A CRITICAL STATE APPROACH TO THE MECHANICAL BEHAVIOR OF EARLY-AGE CEMENTED PASTE BACKFILL

by

AMIN B. GHORBANPOUR

Presented to the Faculty of the Graduate School of

The University of Texas at Arlington in Partial Fulfillment

of the Requirements

for the Degree of

DOCTOR OF PHILOSOPHY

THE UNIVERSITY OF TEXAS AT ARLINGTON

December 2019

Acknowledgements

I would like to thank Dr. Xinbao Yu for his support and guidance through the completion of this research. I am grateful to have had a supervising professor who was always available for questions. I also want to thank my colleague Dr. Reza Moghaddam for his support and willingness to give his time and expertise. I would like to extend my gratitude to other colleagues at Golder Associates whom without their guidance and continuous support the completion of this research would be impossible.

Additionally, I would like to thank the instructors and staff at the Bahá'í Institute for Higher Education (BIHE) during my undergraduate studies in Iran for volunteering and dedicating their efforts to building an exemplary institution to provide an academic education to those who were denied access to higher education due to unrelenting religious persecution.

Finally, I would like to thank my parents and siblings for their support throughout my studies. Your prayers and encouragement have been instrumental in the completion of this thesis.

November 15, 2019

Abstract

A Critical State Approach to the Mechanical Behavior of Early-Age Cemented Paste Backfill

Amin B. Ghorbanpour, Ph.D., P.E.

The University of Texas at Arlington, 2019

Supervising Professor: Xinbao Yu

Low plasticity to non-plastic mine tailings are typically transported to a storage area through pipelines in form of slurry or thickened tailings. The main concern with such tailings deposits is the possibility of liquefaction and the consequent failure of the tailings retaining dams. Tailings can also be used as Cemented Paste Backfill (CPB) material to fill previously mined underground voids. The state of practice to improve the mechanical properties of tailings is to add a small quantity of cementitious materials or binder agents. Portland cement (PC) is the most common binder agent that is used to improve the mechanical properties of mine tailings in underground backfilling applications. To prepare a cheaper and more environment-friendly cemented tailings mix, the application of class C fly ash (FA) both as a single binder agent and supplementary cementitious materials (SCM) to replace PC was evaluated. In this study, laboratory tests indicated potential application for class C fly ash to be used as a single binder to improve the mechanical properties of tailings at the paste consistency. Additionally, class C fly ash can be used to replace a significant portion of Portland cement (PC) in CPB. Fairly similar UCS values were obtained for 3%PC and 1.5%PC:3%FA specimens. The reduction of PC to half and addition of class C fly ash increased the initial and final setting times by approximately 3.5 times.

After developing a CPB mix design the liquefaction of early-age CPB through a comprehensive framework of critical state soils mechanics was studied. The critical state soil mechanics is a robust approach to evaluate the liquefaction behavior of sands, silts, and early-age CPB at a broad range of void ratios.

Previous studies have indicated early-age CPB is not susceptible to static liquefaction. A critical state approach taken in this study shows why the CPB specimens in literature did not experience static liquefaction. Taking this comprehensive approach to explain the mechanics of CPB is critical as the field void ratios of CPB, and consequently its liquefaction behavior, may vary from those tested in the laboratory. The early-age behavior of CPB was evaluated when the samples reached the initial set time at 22-hour curing period, and the UCS values ranging from 78 kPa to 92 kPa. A critical state line of uncemented tailings and CPB specimens was developed using a set of drained and undrained triaxial tests. The triaxial confining pressures targeted common vertical effective stresses in stopes. The static liquefaction behavior of early-age CPB can be predicted using the state parameter (ψ) of the tailings or early-age CPB. In addition to the static liquefaction, the cyclic mobility of tailings and early-age CPB were evaluated using a set of cyclic direst simple shear tests. The cyclic tests were performed using the cyclic stress ratios appropriate for most seismic regions. Based on the cyclic test results, the CPB prepared with 50% replacement of PC with fly ash indicated adequate resistance against liquefaction at its initial setting time for reasonably large earthquakes in most seismic regions.

Finally, the applicability of a select existing constitutive model (NorSand) to predict the behavior of early-age CPB was evaluated. NorSand was found to be applicable to early-age CPB particularly post peak strength, approximately after 1% axial strain, due to breakage of cementitious bonds.

Table of Contents

List of Illustrations

List of Tables

Chapter 1

Introduction

Mine tailings are the unwanted materials after the process of extracting valuable minerals from an ore. The mining industry produces large quantities of fine-grained mine tailings daily. Mine tailings are often stored in impoundments behind dams. Annually, mines in the United States generate waste equivalent in weight to nearly nine times the trash produced by all US cities and towns combined (United States Environmental Protection Agency, 2003). The main waste stream worldwide is tailings with the rate of approximately 500 million tons per year (Kossoff et al., 2014; Collins & Ciesielski, 1994). On a global scale, the rate of mine waste production is increasing (Kossoff et al., 2014). One of the most common methods of tailings disposal is transporting in the form of slurry through pipelines to suitable disposal ponds retained by tailings dams. The main concern with such tailings deposits is the possibility of seismic liquefaction (cyclic mobility) and the consequent failure of the retaining dams during cyclic loading. Cyclic mobility can be triggered by different seismic events including earthquakes, rock bursts, and blasting. The current rate of major tailings dam failure has been estimated approximately two to five per annum (Davies, 2001). Adding a binder agent (i.g., fly ash, cement) to tailings can improve the resistance of tailings against liquefaction.

Tailings can also be used as Cemented Paste Backfill (CPB) material to fill previously mined underground voids (also known as stopes). Once the CPB mix is ready, it will be transferred to the mine voids through pipelines. The main reason to backfill is to provide support to the surrounding rock which allows the extraction of more mineral-rich rocks between the previously mined voids. To retain the fill within the stope features are constructed at the bottom of the stope which are called bulkheads (or barricades). If liquefaction is triggered inside the stope, the pressure on the bulkheads may reach up to

full hydrostatic pressure (Suazo, 2017). Historical cases of barricade failures cases have been reported (Revell and Sainsbury 2007; Helinski 2008). The barricade failure will endanger the safety of workers because of the inrush of material into the work zone. Therefore, the integrity of bulkheads under all loading conditions including cyclic loading should be considered. The resistance of CPB against liquefaction is an important criterion that needs to be considered in the mix design. The application of backfill in underground mine voids also reduces the number of mine tailings that need to be stored on the surface.

Portland cement is the most common binder agent that is used improve the mechanical properties of mine tailings in underground backfilling application. Upon the availability of fly ash, mine owners and practitioners consider the use of fly ash in the mix design to reduce the costs since fly ash tends to be less expensive than Portland cement.

1.1 Problem Statement

Low plasticity to non-plastic mine tailings, particularly when they are transported to the storage area through pipelines in form of slurry or thickened tailings, may be susceptible to liquefaction under monotonic and cyclic loading even after they consolidate. In upstream raised tailings dams the failure of the foundation tailings can result in catastrophic environmental consequences and endangers the lives of people. Adding a binder agent (i.e., lime, fly ash, and cement) to tailings can improve their mechanical behavior. The improvement of slurry or thickened tailings in surface disposal by adding a binder agent has not garnered enough attention by researchers.

Cemented paste backfill (CPB) is a mixture of mine tailings, mine process water, and binder agents used to fill previously mined underground openings (stopes). The use of mine tailings in the stope backfill application will reduce the amount of mine tailings that need to be disposed on the surface behind the mine tailings dams and provides

stability for the underground mining in the vicinity of the stopes. Although the long term stability provided by using CPB is important, the short term stability of fresh CPB, including its resistance to liquefaction, is of concern.

The state of practice in CPB technology is to add a small quantity of cementitious materials (i.e., binder agents) to mine tailings as backfill material in order to improve short term and long term strengths. The 'rule of thumb' criterion used to consider backfill as liquefaction resistant is to obtain an unconfined compressive strength (UCS) of 100 kPa based on special case study on clean rounded cemented sand (Clough et al., 1989). It has been shown that the 100 kPa UCS can be achieved by adding a small quantity of binder to CPB in a short period of time (Aref, 1988; Pierce, 1997, Le Roux, 2004). The CPB at its early-age conditions may be susceptible to liquefaction since hydration takes time to progress. The most common binder agent that is used to prepare CPB is Portland cement. The full or partial replacement of Portland cement with fly ash may significantly reduce total CPB costs and provide environmental benefits.

The tailings for mine backfilling are commonly dewatered to a paste consistency and transported by pipeline into a previously mined stope at a controlled filling rate. The filling rate depends on the strength development of CPB over time due to the hydration of cementitious binders. The susceptibility of early-age CPB to static liquefaction during the backfilling of a stope (i.e., static loading) is of paramount importance for the safety of workers underground in the vicinity of the backfilled voids and other economic implications.

In addition to static (monotonic) liquefaction, the dynamic (cyclic) response of CPB to liquefaction induced by a seismic event is of concern. The freshly placed CPB may be susceptible to liquefaction during seismic loading due to a natural seismic event

such as earthquake or mining activities such as blasting during the excavation of adjacent stopes or rock bursts.

The static liquefaction of early-age CPB has been studied by previous researchers (Aref, 1988; Le Roux et al., 2004; Saebimoghaddam, 2010; Suazo et al., 2017) using the interpretation of individual triaxial tests. These studies have indicated early-age CPB is not susceptible to static liquefaction. However, the liquefaction of early-age CPB through a more comprehensive framework of critical state soils mechanics has not been studied. A critical state approach can provide an explanation why the CPB specimens in literature did not experience static liquefaction. Taking this comprehensive approach to explain the mechanics of CPB is critical since the field void ratios of CPB, and consequently its liquefaction behavior, may vary from those of tested in the laboratory. The critical state soil mechanics is a robust approach to evaluate the liquefaction behavior of CPB at any void ratio.

Also, the influence of fly ash on CPB strength and susceptibility to static and cyclic liquefaction has not received enough attention. The application of class C fly ash as a single binder agent to improve the mechanical properties of mine tailings in the mining industry has not been studied enough either.

1.2 Objectives

The mechanical properties of mine tailings, including static and dynamic strengths, have been studied for a wide range of particle sizes and mineralogy. The static and dynamic strengths of CPB that was prepared with Portland cement have also been studied by several researchers. However, the mechanics of CPB has not been evaluated through a comprehensive framework of critical soil mechanics. Additionally, the influence of fly ash as a binder agent or supplementary cementing materials (SCM) on the mechanical properties of early-age CPB including its static and dynamic strengths (i.e.,

resistance to liquefaction) has not received enough attention. Therefore, determining the laboratory responses of early-age CPB that was prepared with Portland cement and/or flyash to monotonic and cyclic loadings through the framework of critical state soil mechanics is the main objective in this thesis. A better understanding of the influence of fly ash on the hydration process and mechanical properties of CPB through the unconfined compressive strength testing is another objective of this study. Also, the application of fly ash to improve the mechanical properties of mine tailings as a single binder agent for the surface disposal method or for underground backfilling is another question to be answered during this study. Subsequently, the cyclic response of early-age CPB with fly ash in the mix design needs to be studied to determine the dynamic behavior of CPB.

1.3 Plan of Work

This thesis aims to understand the liquefaction behavior of CPB through a comprehensive framework of critical state soil mechanics.

The application of fly ash in improving the mechanical properties of tailings (e.g. CPB) will be studied. The remainder of the thesis will examine the liquefaction potential of early-age CPB under monotonic and cyclic loading conditions. An applicability of existing constitutive models for uncemented soils to early-age CPB will be also evaluated. The new work will be synthesized and recommendations will be made for future research.

1.4 Thesis Organization

Chapter 2 describes the methods which mine tailings are disposed. CPB, its ingredients and the basic properties of mine tailings and binder agents will be described. The definition of liquefaction in the context of geotechnical earthquake engineering and the state of the practice for evaluating the liquefaction susceptibility of soils will be

provided. A literature review of relevant works to this study will be presented in this chapter.

Chapter 3 presents the basic properties of the mine tailing, cement, and fly ash used in this study. The experimental design, the sample preparation technique and equipment used are also discussed.

Chapter 4 presents the results of unconfined compressive strength tests. The strength of CPB prepared with PC and/or fly ash will be investigated in this chapter.

Chapter 5 presents the results of monotonic tests on mine tailings and CPB at different effective confining stresses in undrained and drained conditions. The critical state line will be developed and the susceptibility of CPB will be explained using the critical state approach.

Chapter 6 presents the results of cyclic tests for mine tailings and CPB at different cyclic stress ratios.

Chapter 7 presents the constitutive models of the mine tailings and the early-age CPB using the NorSand model.

Chapter 8 presents the conclusion and plan for future work.

Chapter 2

Literature Review

The objective of this chapter is to review the major disposal methods of mine tailings, test material characteristics, unconfined compressive strength studies of CPB, liquefaction of soils subjected to monotonic and cyclic loading and existing constitutive models to predict the behavior of silts.

The major disposal methods of mine tailings will be described to better understand why the laboratory study of mine tailings is important. Then general characteristics of the test materials will be provided. Definiens related to liquefaction will be briefly reviewed. Then a literature review of CPB unconfined compressive strength (UCS), liquefaction potential of silts, silt-sized mine tailings and CPB will be reviewed.

2.1 Major Disposal Methods of Tailings

One of the most common methods of tailings disposal is transporting them in the form of slurry through pipelines to suitable disposal ponds retained by tailings dams. The main concern with such tailings deposits is the possibility of liquefaction.

Liquefaction has been one of the known failure mechanisms in mine tailings sites (Dobry and Alvarz, 1967; Ishihara et al., 1980; Davies et al., 2002; Kossoff et al., 2014). Although flow liquefaction under monotonic loading is known to be the main mechanism in most tailings dam failures (Davies, 2002), cyclic liquefaction due to earthquake (cyclic) loading is still a concern, particularly in upstream raised tailings. Figure 2-1 shows the different types of commonly constructed tailings dams. The upstream raising of tailings dam is a cost-effective method, typically requiring only minimal volumes of fill materials from borrow sources. However, this type of tailings dams has an inherent risk of failure due to the potential for static or seismic liquefaction of the foundation tailings (Etezad,

2016). The liquefaction susceptibility of the foundation tailings upon which the dam is raised is a key design concern for the upstream construction method.

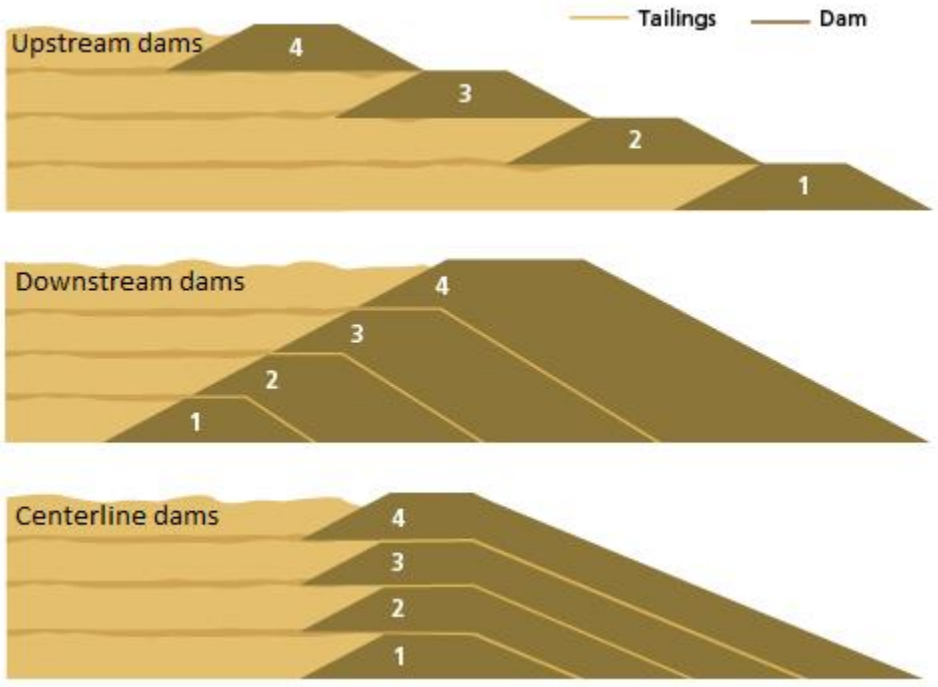

Figure 2-1 Common methods of tailings dam construction (Vick, 1983)

Tailings from a typical hard rock mine operation primarily include angular sand-size and silt-size particles. The tailings are often transported through pipelines in slurry form to be stored behind the retaining dam. The as-placed tailings are generally considered susceptible to liquefaction because of the nature of deposition, high degree of saturation, and relatively loose densities (Wijewickreme et al., 2005).

A considerable amount of research has been conducted to understand the liquefaction susceptibility of uncemented silty and silty sand materials (Seed and Idriss 1982; Boulanger et al., 1998; Erten and Maher, 1995) or mine tailings (Al Tarhouni, 2008; Crowder, 2004; Dobry and Alvarez, 1967; Fourie and Papageorgiou, 2001; Garga and McKay, 1984; Ishihara et al., 1980; Okusa et al., 1980; Poulos et al., 1985). These

studies reported that mine tailings are vulnerable to earthquake-induced liquefaction as well as flow liquefaction. Although the cyclic and monotonic response of tailings has received adequate attention, published data on the cyclic and monotonic response of tailings amended with a binder agent, including fly ash, is surprisingly limited or not available, despite the potential implications.

Another major method of mine tailings disposal is to mix them with a binder agent to backfill the underground mine voids at the mine site. Cemented paste backfill (CPB) is a mixture of mine tailings, mine process water, and binder agents used to fill previously mined underground openings (stopes). Typically, CPB is produced in a paste plant by mixing water and binder agents to fine tailings to make the mixture pumpable. CPB is mixed using the “batch” or “continual” technique and then delivered into a previously mined stope in pipelines, predominantly by gravity transport (Hassani and Archibald, 1998). Once CPB is delivered to the stope through a pipeline it will be discharged into the stop that is closed at the bottom using a rock pile barricade. Figure 2-2 shows the basic configurations for CPB distribution systems and the schematic of a backfilled stope.

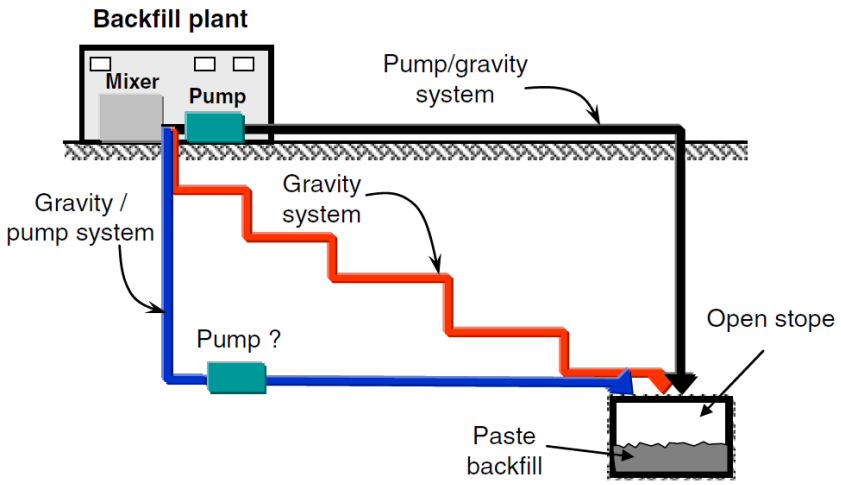

(a)

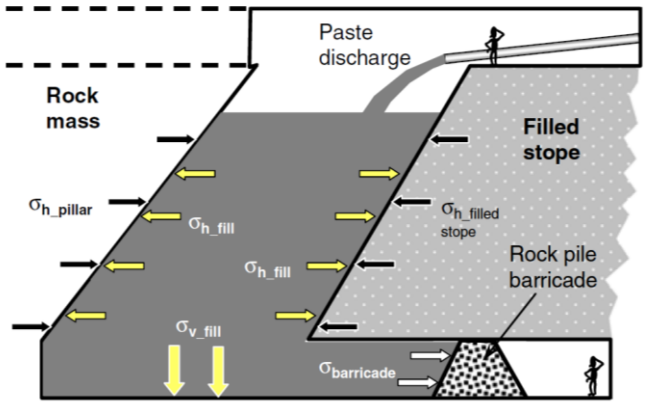

(b)

Figure 2-2 a) Basic configurations for paste backfill distribution systems, b) Schematic diagram of backfilled stope components and stress field distribution (Belem & Benzaazoua, 2008)

The mechanical properties of CPB including its strength are governed by the characteristics of mine tailings on one hand and the characteristics of binder agents on the other. Portland cement (PC) is the most commonly used binder agent to make CPB. The mine owners and practitioners usually consider the use of fly ash as supplementary

cementing materials to develop a cheaper mix design. The costs of mine void backfilling with CPB typically range from 10% to 20% of total mine operating costs. Binder agents account for up to 75% of backfilling costs (Grice 1998; Fall and Benzaazoua, 2003).

According to data from the U.S. Geological Survey, the average price of cement in 2010 was $92 per ton. A survey of fly ash providers nationwide found the average price for a ton of fly ash is $40 (Transportation Development Foundation, 2011). The major portion of the cost of fly ash is transportation. In the concrete industry, the substitution ratio for fly ash to Portland cement is typically 1:1 to 1.5:1 (Federal Highway Administration, 2017). The average prices for Portland cement and fly ash suggest that the replacement of Portland cement with fly ash can potentially result in much cheaper mix design if the engineering properties criteria are met.

The mechanical properties of CPB change as the hydration processes progress. Early-age CPB has low strength and may be susceptible to liquefaction due to static and dynamic loads during a transient period after preparation. After the transient phase, there is a hardening phase where CPB gains an adequate strength for underground support.

2.2 Hard Rock Mine Tailings

The basic properties of mine tailings, such as particle size distribution, mineralogy, and chemical composition varies from mine to mine and within individual mines. Usually, the mine tailings that are used to prepare the CPB should contain a minimum weight of 15% of the particles that are smaller than 20 microns. The role of fine particles (<20 microns) is to prevent the water/solids separation (Landriault, 1995, Cincilla et al., 1997; Tenbergen, 2000).

Particle size distribution influences several properties of mine tailings, such as bulk density and effective surface area of particles. The effective surface area of the particles affects the rheological properties of mine tailings. The finer particle size

distribution will result in more water surrounding the particle surface areas. Consequently, more water in CPB will result in more “workability” or consistency (i.e., slump). Furthermore, finer particles will have a greater effective surface area that the cementitious materials must act on. The angularity of particles also can impact strength. The use of a binder agent in soils with angular particles instead of round-shaped particles typically results a higher strength (Clough et al., 1989).

Mine tailings that are typically used to make CPB in hard rock mining can be categorized as fine-grained soil with zero to low plasticity index (PI). Mine tailings particle sizes usually range from clay sized particles to sand sized particles depending on the mineralogy and the mining operation. The approximate range of hard rock mine tailings particle size is shown in Figure 2-3. Hard-rock mining tends to produce fine tailings that can range from clay sized through silts, with particle diameters of less than 0.08 mm (James et al. 2011). The plasticity index of mine tailings ranges from zero plasticity to high plasticity based on the ore mineralogy and the particle size distribution.

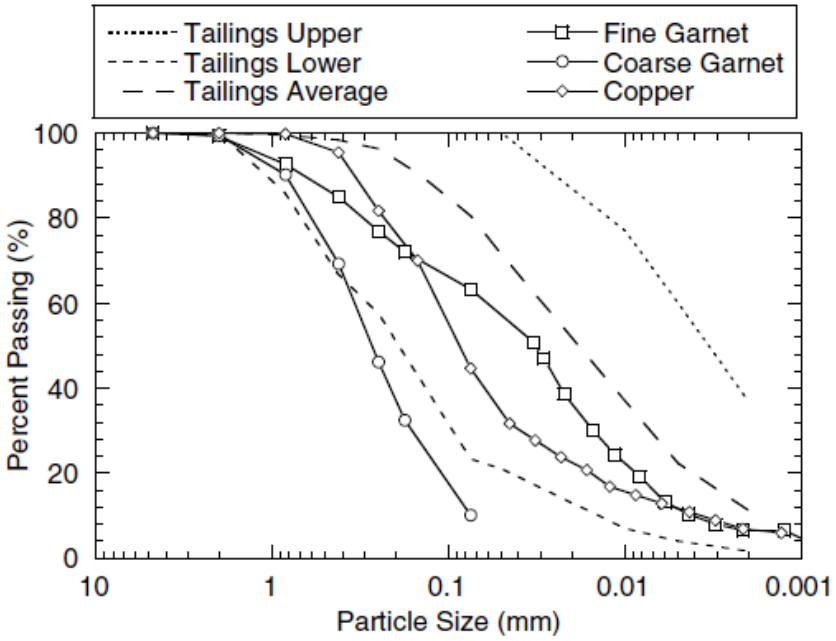

Figure 2-3 Particle size distribution of hard rock mine tailings (Gorakhki & Bareither, 2017)

The mineralogy of mine tailings depends on the type of host rock. The major constituent of mine tailings minerals is quartz. The effects of particle size distribution and PI on the mechanical properties of CPB will be discussed later in this chapter.

2.3 Binder Agents

Binder agents such as Portland cement (PC) and supplementary cementing materials (SCM) (e.g., ground-granulated blast-furnace slag (GGBS), fly ash) can be added to mine tailings-water mixtures to improve the mechanical properties of CPB. Portland cement at various contents have been the main constituent of the binder agents in CPB. Cemented paste backfill plants typically mix tailings, cement, and water to solids contents (SC; i.e., the weight of solids over total weight) ranging between 75 and 85% and cement content between 3 and 7% by dry total weight (Benzaazoua et al., 2004). To design a cheaper mix design the use of SCM is usually considered. In addition, chemical

additives, such as flocculants, super-plasticizers, and accelerators may be employed to improve the permeability or consolidation of fills or to increase the flowability of CPB. The main characteristics of Portland cement and fly ash are briefly discussed in the following subsections.

2.3.1 *Portland Cement*

Portland cement clinker mainly contains four mineral components: tricalcium silicate or alite ($3CaO.SiO_2$ or C_3S), dicalcium silicate or belite ($2CaO.SiO_2$ or C_2S), tricalcium aluminate ($3CaO.Al_2O_3$ or C_3A), and tetracalcium alumina ferrite ($4CaO.Al_2O_3.Fe_2O_3$ or C_4AF). The properties of major constituents of Portland cement clinker are shown in Table 2-1.

Table 2-1 Major components of Portland cement clinker

Constituent	**Percentage**	**Grain shape**	**Rate of hydration**
C_3S	50%	Equidimensional	Rapid
C_2S	20%	Rounded	Slow
C_3A	3-8%	Rectangular	Instantaneous
C_4AF	-	-	Very rapid

The minor constituents of Portland cement include MgO, TiO_2, Mn_2O_3,K_2O, and Na_2O. The range of chemical compositions of Portland cement in a ternary diagram including CaO, SiO_2, and Al_2O_3 is shown in Figure 2-4.

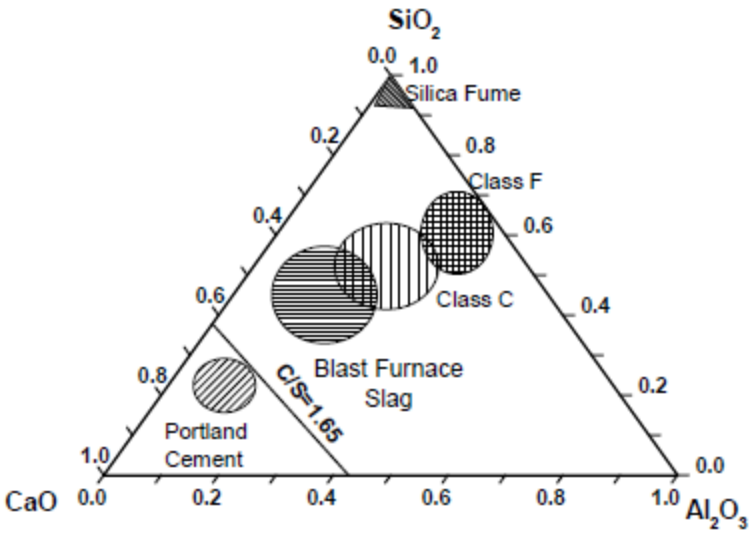

Figure 2-4 Ternary phase diagram of chemical composition of common binders phase diagram (Livingston and Bumrongjaroen, 2005)

The reaction of enough Portland cement with water forms hydrates that produce a stiff mass after enough time. The typical hydration products are: calcium hydroxide (Ca(OH)2 or CH), calcium-silicate-hydrate (C-S-H), and calcium sulphoaluminate known as ettringite ($3CaO.Al_2O_3.3CaSO_4.31H_2O$). To control the violent reaction between C3A and water, gypsum is added to Portland cement during grinding.

The hydration process of Portland cement typically occurs in four stages, as follows:

I) Initial reactions (0-15 min.): initial dissolution of C_3A, C_3S, and gypsum (if applicable) is the first chemical reaction to occur in the cement paste resulting in the release of Na, K, Ca, OH ions into the pore solution.

II) Induction, or dormant, period (1-3 hrs.): an amorphous, semi-permeable gel, rich in calcium, silica, and alumina will form around the cement grains, along with ettringite and

CH during this period (Soroka, 1980). Further hydration might be retarded due to the formation of this gel and ettringite around C_3S and C_3A grains, respectively.

III) Setting period (3-17 hrs.): the end of dormant period is associated with the rupture of gel formed around the cement grains due to excess pressure. This results in the formation of C-S-H gel due to the contact of the silica rich solution from the gel with the external solution. In this stage, large crystals of CH might form out of the supersaturated solution (Soroka, 1980).

IV) Hardening period (17 hrs. to 90 days): short fibers of C-S-H and massive deposition of CH continue to form at a very slow rate resulting in further de$_{cr}$ease in paste porosity (Neville, 1995).

Low-calcium fly ash or class F fly ash can be used as a SCM in conjunction with Portland cement to prepare CPB. The contribution of class F fly ash to the strength of CPB is through the pozzolanic reactions. Unless the porewater in CPB is highly alkaline (pH>13), class F fly ash needs to be used in conjunction with Portland since it does not contain enough calcium oxide content. On the other hand, high-calcium fly ash or class C fly ash will increase the strength of CPB through both pozzolanic and cementitious reactions and can exhibit self-cementitious behavior (Papadakis, 2000).

2.3.2 *Fly Ash*

Fly ash is a residual material produced in coal-fired power plants by burning pulverized coal in boilers to generate electricity. Fly ash is usually categorized into two main groups, class C fly ash and class F fly ash. When the calcium oxide (CaO) in PC or class C fly ash reacts with water calcium hydroxide will be produced. Both class F and class C fly ashes contain amorphous silica and alumina which in the presence of calcium hydroxide will produce calcium-silicate-aluminate hydrates (hydration gel).

Table 2-2 shows the chemical requirements for fly ashes to be classified as either class F or class C fly ashes (ASTM C618, 2017). The fly ashes that do not meet the requirements listed in in Table 2-2 are classified as off specification fly ash. The fly ash in CPB is not required to meet the requirements for class F and class C fly ash.

Table 2-2. Chemical requirements for fly ash classification (ASTM C618, 2017)

Parameter		class F	class C
$SiO_2 + Al_2O_3 + Fe_2O_3$	min%	70	50
Sulfur trioxide (SO_3)	max%	5	5
Moisture Content	max%	3	3
Loss on ignition (LOI)	max%	6	6

Notes: SiO_2=Silicon dioxide, Al_2O_3= Aluminium oxide, FE_2O_3= Iron oxide

Fly ash has a relatively high glass content. The glass phase consists primarily of ordered silicate and aluminosilicate phases. class C fly ash has a higher CaO content than class F fly ash and has self-cementing properties in the presence of water. Based on Thomas et al. (1999) class C fly ash has more than 20% calcium oxide while class F fly ash has less than 20% calcium oxide. The glass phase for class C consists primarily of substituted calcium aluminate and calcium aluminate silicate phases. Fly ash particles are spherical, ranging in size from 1 μm to 100 μm based on differences in power plant operations. The typical value of the specific gravity for fly ash ranges from 2.2 to 2.5 (Neville, 1995).

The glass content in fly ash in the presence of an alkaline agent and when the mixture pH is more than 12 forms cementation through a different set of dissolution reactions which is beyond the scope of this study.

2.4 Strength of Cemented Paste Backfill

The required strength for CPB depends on the intended function. Belem and Benzaazoua (2008) reviewed the design unconfined compressive strength (UCS) required for different backfill applications, such as vertical roof support, pillar recovery, ground support, and working platforms. The UCS values for free-standing backfill applications usually range from 0.2 MPa to 4 MPa (Stone 1993; Li et al. 2002) while the USC values for surrounding rock mass range from 5 MPa to 240 MPa (e.g., Grice 1998; Revell, 2000). A UCS of 100 kPa is historically adopted as the liquefaction potential limit (Grice 2001; le Roux et al. 2002). Suazo et al. (2017) recently showed that CPB becomes resistant to liquefaction when the UCS reaches a minimum value of 60-75 kPa assuming a reasonably large earthquake for most seismic regions.

In the following subsection the main factors that affect the UCS of CPB, such as binding agents, tailings characteristics (specific gravity, mineralogy, particle size distribution), and mixing water chemistry, will be reviewed.

2.4.1 *General Parameters Affecting the UCS of CPB*

The strength of CPB is determined by many factors including curing age, particle size distribution, particle shapes, binder type, binder content, initial void ratio, and solid contents.

The longer curing age will result in more hydration products and higher strength (Mozaffaridana, 2011). The lower initial void ratio and higher density will increase the strength (Suazo et al., 2017). The higher tailings solid content will increase strength (Gorakhki & Bareither, 2017). Solid content in this thesis is defined as the ratio of the mass of solid particles to the total mass of CPB. The higher binder content will result in a higher UCS value.

Fly ash impacts the strength of CPB through two mechanisms. One mechanism is the replacement of angular tailings particles with rounded fly ash particles and the other mechanism is the participation in the hydration process to generate cementitious bonds. The replacement of the angular particles with rounded particles may decrease the CPB strength while more cementitious bonds will increase the strength (Gorakhki & Bareither, 2017). The contribution of class C fly ash to the CPB strength will be further assessed in this thesis.

It has been shown that the particle size distribution of mine tailings has a strong influence on the strength of CPB (Fall et al., 2005; Gorakhki & Bareither, 2017). Larger amounts of fine particles (i.e., <20 μm) in tailings will result in lower UCS values. Fall et al. (2005) showed that the UCS of CPB decreases as the percentage of fine particles increases for different CPB specimens, as shown in Figure 2-5. In this figure, PCI and PCV are ASTM Portland cement type I and V, respectively. The PCI to PCV ratio was 50/50, while the PCI to the SCM (slag) ratio was 20/80 for the samples.

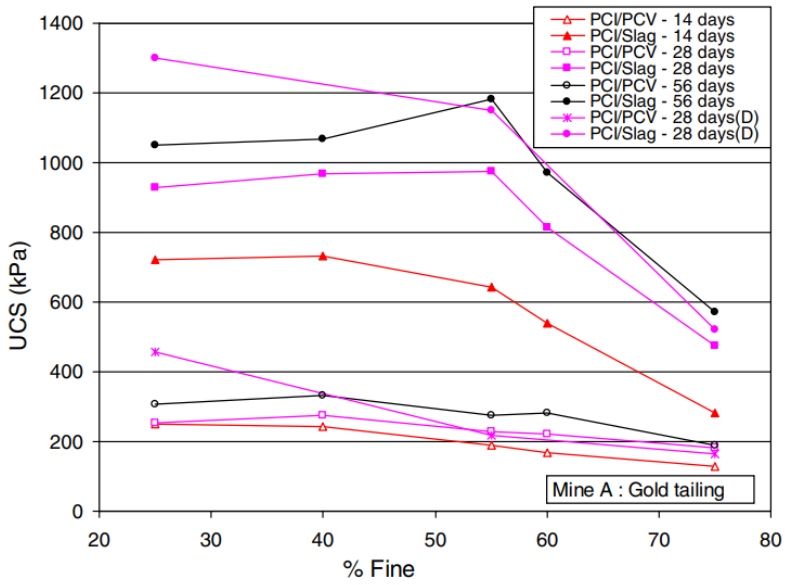

Figure 2-5 Effect of tailings fineness on strength of CPB (Fall et al., 2005)

The quality of water used in CPB is another parameter that can influence the strength of CPB. The pH and sulphate salts content of the water are two important factors. Acidic water and sulphate salts result in strength loss in CPB (Benzaazoua et al. 2002, 2004).

2.4.2 *Effect of pH on the Role of Fly Ash in Cementation*

The pH of the fluid phase in the tailing mixture amended with fly ash has a significant role in the strength of the mixture. In highly alkaline environments (pH>12) different reactions through dissolution of fly ash in alkaline media take place which can significantly contribute to the strength of tailings amended with fly ash. Increasing the pH of the fluid phase with additions of lime and/or alkali hydroxides to the mixing water would facilitate the reaction of fly ash. (Ramlochan et al., 2004). However, the use of an alkaline agent might be expensive and introduce health and safety hazards. The use of an alkaline agent to facilitate the reaction of fly ash in CPB is not a common practice in the mining industry.

2.4.3 *Shear Strength Development*

The microstructure of cemented tailings (e.g., CPB) have been studied using the scanning electronic microscope (SEM) technique by several researchers (Ouellet et al., 1998; Benzaazoua, et al., 1999; Benzaazoua, et al., 2002; Mohamed et al., 2003). In these studies, fractured or cut surfaces of CPB specimens were investigated. However, those surfaces may not be necessarily representative of the microstructures since fractured surfaces are obtained from naturally weak planes in the material and cut surfaces are disturbed by the cutting process.

Ramlochan et al. (2004) suggested the backscattered-electron (BSE) imaging is a better method to study the microstructure of CPB. They investigated the microstructure of four cured CPB specimens using several mix designs. One mix design consisted of

50% PC and 50% fly ash. The microstructure of CPB specimen with the total binder content of 15% by mass (7.5% PC+7.5% FA) is shown in Figure 2-6. Some hydration products can be seen at the surface of tailings particles and sparsely infilling the interstitial space. The void space is filled with epoxy and appears near black in the BSE image.

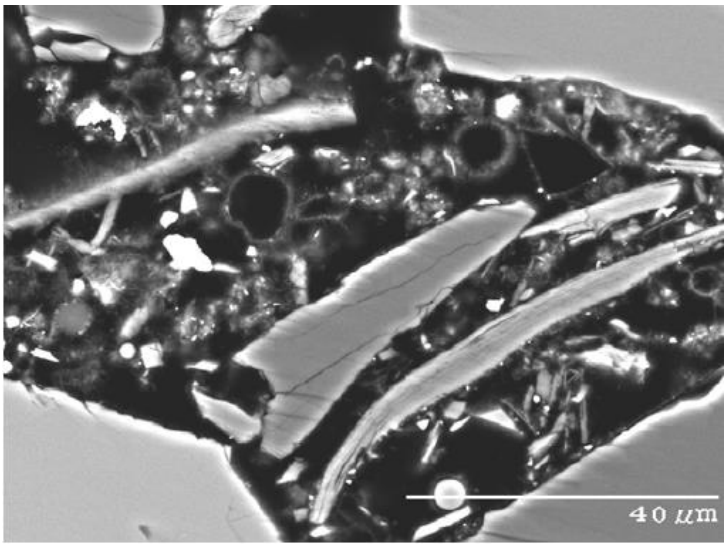

Figure 2-6 BSE image of the interstitial space in the 50%FA:50%PC CPB specimen (Ramlochan et al., 2004)

As shown in Figure 2-6, the hydration products did not fully fill the interstices separating the tailings particles, which resulted in relatively low strength CPB. Figure 2-7 shows the typical BSE image of a Portland mortar with its microstructural constituents. As it is shown in Figure 2-7 most interstices between sand aggregates are filled with the hydration products forming a stronger matrix.

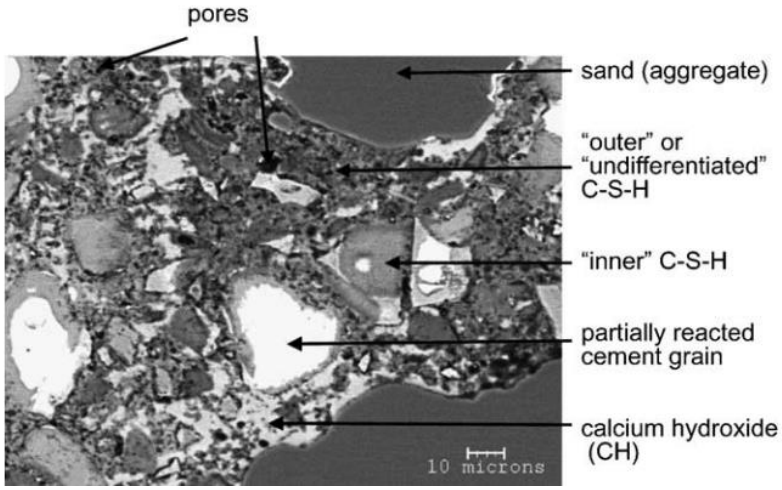

Figure 2-7 Typical BSE image of a Portland cement mortar (200 days old, w/c =0.4) with the microstructural constituents distinguished (Scrivener, 2004)

2.5 Unconfined Compressive Strength of CPB

2.5.1 *Unconfined Compressive Strength Criteria*

The UCS testing is a fairly simple and inexpensive way to determine whether the use of a binder agent will improve the mechanical properties of mine tailings. The required strength for paste backfill depends on the intended function. To provide adequate ground support, the required uniaxial/unconfined compressive strength (UCS) of the fill should be at least 5 MPa, whereas for free-standing fill applications, UCS is commonly lower than 1 MPa (Stone 1993;Li et al. 2002). A UCS of 100 kPa is commonly adopted as the liquefaction potential limit (Grice 2001; le Roux et al. 2002). Suazo et al. (2016) reported a UCS of 70 kPa is adequate to resist liquefaction under a CSR typically generated by a maximum ground acceleration of 0.3 g. Required static strength for paste without exposures may be arbitrarily selected at 200 kPa (e.g., Li et al. 2002).

2.5.2 *Previous UCS Studies on CPB Made with Portland Cement and Fly Ash*

The UCS of CPB made with PC has been extensively studied (Simon, 2005; Mozaffaridana, 2011). However, the application of fly ash to substitute PC in CPB has not received enough attention by researchers. The optimum amount of fly ash in CPB must be determined on a case-by-case basis since it depends on a wide range of parameters.

Mozaffaridana (2011) evaluated the impact of fly ash on the strength of CPB at early and later curing ages by comparing the UCS results for the CPB specimens made using 3% PC and 1.5%PC:1.5%FA binder contents. Fly ash with 14.5% calcium oxide content was used and the specimens were prepared at 72% initial solid contents. The UCS results are shown in Figure 2-8. Although initially, the specimen with 3%PC gained higher strength, the strength of the specimen with 1.5%PC:1.5%FA gradually increased and exceeded that of the 3%PC specimens after a few weeks. Mozaffaridana (2011) stated that fly ash delays set and lowers the early strength development while it contributes greatly to the strength through the pozzolanic reactions at later ages.

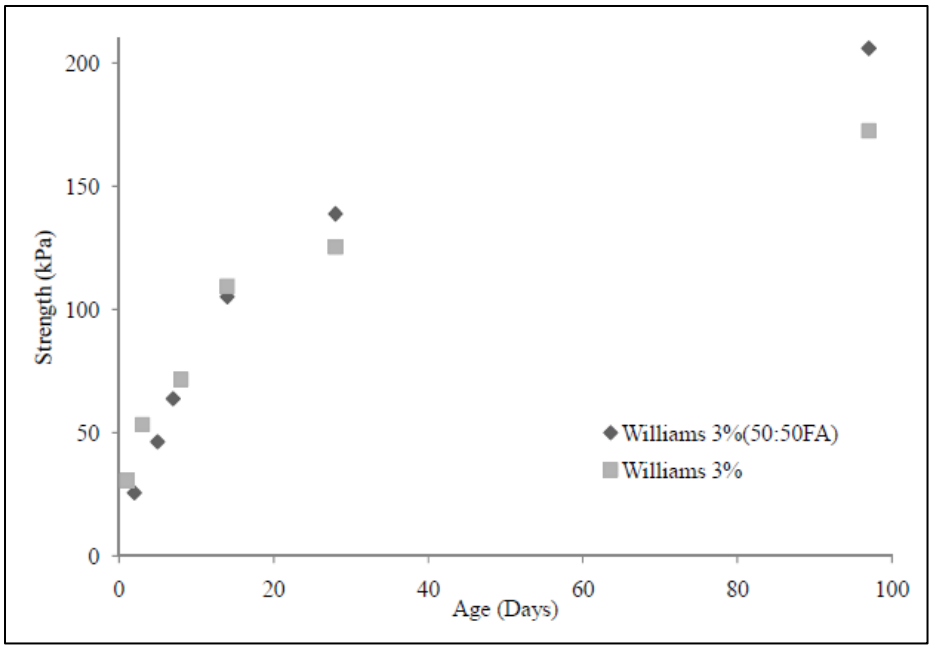

Figure 2-8 Impact of fly ash on the strength gain of CPB (Mozzafaridana, 2011)

2.5.3 *Previous UCS Studies on Mine Tailings Amended with Fly Ash*

Unlike Portland cement, the use of fly ash as a single binder agent has not received enough attention despite the potential implications. Gorakhi and Bareither (2017) mixed tailings with two different samples of fly ash and performed UCS tests under different conditions such as binder content, degree of saturation, solid content (SC=mass of solid particles/total mass), and water to binder ratio. They used 10% and 20% fly ash content (mass of fly ash by mass of dry tailings) at different solid contents to determine the suitability of mine tailings amended with fly ash as fill materials in earthworks such as road subbase and embankments. They concluded that the mine tailings amended with fly ash at a solid content higher than 80% can successfully be used for the application studied.

2.6 Definition of Liquefaction

The term liquefaction has been used in conjunction with a variety of phenomena that involves soil deformations caused by monotonic, transient, or cyclic loading of mainly

saturated soils under undrained conditions. The tendency for densification in saturated cohesionless soils under undrained loading conditions causes an increase in excess pore pressures resulting reduction in effective stresses. The process of transforming any substance into a liquid as a consequence of increased pore pressure and reduced effective stress is defined as liquefaction (Committee on Soil Dynamics of the Geotechnical Engineering Division, American Society of Civil Engineering,1978). Therefore, the generation of excess porewater pressure is a key feature in liquefaction.

Generally, when saturated soils are subjected to rapid loading under undrained conditions the tendency for contraction causes excess porewater pressures to increase and effective stresses to de$_{cr}$ease. In other words, the generation of excess porewater pressure due to static or dynamic loading, might be enough to bring the soil to the steady state condition or a condition of zero effective stress leading to large deformations. Depending on stress and state conditions at which liquefaction might occur and the resultant deformation, liquefaction can be divided into two main groups: flow liquefaction and cyclic mobility (Kramer, 1996). In this study, both flow liquefaction and cyclic mobility are referred to as “liquefaction”.

Flow liquefaction can occur when the shear stress required for static equilibrium of a soil mass is greater than the shear strength of the soil in its liquefied state (Kramer, 1996). Both monotonic and cyclic loading may bring the soil to an unstable state at which its strength drops sufficiently to allow the static stresses to produce the flow failure.

Cyclic mobility occurs when the static shear stress is less than the shear strength of the liquefied soil (Kramer, 1996). Cyclic loading such as the earthquake load may cause cyclic mobility. Flow liquefaction and cyclic mobility of cohesionless soils will be reviewed in the following sections.

2.7 Liquefaction Susceptibility and Its Mechanisms

Liquefaction susceptibility can be evaluated using several criteria. Generally, liquefaction susceptibility criteria for soils can be categorized as historical, geological, state and compositional criteria (Kramer, 1996). The historical and geological criteria consider the history and origin of the soil. In this chapter, the state criteria will be reviewed since it's the main tool used in this study to evaluate the liquefaction behavior.

2.7.1 *State Criteria*

Liquefaction susceptibility depends on the initial state of the soil. The initial state of the soil refers to both initial density and stress conditions at the time of loading (e.g., earthquake). The initial state of the soil determines the porewater pressure generation behavior of soil during the loading (Kramer, 1996). To explain the methods for evaluating state criteria, some basic concepts relevant to the behavior of cohesionless soils will be reviewed in the following sections.

2.7.1.1 Critical Void Ratio

Studies have shown that initially loose specimens contract during shearing and initially dense specimens dilate after a quick contraction at the beginning in a drained, strain-controlled monotonic triaxial test. At large strains, both loose and dense specimens approach the same density and continue to shear with constant shearing resistance. The void ratio, e, corresponding to this constant density is called the critical void ratio (CVR). Critical void ratio line, critical state line (CSL), and steady-state line (SSL) are terms that that have been interchangeably used in this chapter. The technical definition of CSL will be explained further in the Steady State of Deformation section. More information on the historical background of different terminologies for the critical state line has been provided in the book titled *Soil Liquefaction- A Critical State Approach* by Jefferies and Been (2016). The CVR is uniquely related to a specific effective confining pressure, σ'_{3c}.

The CVR line can be developed using critical void ratios at different effective confining pressures. Figure 2-9 shows the use of the CVR line as a boundary between loose (contractive) and dense (dilative) states.

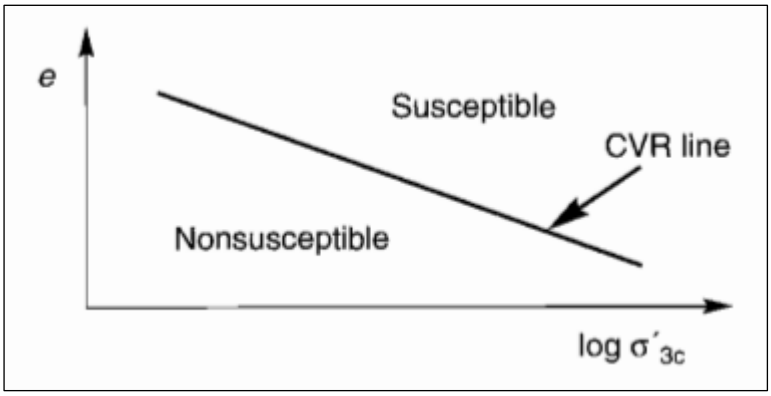

Figure 2-9 Use of the CVR line as a boundary between loose contractive states and dense dilative states

The tendency of soil to contract or dilate can be evaluated by comparing the initial state of the soil in terms of void ratio and effective confining pressure with respect to the CVR line. The state parameter (ψ) as defined in Figure 2-10 is a useful tool to predict the behavior of cohesionless soils. In Figure 2-10, e, is the in-situ void ratio of soil and e_{ss} is the void ratio of the steady-state line at the effective confining pressure of interest.

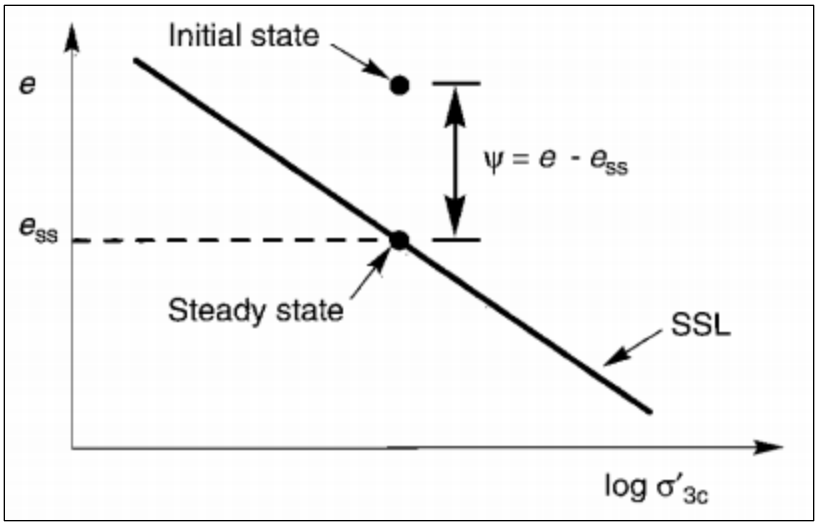

Figure 2-10 State parameter

Generally, saturated soils with initial void ratios above the CVR line are considered susceptible to flow liquefaction and those with void ratios below the CVR are then considered non-susceptible to liquefaction. Jefferies and Been (2016) had suggested that coarse-grained ideal soils with a state parameter smaller than –0.05 will tend to dilate at large strains when loaded in drained shear.

In other words, when the state parameter is positive, the soil exhibits contractive behaviors and may be susceptible to flow liquefaction. When the state parameter is negative (less than -0.05), dilative behavior will occur and the soil is not susceptible to flow liquefaction. The accuracy with which the state parameter can be determined depends on the accuracy of the SSL that is developed using the laboratory test results. The state parameter is also correlated to the CPT resistance and other in-situ testing techniques.

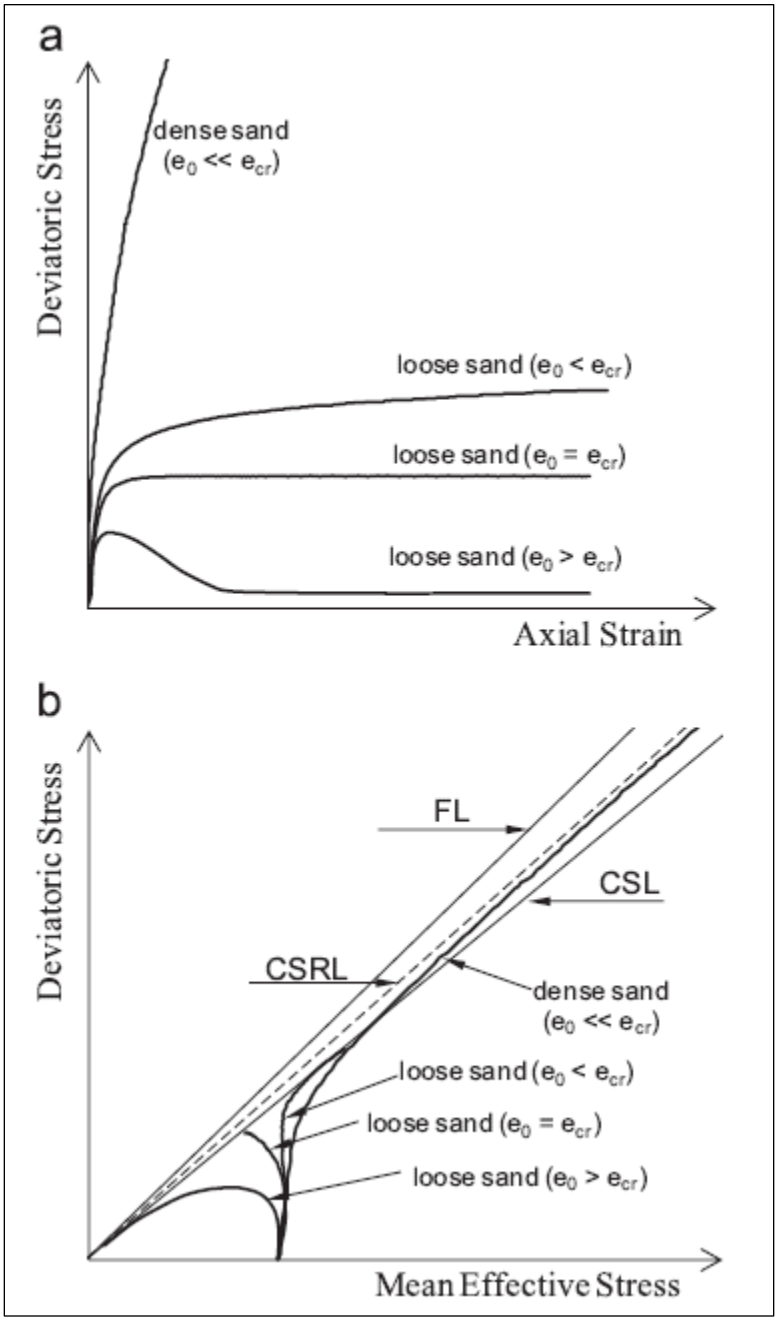

Figure 2-11 Typical behavior of loose and dense sand under undrained conditions. a) stress-strain curves, b) effective stress paths (Chu et al., 2015)

The stress-strain behavior of cohesionless soils under undrained conditions is shown in Figure 2-11 (e_0, is the initial void ratio of the sand tested and e_{cr} is the critical void ratio). Loose samples with a void ratio larger than the critical void ratio $e_0>e_{cr}$ indicate strain-softening behavior caused by the generation of significant excess pore pressure or liquefaction. Loose (i.e., contractive) samples with the void ratio larger than the critical void ratio $e_0>e_{cr}$ indicate strain-softening behavior caused by the generation of significant excess pore pressure, or liquefaction. Loose samples with the void ratio equal to the critical void ratio $e_0=e_{cr}$ indicate a constant deviatoric stress after the peak strength. For loose sand with $e_0<e_{cr}$ the effective stress path in undrained conditions increases towards the peak and then follows the CSL. For dense sand with an initial void ratio much smaller than the critical void ratio ($e_0<<e_{cr}$) or the state parameter smaller than -0.05, the effective stress path will increase monotonically and approach a constant stress ratio line (CSRL). For dense (i.e., dilative) sands with $e_0<<e_{cr}$ the critical state cannot be determined because the specimen exhibits strain hardening behavior and the deviatoric stress increases with axial strain throughout the shearing (Chu et al. 2015).

2.7.1.2 Steady State of Deformation

The stress-strain behavior of soil specimens at three different states under undrained monotonic loading are shown in Figure 2-12. Loose specimens (specimen A) exhibit stain softening behavior with peak strength at a small shear strain and then collapse to follow to large strains. This behavior is considered as flow liquefaction. Dense specimens (specimen B) exhibit strain hardening behavior with an initial contraction and then dilation at large strains. At intermediate densities (specimen C) a peak strength at low strain is followed by a limited period of strain softening behavior and then end with strain hardening behavior at intermediate strain. The transformation between strain

softening (contractive) and strain hardening (dilative) occurs at a point known as the phase transformation point. This type of behavior is called limited liquefaction.

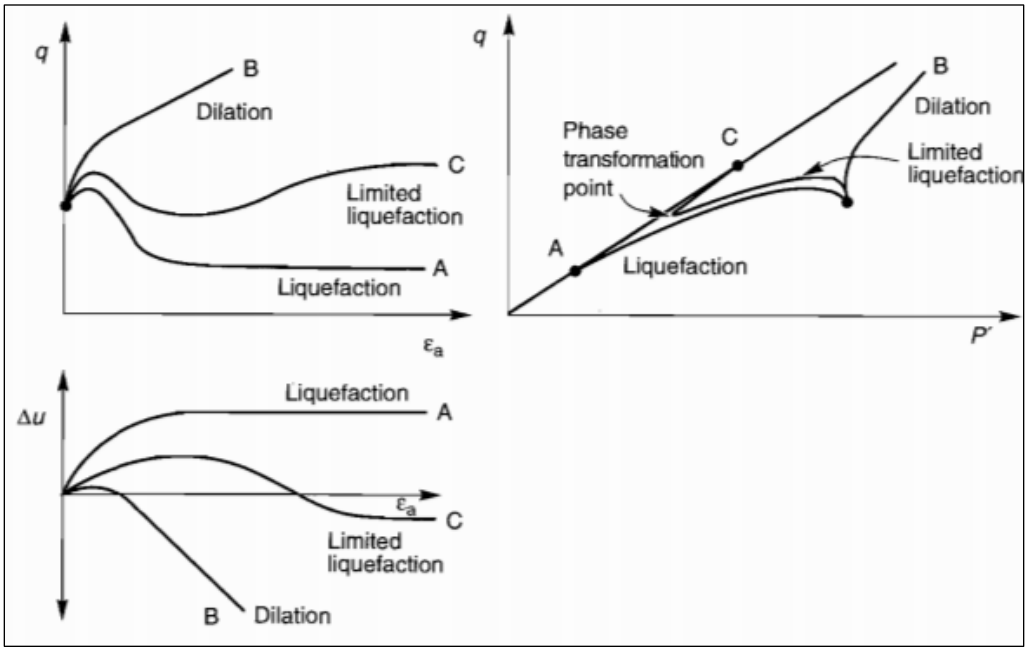

Figure 2-12 Stress-strain behavior and liquefaction susceptibility soils at different initial states under monotonic loading (Kramer, 1996)

The state in which the soil flows continuously under constant shear stress and constant effective confining pressure at constant volume is defined as the steady state of deformation (Castro and Poulos, 1977; Poulos 1981). The steady state of deformation is reached at large strains. Specimens A and C show two examples of the steady state of deformation at large strains. Constant Δu (excess porewater pressure) shows constant volume change and constant deviator stress (q) is corresponding to constant shear stress while strained in an undrained condition. Therefore, there is a unique relationship between void ratio and effective confining pressure at large strains. The locus of points describing this relationship in the steady state of deformation is called the steady state line (SSL). The SSL can also be expressed in terms of the steady state strength, S_{su}. The

SSL can be used to identify the susceptibility of a cohesionless soil to flow liquefaction. Generally, a cohesionless soil is not susceptible to flow liquefaction if its initial state lies well below the SSL (ψ<-0.05) while soils with a state lying above the SSL will be susceptible to flow liquefaction as shown in Figure 2-13.

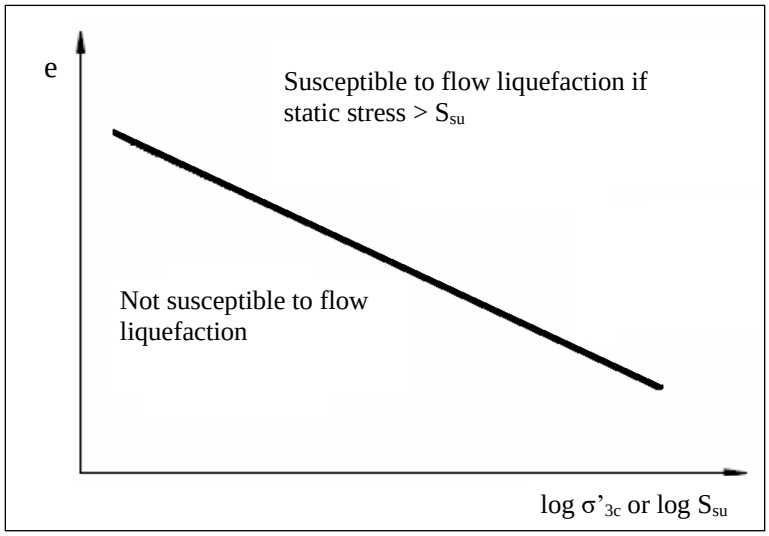

Figure 2-13 State criteria for flow liquefaction susceptibility (Kramer, 1996)

It is common to treat the CSL as semi-logarithmic for all soils. Ideally the CSL is a curved line as shown in Figure 2-14; however, a straight line is usually used as an acceptable approximation for engineering practices (Jefferies & Been, 2016).

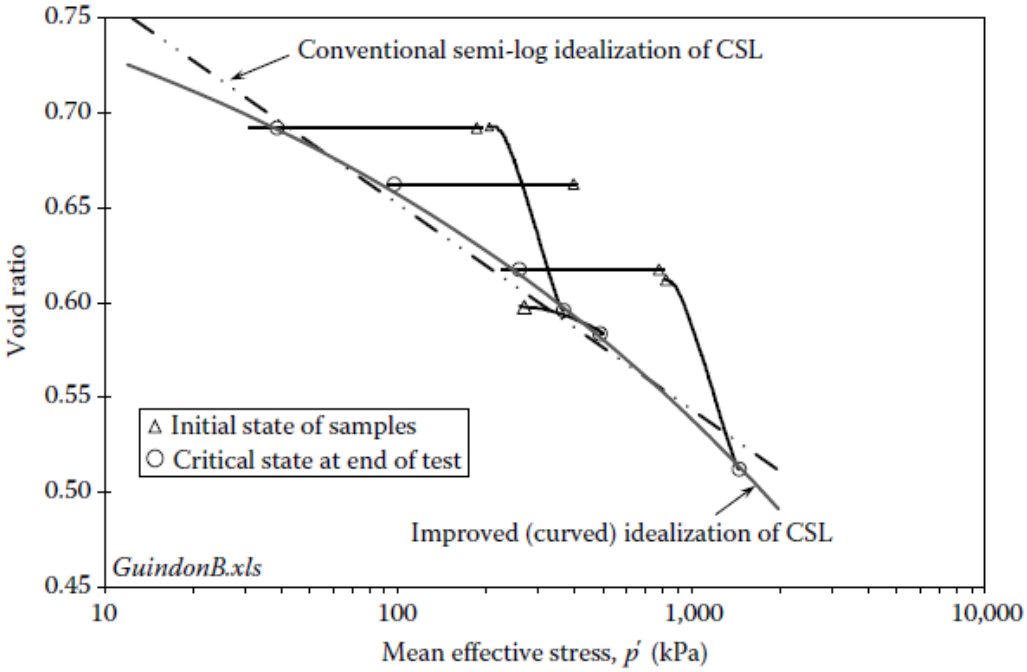

Figure 2-14 Improved idealization of CSL (Jefferies & Been, 2016)

In contrast to flow liquefaction, cyclic mobility can occur in both loose (above the SSL) and dense (below the SSL) soils. In the following sections the state of soil in which it is susceptible to the flow liquefaction or cyclic mobility will be explained.

2.7.2 *Flow Liquefaction Surface*

A stress path can be used to demonstrate the effective stress conditions at which the initiation of flow liquefaction is triggered. The flow liquefaction surface (FLS) is a three dimensional surface determined in the stress path to describe the effective stress conditions at the initiation of flow liquefaction (Vaid and Chern, 1985). The initiation of flow liquefaction can be easily seen when the soil is subjected to monotonic loading.

The monotonic response of five specimens isotropically consolidated to the same initial void ratio at different effective confining pressures is shown in Figure 2-15. The

states of specimens A and B are below the SSL, therefore they are in the dense states while the other three (C, D and E) have states above the SSL and loose states.

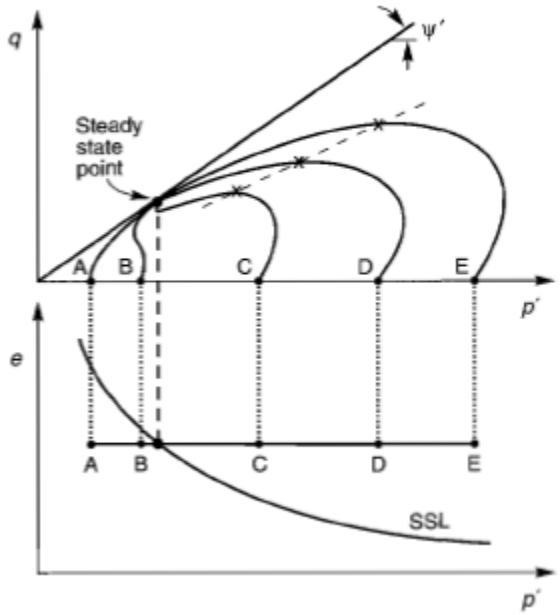

Figure 2-15 The monotonic response of five isotropically consolidated specimens (Kramer, 1996)

All these specimens will reach the same effective stress conditions at the steady state, but the stress paths are different for each of them. The dense specimens show dilative behavior while the loose specimens show contractive behavior. Specimens C, D and E reach maximum points on the stress paths where flow liquefaction is initiated (points are marked with an × in the figure). The locus shows the initiation of flow liquefaction is a straight line that projects through the origin of the stress path, known as flow liquefaction surface (FLS).

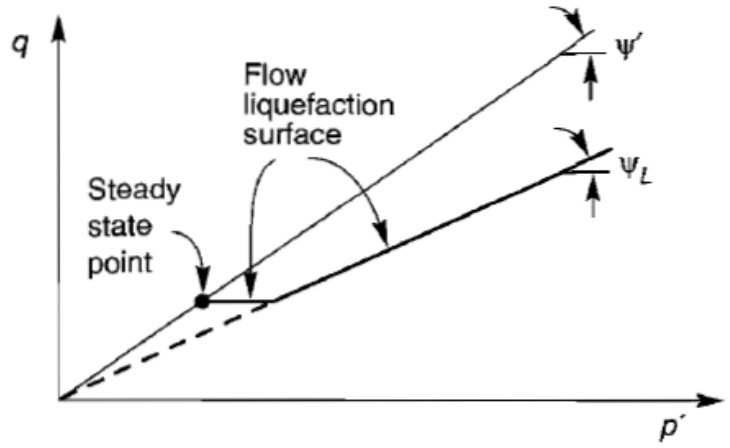

Figure 2-16 Truncated flow liquefaction surface in stress path space (Kramer, 1996)

The FLS is truncated since flow liquefaction cannot occur if the stress path is below the steady-state point, as shown in Figure 2-16.

2.7.2.1 Flow Liquefaction

If initial stress conditions of a soil fall within the shaded zone of Figure 2-17, flow liquefaction will occur if a strong undrained disturbance brings the effective stress path from the initial conditions to the FLS. Both monotonic (ABC) and cyclic (ADC) loadings may trigger the flow liquefaction as shown in Figure 2-18.

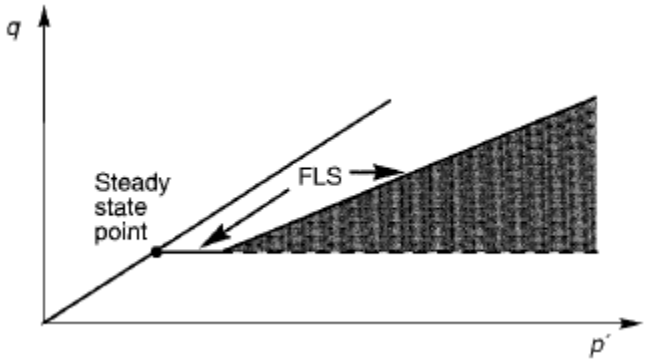

Figure 2-17 Zone of susceptibility to flow liquefaction (Kramer, 1996)

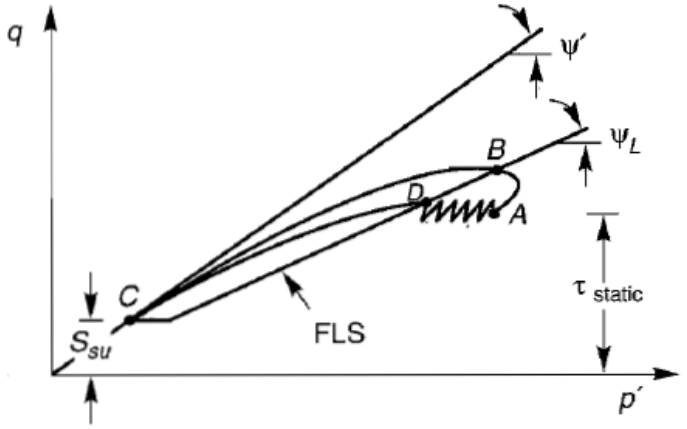

Figure 2-18 Zone of susceptibility to flow liquefaction (Kramer, 1996)

2.7.2.2 Cyclic Mobility

When the static shear stress is smaller than the steady state shear strength flow liquefaction cannot occur. However, cyclic mobility can occur even when the static shear stress is smaller than the steady state shear strength. If the initial stress state of a soil falls within the shaded zone of Figure 2-19, the soil is susceptible to cyclic mobility.

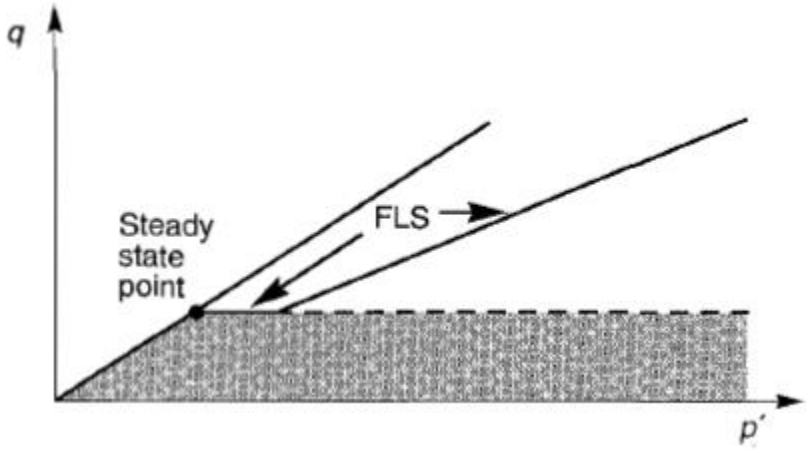

Figure 2-19 Zone of susceptibility to cyclic mobility (Kramer, 1996)

The susceptibility of soil to cyclic mobility can be investigated by cyclic triaxial or cyclic direct simple shear (CDSS) tests. Initial stress conditions and cyclic loading

conditions that might develop cyclic mobility can be divided into three cases as follows: i) no stress reversal ($\tau_{static} > \tau_{cyclic}$) and the total stresses are less than steady state strength ($\tau_{static} + \tau_{cyclic} < S_{su}$) as shown in Figure 2-20a; ii) no stress reversal ($\tau_{static} > \tau_{cyclic}$) and steady state strength is surpassed temporarily ($\tau_{static} + \tau_{cyclic} > S_{su}$) as shown in Figure 2-20b; iii) stress reversal occurs ($\tau_{static} < \tau_{cyclic}$) and steady state strength is not surpassed ($\tau_{static} + \tau_{cyclic} < S_{su}$) as shown in Figure 2-20c. In the third case, each time the effective stress path passes through the origin the specimen is in an instantaneous state of zero effective stress.

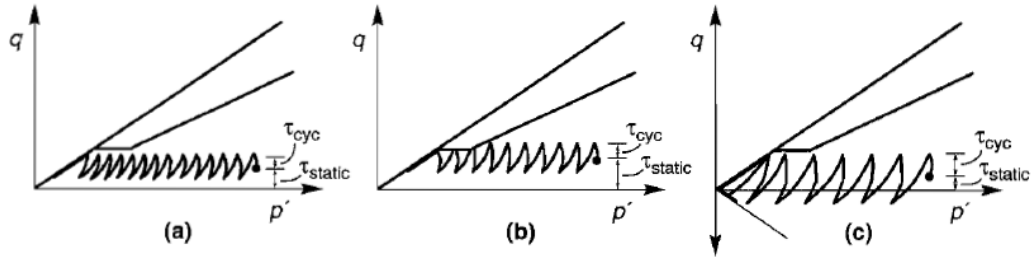

Figure 2-20 Three cases of cyclic mobility (Kramer, 1996)

The state at which the cyclic mobility initiates may not be as defined as that of the flow liquefaction. Permanent deformations take place during cyclic mobility to different extent depending on the static shear stress and the duration of the ground motion. Earthquakes are the main source of the ground motion that results in cyclic mobility. Additionally, liquefaction can be induced by other types of dynamic loads such as blasting or rock bursts.

2.8 Liquefaction Triggers

2.8.1 *Monotonic Loads*

The triggering mechanisms for the flow liquefaction are mainly change in the water level and/or the overloading (e.g. a rapid rate of loading). The change in water level

can cause reduction in mean effective stress, which can move the stress path toward the FLS (Martin&McRoberts, 1999).

2.8.2 *Dynamic Loads*

The main sources of dynamic loading in geotechnical engineering are shown in Figure 2-21. Earthquakes, rock bursts, and blasting are the main sources of dynamic loading in mining sites which may cause the uncemented tailings or the early-age CPB to liquefy.

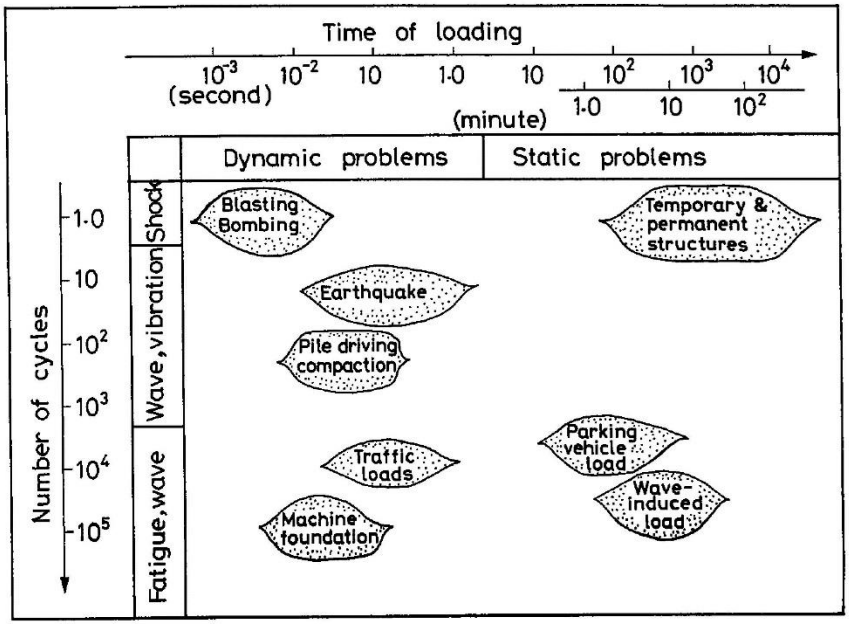

Figure 2-21 Classification of dynamic problems (Ishihara, 1996)

2.8.2.1 Simplified Procedure

For practical purposes, the liquefaction potential of a soil induced by an earthquake can be estimated by the cyclic stress ratio (CSR). The CSR for the direct simple shear test is defined as:

$$CSR = \frac{\tau_{cy}}{\sigma'_{vc}}$$

Where

τ_{cy}= cyclic shear stress

σ'_{vc}= effective vertical stress

This CSR induced by an earthquake can then be compared with the cyclic resistance ratio (CRR) of the soil that represents the liquefaction resistance of the in situ soil. The CRR can be determined in the laboratory or using in-situ testing (e.g., CPT). If the CSR caused by the anticipated earthquake exceeds the CRR, liquefaction is likely to be triggered.

2.9 Liquefaction Studies on Cemented Paste Backfill

The susceptibility of mine tailings to earthquake-induced liquefaction have been shown by several researchers (Al Tarhouni, 2008; Crowder, 2004; Dobry and Alvarez, 1967; Fourie and Papageorgiou, 2001; Garga and McKay, 1984; Ishihara et al., 1980; Okusa et al., 1980; Poulos et al., 1985). The mine tailings used in these studies range from sandy silts to silty sands. The contractive behavior of mine tailings resulting in static liquefaction has also been reported (Li et al., 2018). A full static liquefaction of silt-sized gold tailings at low confining pressures was demonstrated by Li et al. (2018). When clayey silt and silt mine tailings were loaded using simple shear test equipment the cyclic mobility type stress-strain response was observed (Wijewickreme et al., 2005).

Previous studies on the liquefaction potential of CPB have indicated that the response of CPB to monotonic loading in triaxial tests is dilative and CPB is not susceptible to static liquefaction (Aref, 1989; Been et al., 2002, le Roux et al., 2004; Saebimoghaddam, 2010). Been et al. (2002) investigated the critical state behavior of CPB samples collected from a trial stope at Neves Corvo mine. They performed a set of triaxial tests on undisturbed samples that had been placed and cured underground in the stope. The CPB specimens showed dilative behavior with no significant pore pressure development during monotonic loading. Saebimoghaddam (2010) made CPB specimens

using 3% PC and subjected the specimens after four hours to triaxial compression. He reported that the CPB specimens did not experience static liquefaction as shown in Figure 2-22.

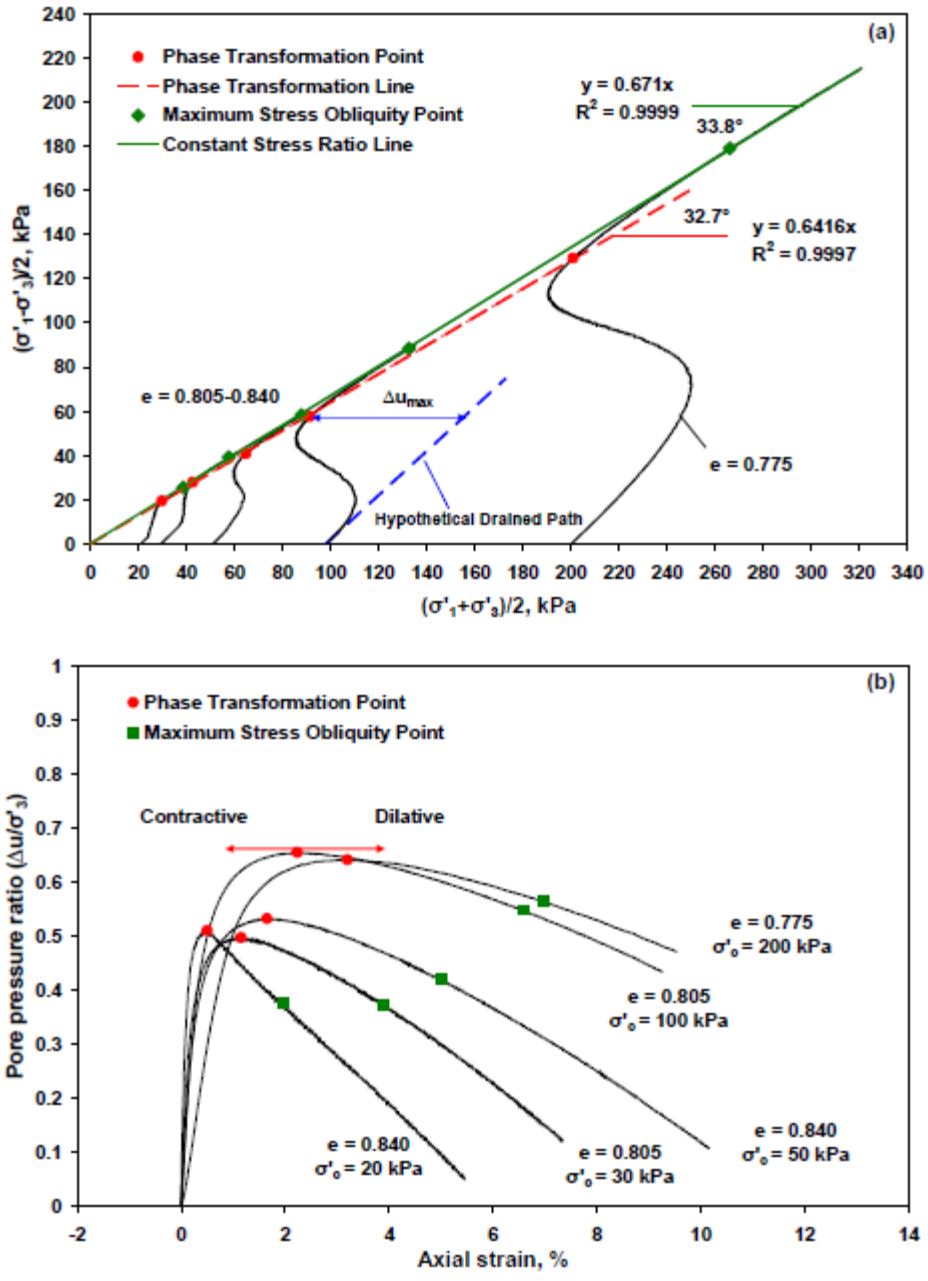

Figure 2-22 The monotonic compression response of CPB specimen, a) stress path, and b) pore pressure ratio versus axial strain (Saebimoghaddam, 2010)

Le Roux et al. (2004) made CPB specimens using 5% binder content with cement to fly ash ratio of 1:1 and subjected the specimens to monotonic and cyclic loading. They concluded the early-age CPB is unlikely to liquefy under monotonic loading; however, cyclic loading may cause cyclic liquefaction or large deformations. Suazo et al. (2016) evaluated the cyclic shear response of CPB made using various Portland cement contents and curing ages. They used a cyclic direct simple shear (CDSS) apparatus and applied different CSRs to the specimens. In addition to cyclic testing, they also performed the UCS testing to correlate the cyclic resistance ratios with the UCS results.

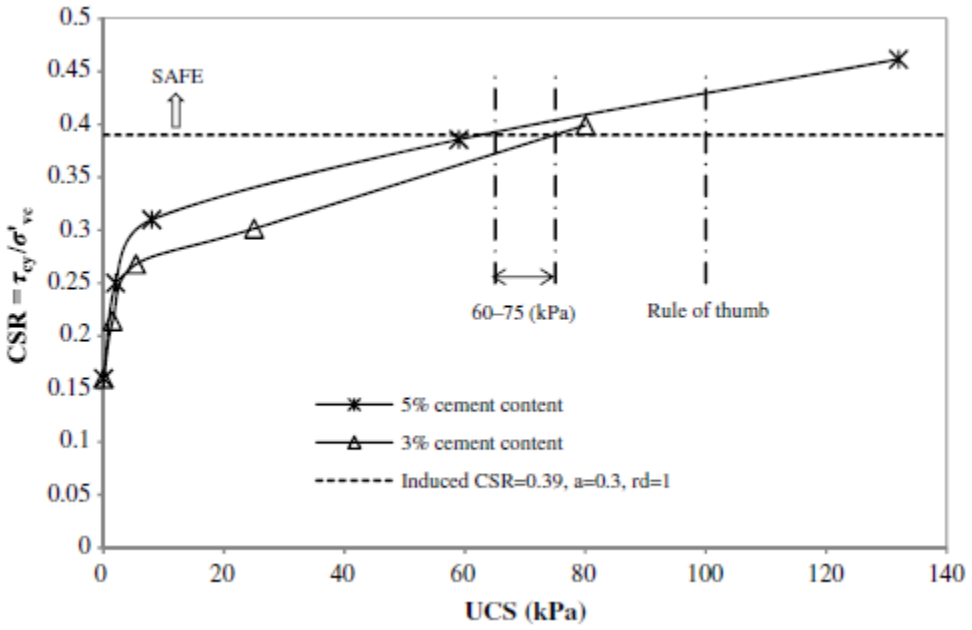

Figure 2-23 The Evolution of liquefaction resistance versus unconfined compressive strength over time for CPB specimens (Suazo et al., 2016)

Suazo et al. (2016) concluded that a UCS of approximately 70 kPa was found adequate to resist liquefaction under a CSR=0.39, a reasonable large value for most seismic regions as shown in Figure 2-23. For simplicity in comparing results under a

unique criterion, Suazo et al. used 10 equivalent cycles (N=10) to simulate earthquakes with a magnitude of 7 as determined by Idriss (1999) for clean sands.

2.10 Parameters Impacting the Liquefaction Behavior

The major factors affecting the liquefaction of silt-sized soils can be listed as follows: degree of saturation, void ratio and particle characteristics, and confining pressure. The effect of these factors will be reviewed in the following section.

2.10.1 *State of Saturation and Occluded Air*

The presence of occluded air bubbles in tailings and CPB has been reported by Fourie et al. (2001) and le Roux (2004). The presence of bubbles in tailings or CPB may increase the resistance against liquefaction. The contractive behavior of mine tailings was shown to be de$_{cr}$eased by the presence of bubbles (Fourie et al., 2001). The air bubbles in CPB may be entrapped during mixing, transport and placement processes (Grabinsky and Simms, 2006). However, the amount of gas (i.e., air or mostly nitrogen) dissolved in porewater is not significant in CPB due to low solubility of air in water.

2.10.2 *Relative Density and Particle Characteristics*

Relative density is one of the most important factors that may affect the liquefaction potential of soils (Lee and Seed, 1967). Loose sands and silts are more susceptible to liquefaction than dense sand because of the tendency of loose sand and silt to contract. The gradation also affects the liquefaction susceptibility of soils. Uniformly graded sands are shown to be most susceptible to liquefaction (Rischbieter, 1977; Prakash, 1981; Charlie et al., 1985a). Soil particle characteristics that influence liquefaction potential include roughness, roundness, and crushability. Angular to sub-angular sands are shown to be more stable than rounded sands (Fragaszy and Voss, 1981).

2.10.3 *Confining Stress*

Effective confining stress is known to be a major factor affecting the liquefaction potential of soils. The full static liquefaction has been shown to be possible only at low confining pressures (Li et al., 2018). The confining pressure will determine the position of the state of soil in reference to the critical state.

2.11 Constitutive modeling to predict the liquefaction of silts

Various constitutive models have been developed by researchers and engineers to predict the behavior of cohesionless soils, particularly the liquefaction behavior. Soils can have a broad range of void ratios. The constitutive behavior of soils is different at various void ratios. A functional soil constitutive model must explain the changes in soil behavior caused by changes in its void ratio. Critical State Soil Mechanics (CSSM) with its most famous model Cam Clay (Schofield & Wroth, 1968), in the form of its derivative Modified Cam Clay (Roscoe & Burland, 1968) is one framework that incorporates the effect of density.

The original critical state models such as Cam Clay or the other variants of Modified Cam Clay have been successful to explain the effect of void ratio on soil behavior, particularly for overconsolidation on clay strength; however, neither Cam Clay, nor the variants of Modified Cam Clay, dilate anything like actual dense soils. Also, original critical state models poorly predict the behaviors of loose sands and silts, particularly the liquefaction behavior.

The NorSand model was developed based on critical state soil mechanics for sand and incorporates seven non-dimensional parameters. It is an isotropic model based on the associated flow rule, capable of predicting unstable behavior of sands and silts in undrained loading, such as limited and full static liquefaction.

Constitutive models can be used to assess the impacts of liquefaction on earth structures. They are powerful tools to analyze whether liquefaction will be triggered, and if so whether the structure will be stable. Among various constitutive models have been developed, state-of-art liquefaction constitutive models of UBCSAND (Byrne et al., 1995; Beaty & Byrne, 1998; Beaty & Byrne, 2011) for dynamic liquefaction and NorSand (Jefferies, 1993; Jefferies and Been, 2016) for static liquefaction can be mentioned.

2.11.1 NorSand

NorSand was the first CSSM developed for sand and silt. Although NorSand was originally developed for sands, later it was shown that the model is also applicable to silts. NorSand is a plasticity model applicable to any soil in which particle to particle interactions are controlled by contact forces and slips rather than bonds (Jefferies & Been, 2016). Plasticity models comprises three items in general: (1) a yield surface; (2) a flow rule; and, (3) a hardening law.

NorSand constitutive model equations are summarized in Table 2-3. The variables and parameters in Table 2-4 are defined as follow:

ψ : state parameter

i: image condition on yield surface

λ: slope of CSL in e-ln(σ_m) space, a model parameter

$\bar{\sigma}_m$: mean effective stress (= p′ under triaxial conditions= $(\bar{\sigma}_1 + \bar{\sigma}_2 + \bar{\sigma}_3)/3$)

χ: dilatancy constant, a model parameter

tc: triaxial compression condition (θ = π/6)

M: critical friction ratio, a model parameter

N: volumetric coupling coefficient, a model parameter

Γ: reference void ratio on CSL, a model parameter

η: dimensionless shear measure as ratio of stress invariants $\eta = \bar{\sigma}_y/\bar{\sigma}_m$

H: plastic hardening modulus, a model parameter

θ: lode angle

D^P: plastic dilatancy, $\dot{\varepsilon}_v^p/\dot{\varepsilon}_q^p$

G: shear modulus, a model parameter

I_r: soil rigidity, $G/\bar{\sigma}_m$

ν: elastic Poisson's ratio, a model parameter

Table 2-5 Summary of NorSand (Jefferies & Been, 2016)

Aspect of NorSand	*Equations*
Internal model parameters	$\psi_i = \psi - \lambda \ln(\bar{\sigma}_{m,i}/\bar{\sigma}_m)$ where $\psi = e - e_c$ $\chi_i = \chi_{tc}/(1 - \chi_{tc}\lambda/M_{tc})$ $M_i = M(1 - \chi_i N\lvert\psi_i\rvert/M_{tc})$
Critical state	$e_c = \Gamma - \lambda \ln(\bar{\sigma}_m)$ and $\eta_c = M$ where… $M = M_{tc} - (M_{tc}^2/(3 + M_{tc}))\cos(3\theta/2 + \pi/4)$
Yield surface and internal cap	$\frac{\eta}{M_i} = 1 - \ln\left(\frac{\bar{\sigma}_m}{\bar{\sigma}_{m,i}}\right)$ with $\left(\frac{\bar{\sigma}_{m,i}}{\bar{\sigma}_m}\right)_{max} = \exp(-\chi_i\psi_i/M_{itc})$
Hardening rule	$\frac{\dot{\bar{\sigma}}_{m,i}}{\bar{\sigma}_{m,i}} = H\frac{M_i}{M_{itc}}\left(\frac{\bar{\sigma}_m}{\bar{\sigma}_{m,i}}\right)^2\left[\exp\left(\frac{-\chi_i\psi_i}{M_{tc}}\right) - \frac{\bar{\sigma}_{m,i}}{\bar{\sigma}_m}\right]\dot{\varepsilon}_q^p$
Stress–dilatancy	$D^p = M_i - \eta$
Elasticity	$I_r = \frac{G}{\bar{\sigma}_m}$ and ν = constant

Note that these equations are in general stress notation with $\bar{\sigma}_m = p'$.

2.12 Summary

The main constituents of CPB (i.e., mine tailings, binder agents) and their basic characteristics were reviewed in this chapter.

The strength development of CPB and the effective parameters on the strength gain in CPB were also reviewed. The microstructure evaluation shows that because of significantly higher water-to-binder ratio the hydration products in CPB do not fill the interstices between the solid particles to the degree that the hydration products fill the interstices in a concrete mixture. Also, in this chapter it was explained that the strength of CPB is governed by many factors including curing age, particle size distribution, particle shapes, binder type, density and void ratio, saturation, and pH value of water.

Based on the objectives of the thesis, the three aspects of the literature review that were investigated were: i) use of fly ash to improve the geotechnical properties of mine tailings, ii) liquefaction of mine tailings under monotonic and cyclic loading, iii) liquefaction of CPB under monotonic and cyclic loading, and IV) constitutive models available to predict the liquefaction of silts.

It was shown that the use of fly ash to improve the mechanical properties of mine tailings has not received enough attention. Some studies on the liquefaction behavior of silt-sized mine tailings and CPB were mentioned. The CPB specimens evaluated in literature for the liquefaction behavior mainly had Portland cement as the only binder agent (no SCM). The approach to evaluate the liquefaction behavior of CPB has been mostly testing the CPB using several individual triaxial tests. Individual triaxial tests have shown that CPB is not susceptible to static liquefaction. However, a more comprehensive framework of critical state soil mechanics has not been utilized to evaluate the static liquefaction behavior of CPB. A more comprehensive approach is necessary to understand why CPB specimens have shown dilative behavior, since the void ratios in

field conditions may vary from those of tested in the laboratory. The influence of fly ash on the CPB strength and susceptibility to cyclic mobility has not received enough attention.

Chapter 3

Laboratory Study

3.1 Test Materials

3.1.1 *Mine Tailings*

The mine tailings used in this study were collected from a confidential gold mine site in Canada. Samples were collected into 20 liter buckets and transported to Golder's Soil Laboratories in Lansing, Michigan.

The initial water content of tailings ranged from 11% to 28%, with no evidence of oxidation. A SEM image of test tailings is shown in Figure 3-1. The index properties of mine tailings, such as liquid limit, plasticity index, particle size distribution and specific gravity, were then determined.

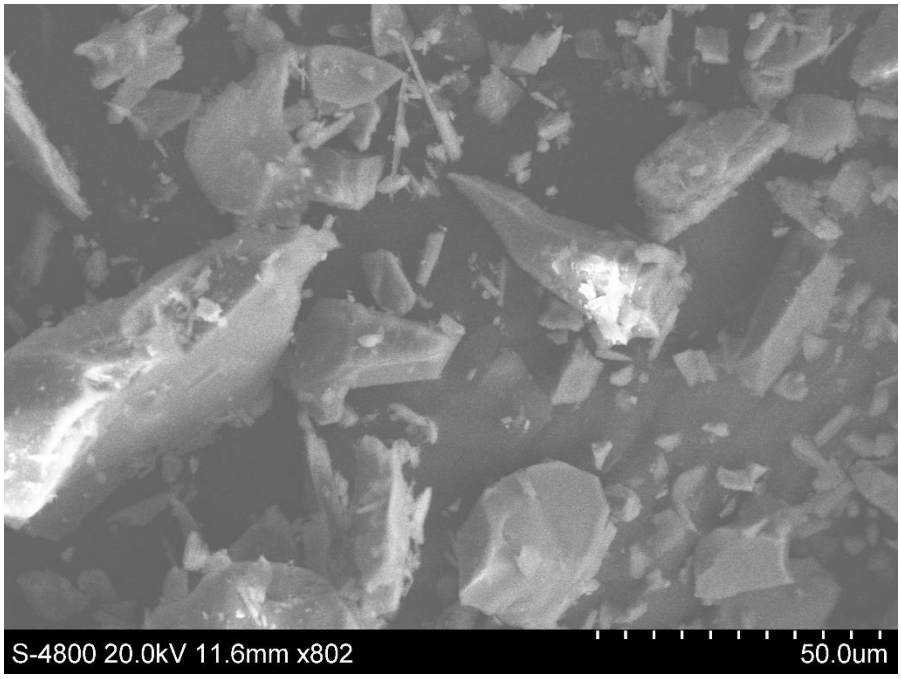

Figure 3-1 Microstructural image of gold mine tailings used in this study

The particle size distribution of the tailings was determined using the standard sieve analysis method (ASTM C136-14), followed by the standard hydrometer test (ASTM D422-63). The sieve analysis test was used to categorize the particles larger than 75 microns while the hydrometer test was used to determine the distribution of the particles smaller than 75 microns. Based on the sieve analysis, the mine tailing sample was classified as non-plastic silt (ML) with sand based on Unified Soil classification System (USCS). The pH of the tailings slurry collected was measured to be 8.8. The specific gravity of the tailings was determined to be 3.25 (ASTM D854-06e1). The percentage particles smaller than 20 microns is approximately 24%.

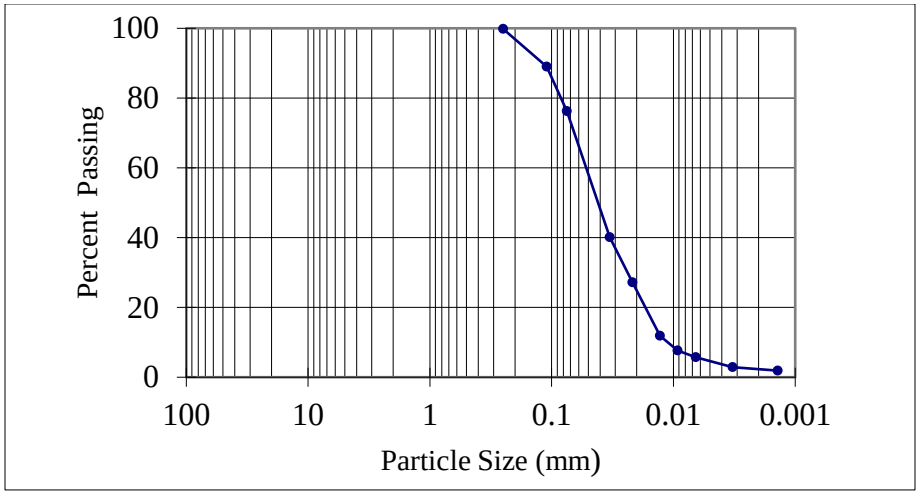

Figure 3-2 Particle size distribution of mine tailings used in this study

To determine the plastic limit (PL) of the tailings, the standard test method (ASTM D4318 – 05) was used. The tailings were determined to be non-plastic. The permeability of tailings was measured to be 1.5×10^{-4} centimeter/second using flexible wall triaxial permeability test (ASTM D5084). The coefficient of permeability of tailings was measured to be 2.6 $inch^2$/minute at the void ratio of 1.03.

The chemical composition of the tailings was determined using the X-Ray Fluorescence Spectroscopy (XRF) method and is shown in Table 3-1.

Table 3-1 XRF results of test tailings

Element	Oxide/Name	XRF %
Si	SiO2	52.6
Fe	Fe2O3	29.1
Al	Al2O3	8.5
Ca	MgO	3.53
Mg	CaO	3.84
H	K2O	0.87
Mn	TiO2	0.44
K	Na2O	0.34
Ti	P2O5	0.11
Na	V2O5	0.02
P	Cr2O3	0.03
V	MnO	0.44

The major compounds are SiO2 and Fe2O3. The X-ray diffraction (XRD) analysis used to identify the mineral components of the tailings showing that quartz and grunerite are the major minerals, as shown in Table 3-2.

Table 3-2. XRD results of test tailings

Composition	**S-Q% ***
Quartz	30.7
Grunerite	22.6
Chamosite	5.1
Biotite	7.9
Albite	--
Anorthite	11
Magnetite	1.1
Pyrope, ferroan	8.6
Diopside	3.8
Pyrrhotite	4.8
Pyrite	1.5
Jarosite	2.8
Thermonatrite	--

Note*: The semi-quantitative analysis of EVA is performed on the basis of relative peak heights and I/Icor values of those detected crystalline phases with PDF files. Amorphous or crystalline mineral species present in trace amounts may go undetected.

3.1.2 *Fly Ash*

Fly ash is a residual material produced in coal-fired power plants by burning pulverized coal in boilers to generate electricity. Fly ash is usually categorized into two main groups of class C fly ash and class F fly ash. Generally, class C fly ash contains more calcium oxide (CaO) than class F fly ash. In this study, a bulk sample of class C fly ash was collected from a coal power plant in Michigan, USA. The chemical composition

of the test fly ashe was measured using X-ray fluorescence (XRF), as presented in Table 3-3. The SEM image of fly Ash is shown in Figure 3-3.

Table 3-3. Chemical composition of Fly Ash by Percent Dry Mass Based on X-ray Fluorescence Analysis

Component %	**Class C Fly Ash**
Na_2O	1.76
MgO	4.61
Al_2O_3	18.94
SiO_2	41.98
P_2O_5	0.73
K_2O	0.72
CaO	20.28
TiO_2	1.1
MnO	0.02
Fe_2O_3	5.92
P.O.C.a	66.84
L.O.I.b	1.77

Note: Balance of chemical composition to 100% includes additional constituents not analyzed. P.O.C. (Primary Oxide Content) calculated as the sum of SiO_2, Al_2O_3, and Fe_2O_3. L.O.I. (Loss on Ignition) calculated as the percentage of weight loss after 2 hours at 900°C.

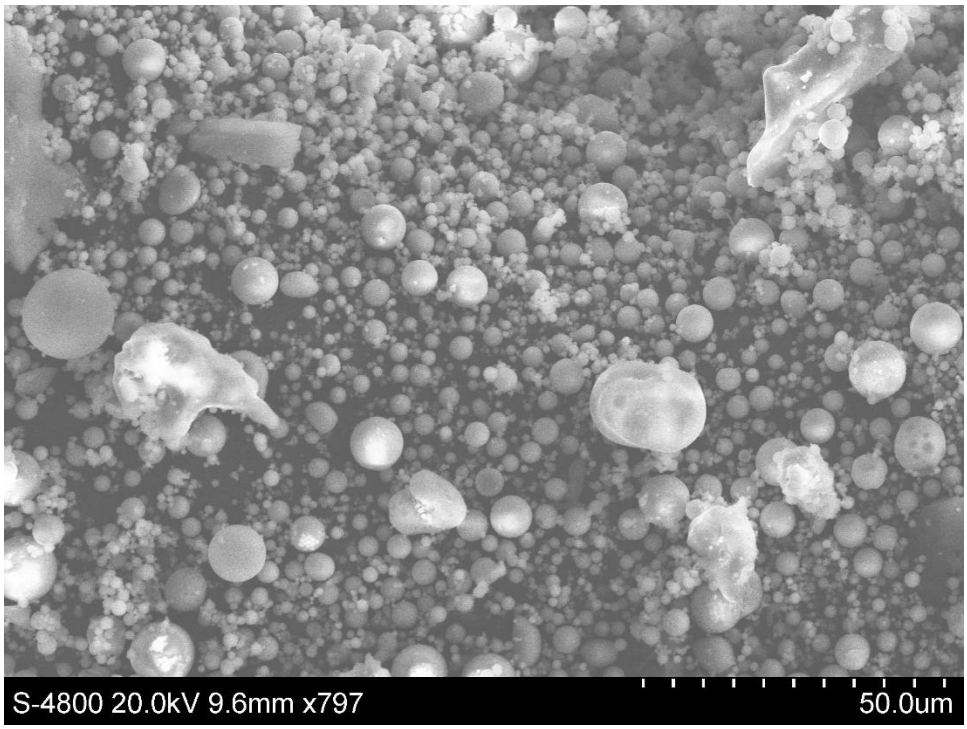

Figure 3-3 Microstructural image of fly ash used in this study

3.1.3 *Portland Cement*

Commercial Type I Portland cement by QUIKRETE® was used in this study. The product used meets the ASTM C 150 Type I requirement. An SEM image of Portland cement used in this study is shown in Figure 3-4.

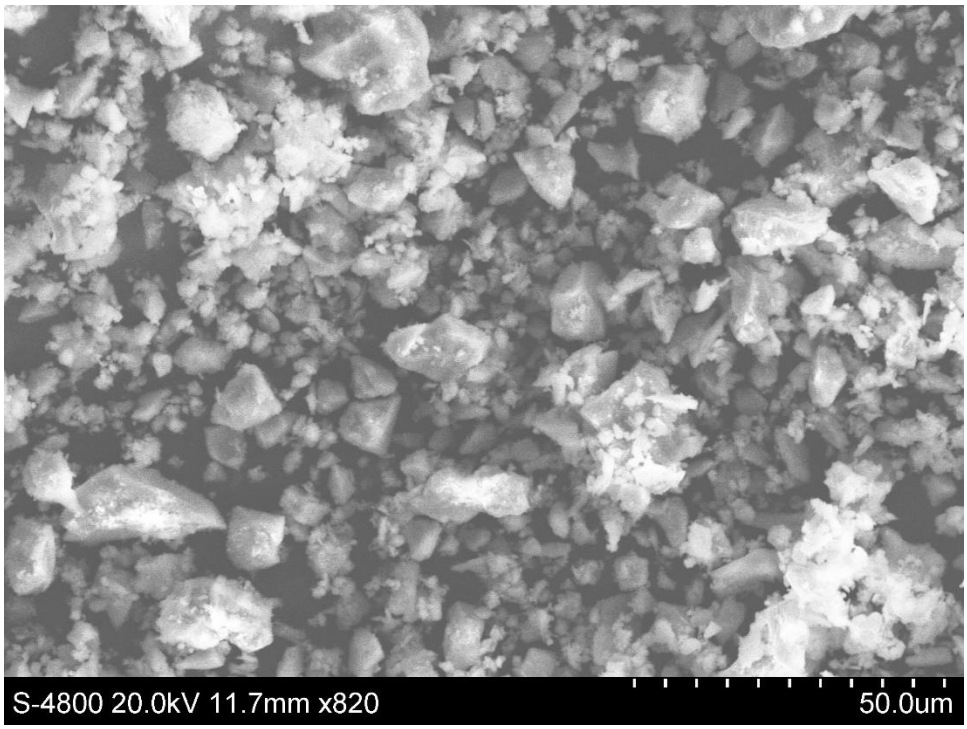

Figure 3-4 Microstructural image of Portland cement used in this study

3.2 Experimental Design and Procedure

The first stage of the experimental program was to evaluate the feasibility of using class C fly ash as a single binder agent to improve the mechanical properties of tailings using UCS testing. In addition to the application of class C fly ash as a single binder agent the influence of cement substitution with fly ash on the set time and the hardening process of CPB was also evaluated in this stage of the study.

Using the results from the first stage of the study, a select CPB recipe was used to prepare specimens for more advanced study of CPB. In the second stage of the experimental program CPB specimens were made for triaxial and CDSS testing.

Table 3-4. Typical tailings consistency (Bussiere, 2007)

Consistency	Solid Content (%)
Slurry	<50
Thickened Tailings	50-70
Paste Tailings	70-85
Filtered Tailings	>85

3.3 Unconfined Compressive Strength

The UCS tests were conducted in accordance with ASTM D5102 (ASTM, 2009). The specimens were mixed for approximately one minute using a rubber blade attached to an electric drill and poured into 1.87” diameter by 4” tall plastic water-proof molds as shown in Figure 3-5. To take the settling into account thickened tailings were poured into the molds to a higher level than the final height. The molds were sealed immediately after pouring the tailings in to prevent evaporation. The specimens were cured for 3 and 28 days at a temperature of 25°C. After specimens were cured they were extruded and trimmed to a height to diameter ratio of 2:1. All specimens extruded were wet and fully saturated as they were kept in sealed molds. The UCS tests were conducted at an axial strain rate of 2%/min using a GEOTAC Sigma-1 Automate Load Test System. The specimens were sheared to maximum 15% axial deformation.

Figure 3-5 a) Rubber blade attached to an electric drill, b) poured materials in mold, and c) tailings specimen in the UCS test setup

3.4 Monotonic Loading

The purpose of investigating the monotonic response of the uncemented mine tailings and the early-age CPB (i.e., 22 hours old) were to develop the critical state line of the tailings, and to determine the contractive or dilative behavior of the CPB at different effective stresses using the critical state approach. A set of drained and undrained triaxial tests were performed for this study. Fully saturated tailings and CPB specimens at the desired effective confining stress were subjected to a monotonic load using a constant strain rate under drained and undrained conditions. Most of the specimens were sheared to maximum 20% axial strain. Based on the permeability of the tailings undrained specimens were sheared at the axial strain rate of 20%/hour. Drained specimens were sheared at the axial strain rate of 5%/hour. The shearing phase of drained specimens took four hours. Based on the results of the Vicat needle tests provided in Chapter 4 the progress of the hydration in four hours for the select recipe used in triaxial testing is not

significant. Therefore, the mechanical behavior of specimens can be assumed consistent during the triaxial shearing phase.

3.4.1 *Triaxial Test Setup and Sample Preparation*

A servo-hydraulic triaxial machine designed by Geotechnical Test Acquisition & Control (GEOTAC) was used in this study as shown in Figure 3-6. The back saturation and consolidation phases were performed manually.

Figure 3-6 GEOTAC setup used in this study

Modified end platens in the triaxial setup were used as shown in Figure 3-7 and Figure 3-8 to obtain the monotonic triaxial responses(Jefferies & Been, 2016). The enlarged and lubricated end platens were used to allow free radial expansion of the specimen and minimize bulging deformation and oozing during shear (Jefferies & Been, 2016).

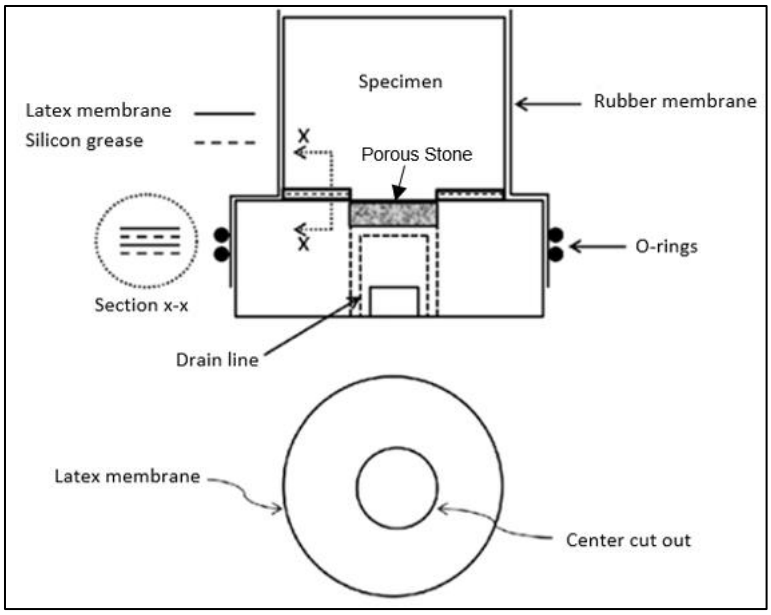

Figure 3-7 Modified end platen details in triaxial setup (Omar & Sadrekarimi, 2015)

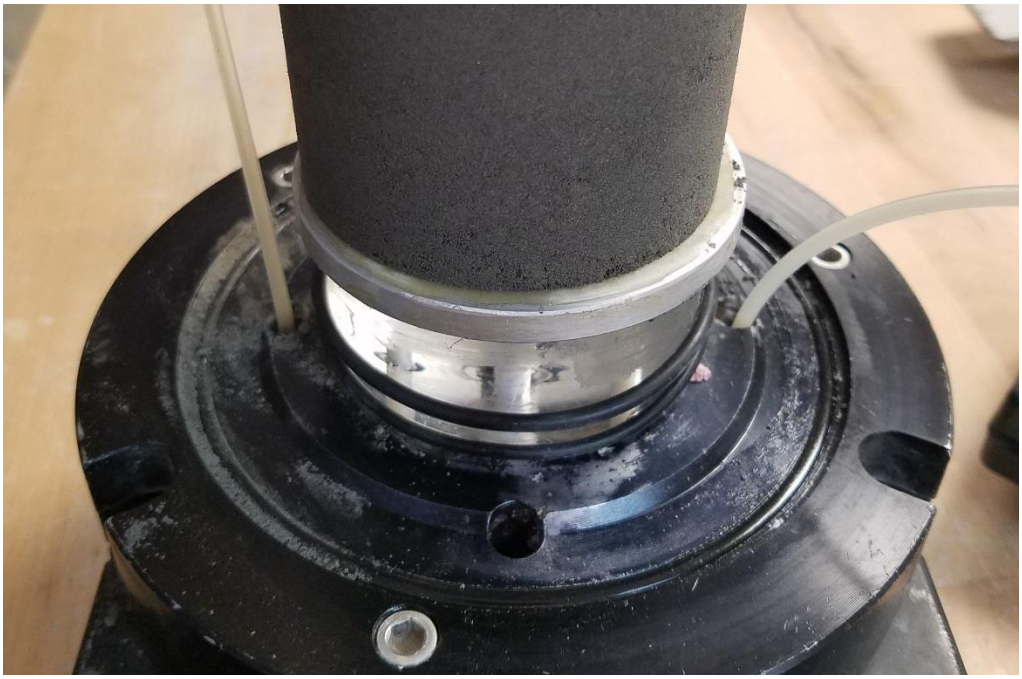

Figure 3-8 Specimen on top of the modified platen

To develop the critical state line of the tailings slurry deposition and moist tamp methods of sample preparation were utilized. There is no standard triaxial specimen preparation method for the paste material, which has a high water content and slump.

Moist tamp is a useful method of sample preparation for developing the critical state line since specimens with a broad range of void ratios can be prepared. The tailings sample with 10% moisture content was compacted in six lifts. The under-compaction method (Ladd, 1978) was used along with the moist tamp sample preparation method to achieve a uniform specimen with consistent density. For the specimens made using the moist tamp technique, the back-saturation process was expedited using the CO_2 percolation through the specimens. The back-saturation and consolidation stations are shown in Figure 3-9.

The liquefaction under monotonic loading is markedly affected by soil fabric and stress path to failure (Vaid & Thomas, 1995). The method of specimen preparation has been shown to determine the structure, or fabric, of the specimen. However, for the CSL determination, this is not a major concern. Samples reach the critical state only after the initial structure has been destroyed, and at that point, samples have a very different particle arrangement at large strain. The main concern for specimen preparation in the CSL testing is therefore that uniform samples are obtained at predetermined void ratios (Jefferies & Been, 2016).

Figure 3-9 Back-saturation and consolidation stations with the CO2 cylinder

Since the slurry deposited specimens are very loose with high water content previous researchers have used dead weight to consolidate the specimen before placing the specimen into the triaxial setup. The consolidation of specimens using the deadweight technique did not result in uniform specimens, therefore, a different method to set up the specimen was used in this study. First, the latex membrane was set up around the bottom platen and secured using typical O-rings. A temporary split mold made with a clear polyvinyl chloride (PVC) binding cover was placed on top of the bottom platen. The latex membrane was passed through the mold. The split mold was made with a vertical cut with two sides taped together. The other end of the tape was attached to the cell axial rod above the top platen. At the end of the back-saturation process and before the start of the consolidation phase the mold's tape was detached with the rotation of the

axial rod and the mold was completely separated at the vertical cut location. With this technique the loose specimen was held inside the temporary mold and consolidated uniformly inside the triaxial chamber under the cell pressure. A slurry deposited specimen was set up using the above technique and is shown in Figure 3-10.

Figure 3-10. Temporary mold made using a PVC binder cover

For the CPB specimens tailings with 10% moisture content were mixed with the binders. Then water was added to the mix to make the desired tailings consistency. A mixer with a rubber blade was used to blend the CPB mix for about two minutes before it was poured into the triaxial temporary mold. The back-saturation process of CPB specimens took three to four hours. The consolidation phase began immediately after the back-saturation phase. Because of high coefficient of permeability, the specimens experienced most of their consolidation within the first hour of the consolidation phase. Therefore, the influence of the consolidation process on the setting process is negligible.

By the end of a triaxial test, the sample is distorted and irregular in shape. Determining the void ratio using the height, diameter and axial strain measurement is likely to result in an inaccurate estimation of void ratio. Sladen and Handford (1987) suggest that the sample to be frozen while it is in the membrane with all valves closed. The frozen sample was then taken out and its water content be determined. The final void ratio of samples was computed using the water content of the sample, assuming 100% saturation and the measured specific gravity of the solids. This method is an accurate way of measuring the initial and final void ratio. For undrained tests, the initial void ratio (pre-shear) and final void ratios are the same. For drained tests, the initial void ratio can be calculated by adding or subtracting the change in volume during the test to the final void ratio.

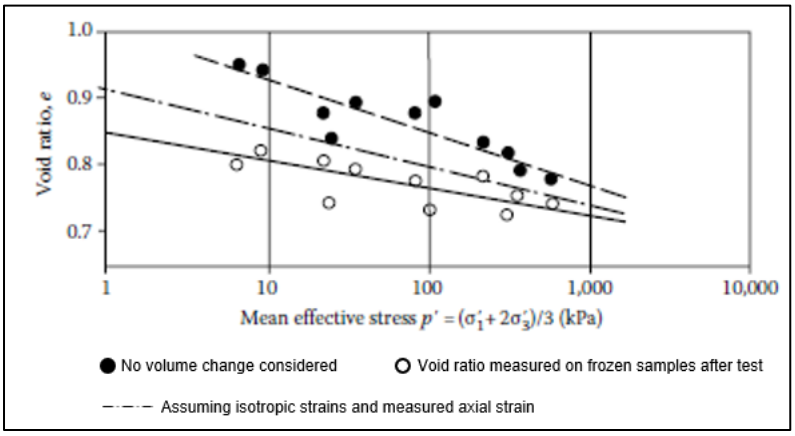

Figure 3-11. Potential error in void ratio if volume changes during saturation are not considered (Sladen & Hanford, 1987)

3.5 Cyclic Loading

The common practice to simulate earthquake loadings in the laboratory is to conduct cyclic tests using a simple direct shear or triaxial machine. The advantage of using the simple shear test over the triaxial test is to better represent the stress conditions due to vertically propagating S-waves induced by earthquakes. In other words,

the specimen in the direct simple shear test is directly subjected to cyclic horizontal shear stresses.

The input parameters for the cyclic tests include cyclic stress ratio (CSR) and the frequency of uniform load cycles as well as the effective vertical stress.

Like monotonic loading, the cyclic response of mine tailings mixtures with no binder should also be investigated to better understand the effect of binder agents on the behavior of the material.

3.5.1 *Cyclic DSS Test Setup and Sample Preparation*

The GDS Instruments (GDS) Electromechanical Dynamic Cyclic Simple Shear Device (EMDCSS) were used in this study to perform cyclic simple direct shear tests. This device is also called constant volume direct simple shear because, during shearing, the specimen height and diameter are kept constant in order to ensure constant volume conditions. The sample diameter was constrained using Teflon-coated stacked rings, whereas constant height was maintained by a vertical rod which prevented vertical displacements. Under these conditions, the change in total vertical stress recorded would be equivalent to the pore pressure. Subsequently, changes in pore pressures, or excess pore pressures, are presented based on measured changes in the total stress.

The slurry deposition method was adopted to prepare specimens for CDSS testing. The procedure involved mixing tailings, binders, and water to 78% solid content for a few minutes at low speed using a portable electric mixer. The mixture was gently poured into a latex membrane attached to a split vacuum mold with Teflon rings inside it. The membrane was stretched against the mold’s wall using a pump with a suction of approximately 30 kPa. Filter paper and porous stones were placed on both the bottom and top caps. Pre-consolidation static weights were placed on the specimen. When specimens were able to stand unsupported, weights were removed, vacuum was

stopped, the split mold was removed. The top cap was attached and secured to the latex membrane using O-rings. The sample preparation and the CDSS mold are shown in Figure 3-12.

During the cyclic loading phase, symmetrical sinusoidal shear pulses were applied at constant cyclic stress ratio amplitudes at a frequency of 0.1 Hz. The loading frequency of 0.1 Hz has been commonly used for the silty soils by previous researchers (Wijewickreme et al., 2005).

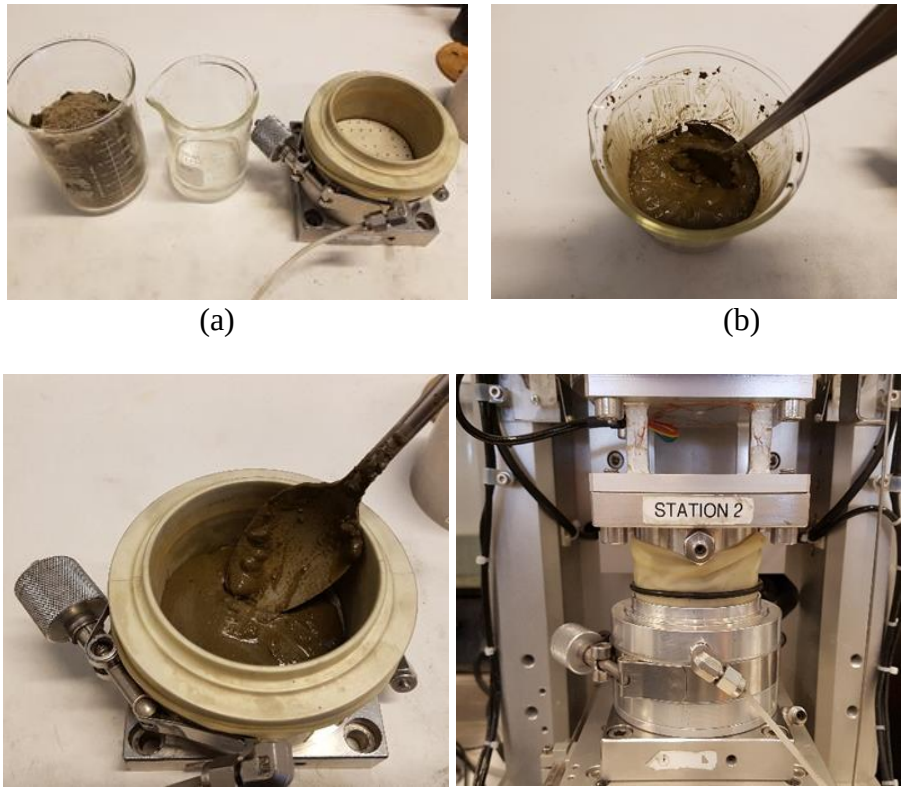

(a) (b)

(c) (d)

Figure 3-12. a) mixing the tailings or CPB specimen at 78% solid content and the test mold, b) prepared mixture, c) slurry specimen in the mold, and d) specimen in the test setup

Chapter 4

Unconfined Compressive Strength of Mine Tailings Amended with Fly Ash

Unconfined compressive strength tests were performed on the specimens of CPB made using different types of binders with varying amounts of each binder. Additionally, the application of fly ash for use as a single binder agent to improve the geotechnical properties of tailings was studied. CPB specimens were cured for up to 90 days. A summary of all UCS tests conducted during this study is presented in Table 4-1. To study the effects of PC partial replacement with fly ash baseline specimens were made using 3% PC. Then specimens with two different mix designs were made using 1.5% PC:1.5% FA and 1.5% PC:3.0% FA ratios.

To study the application of fly ash as a single binder agent to improve the geotechnical properties of tailings initial solid contents of 70% and 78% were used to evaluate the effect of the initial solid content (SC) on the unconfined compressive strength (UCS) of the tailings. The 70% solid content was used to evaluate the application for thickened tailings, or the surface disposal method. The 78% solid content was used to evaluate the application for paste tailings, or the underground backfilling. These solid contents were selected based on the rheological behavior of test tailings as shown in Figure 4-1. Pumping uncemented tailings or CPB at higher solid contents than those selected will be costly and may not be practical.

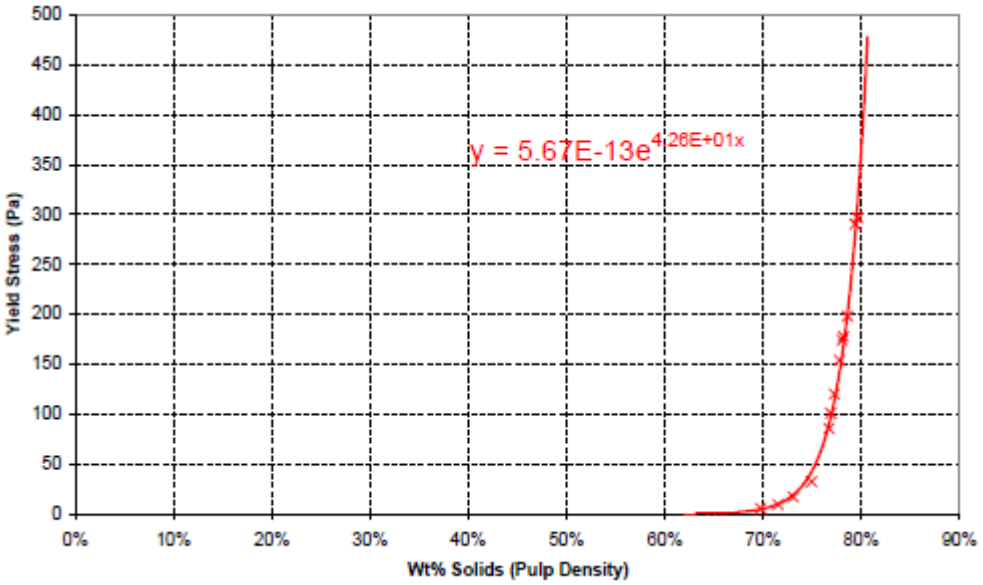

Figure 4-1.Solids content versus yield stress for the test tailings (Golder Associates, 2017)

Specimens were prepared by mixing tailings with 3% and 7% class C fly ash contents by dry mass and cured for up to 90 days. The summary of UCS testing is presented in Table 4-1.

Table 4-1 Summary of Unconfined Compressive Strength Tests Performed for This Study

Test ID.	SC* (%)	WC* (%)	PC* (%)	Class C Fly Ash (%)	Total Binder Content (%)	Water to Binder Ratio	Curing Time (days)	UCS (kPa)
78:1.5:1.5_3	78	28	1.5	1.5	3.0	9.4	3	137
78:1.5:1.5_28	78	28	1.5	1.5	3.0	9.4	28	169
78:1.5:1.5_90	78	28	1.5	1.5	3.0	9.4	90	282
78:1.5:3.0_0.9	78	28	1.5	3.0	4.5	6.3	0.9 (22Hrs)	78
78:1.5:3.0_0.9 TX*	78	28	1.5	3.0	4.5	6.3	0.9 (22Hrs)	92
78:1.5:3.0_3	78	28	1.5	3.0	4.5	6.3	3	178
78:1.5:3.0_28	78	28	1.5	3.0	4.5	6.3	28	221
78:1.5:3.0_90	78	28	1.5	3.0	4.5	6.3	90	306
78:3.0:0_3	78	28	3.0	None	3.0	9.4	3	164
78:3.0:0_28	78	28	3.0	None	3.0	9.4	28	314
78:3.0:0_90	78	28	3.0	None	3.0	9.4	90	327
78:0:7.0_3	78	28	None	7.0	7.0	4.0	3	41
78:0:7.0_90	78	28	None	7.0	7.0	4.0	90	109
70:0:10.0_3	70	42	None	10	10	4.3	3	0
70:0:10.0_28	70	42	None	10	10	4.3	28	0
70:0:10.0_90	70	42	None	10	10	4.3	90	0

Notes: * SC=Solid Content, WC=Water Content, PC=Portland Cement, TX=Triaxial preparation at 100 kPa confining pressure

4.1 Effect of Portland Cement Partial Replacement with Fly Ash on Setting Time

It is well known that the contribution of fly ash to the hydration and cementation process is more time consuming than that of Portland cement. Final setting time were assumed to be achieved when penetrations became limited and constant. CPB may not get as stiff as concrete, particularly at its early-age, since the binder to water ratio of CPB is significantly smaller than that of concrete.

Vicat needle test results indicated longer setting times for the 1.5%PC:3%FA sample comparing to setting times for the 3%PC sample. The initial setting time of 1.5%PC:3%FA and 3%PC samples were estimated to be 22 hours and 6 hours, respectively, based on Vicat needle test results as shown in Figure 4-2. The final setting time of 1.5%PC:3%FA and 3%PC samples were estimated to be 108 hours (4.5 days) and 31 hours, respectively, based on Vicat needle test results as shown in Figure 4-2.

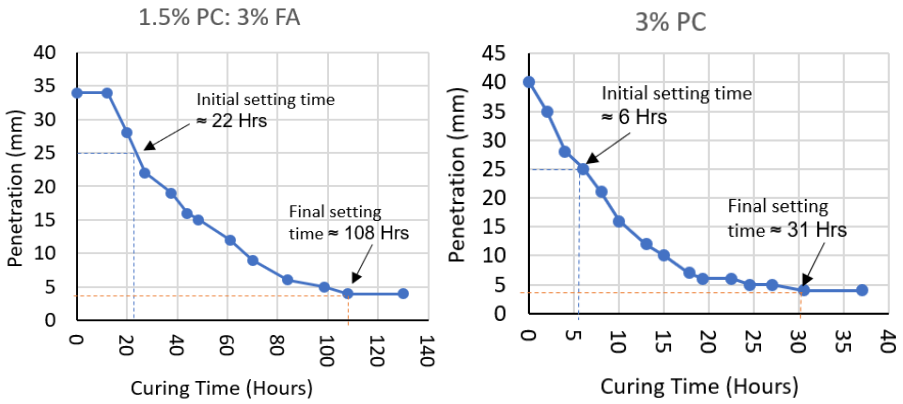

(a) (b)

Figure 4-2 Vicat needle test results for a) 1.5%PC:3%FA sample, and b) 3%PC sample

Based on the Vicat needle test results, reducing the PC amount to 1.5% (instead of 3%) increased the initial and final setting times by approximately 3.5 times. The longer

setting times of CPB with reduced PC should be considered for early-age assessment of CPB behavior.

4.2 The Results of Unconfined Compressive Strength Testing

4.2.1 *Partial Replacement of Portland Cement with Class C Fly Ash in CPB*

The results of UCS testing for specimens made using 3% PC and two different PC:FA ratios are shown in Figure 4-3. At 28 days, the specimens with 3% PC, 1.5% PC:3.0% FA and 1.5% PC:1.5% FA ratios yielded the UCS values of 314 kPa, 221 kPa, and 169 kPa, respectively. At 90 days the specimens with 3% PC, 1.5% PC:3.0% FA and 1.5% PC:1.5% yielded the UCS values of 327 kPa, 306 kPa, and 282 kPa, respectively.

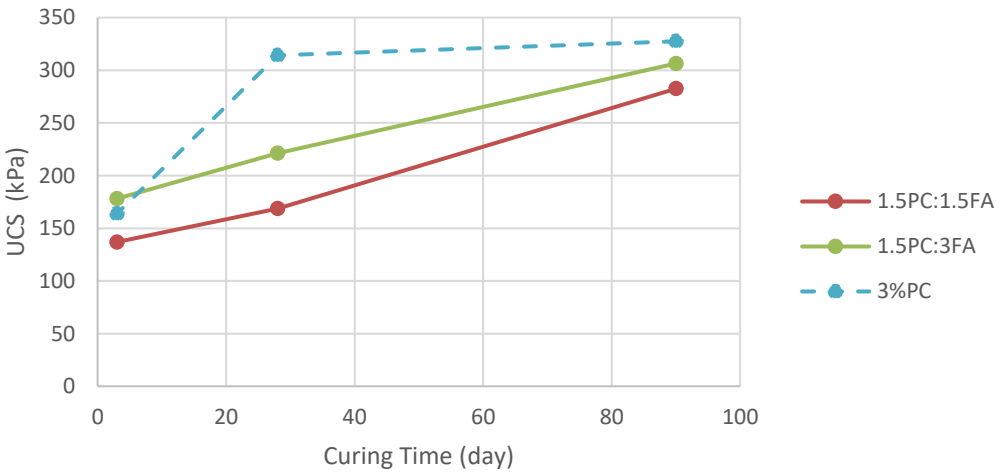

Figure 4-3 Summary of UCS results for specimens made using fly ash class C at 78% solid content

(a) (b)

Figure 4-4 Example photos of a) extruded CPB specimen, and

b) crushed UCS specimen

4.2.2 *Effect of Portland Cement Partial Replacement with Fly Ash on Hardening Process*

The UCS results indicate a slower hydration rate for the samples containing fly ash at the 3-day and 28-day curing time. For example, 90-day UCS values for the 3%PC and 1.5%PC:3%FA samples are 327 and 306 kPa, respectively, while 28-day UCS values for the 3%PC and 1.5%PC:3%FA samples are 314 and 221 kPa, respectively. The 28 day strength value for the 1.5%PC:3%FA was significantly smaller than that of 3%PC while the 90-day strength for the 1.5%PC:3%FA was slightly higher than that of 3%PC.

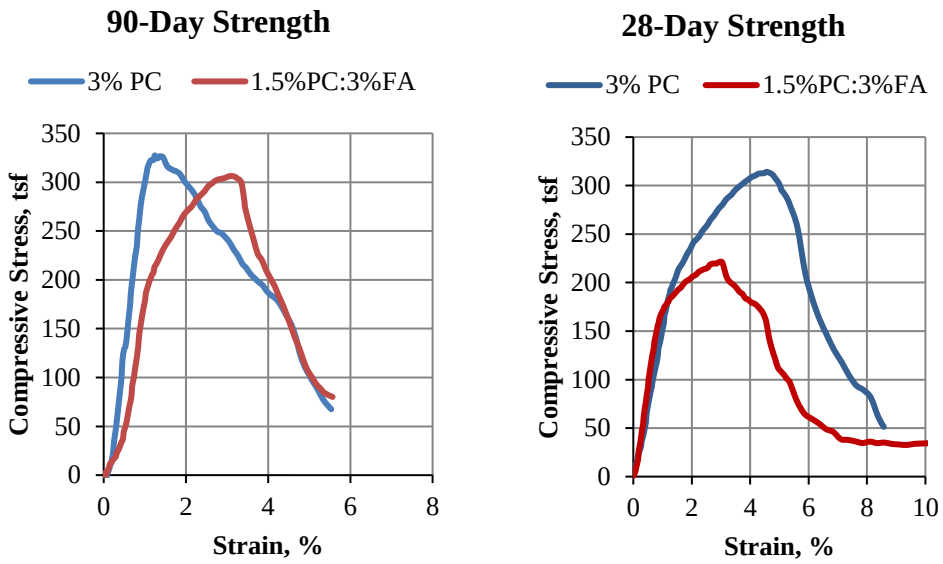

Figure 4-5 Effect of Portland cement partial replacement with fly ash on the hardening process

4.2.3 *Class C Fly Ash as a Single Binder Agent*

The use of fly ash as a single binder agent for surface disposal and underground backfilling applications was evaluated. The solid content of 70% used as an upper bound of solid contents for thickened tailings to evaluate the application of fly ash in the surface disposal method. The solid content of 78% used as an upper bound of solid contents for paste tailings to evaluate the application of fly ash in the surface disposal method.

4.2.3.1 Tailings Amended with Fly Ash at Thickened Tailings Consistency (SC=70%)

Specimens made using 70% initial solid content yielded no measurable UCS value. This result shows the importance of initial solid content. Adding 10% class C fly ash to tailings at 70% initial solid content (thickened tailings) did not improve the geotechnical properties within 28 days.

4.2.3.2 Paste Tailings Consistency (78% SC)

Specimens made at 78% initial solid content and 7% class C fly ash yielded measurable UCS as shown in Figure 4-6. The paste tailings amended with 7% fly ash by dry mass were cured for 90 days. The specimens yielded a 90-day UCS value of 109 kPa.

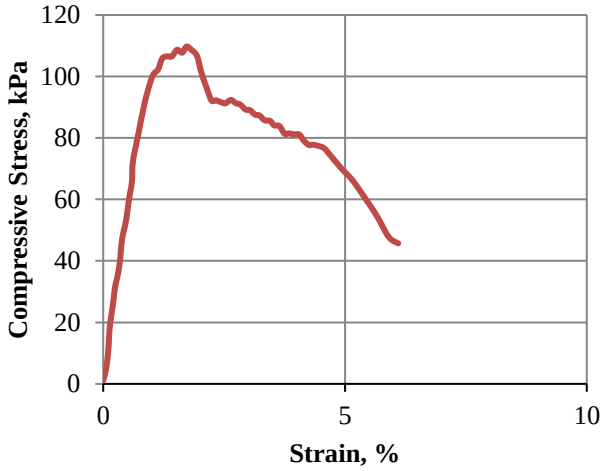

Figure 4-6 UCS of the specimen made at 78% initial solid content using 7% class C fly ash as the binder

4.3 Discussions on the UCS of Mine Tailings Amended with Fly Ash

The application of fly ash as a binder agent to improve the geotechnical properties of tailings was studied through UCS testing in this chapter. Based on the test results provided in this chapter, class C fly ash can be used with or without Portland cement to improve the geotechnical properties of mine tailings at the paste consistency. The class C fly ash was also used to prepare specimens at the thickened tailings consistency to evaluate the application for tailings surface disposal. The specimens made at the thickened tailings consistency (70%) yielded no measurable UCS because of the

low binder to water ratio. The binder content used in this study was 10% by dry mass as the typical upper bound for binder content in ground improvement.

For the paste consistency, the test results indicated that fly ash has applications both as a single binder agent or in combination with Portland cement to make CPB. The Vicat needle test results indicated the partial replacement of PC with fly ash increases the initial and final setting times. However, fairly similar 90-day strength values were obtained when 1.5% PC was replaced with 3% class C fly ash. The bulk price for fly ash varies; however, it is usually significantly cheaper than PC.

In addition to the use of fly ash along with Portland cement, the use of fly ash as a single binder agent was evaluated. The use of 7% class C fly ash yielded the UCS of 109 kPa in 90 days, which is higher than the cyclic mobility resistance criterion of 60-75 kPa for most seismic regions (Suazo et al., 2017). The 3-day UCS strength of the specimen with 7% class C fly ash was obtained to be 41 kPa which indicates the likelihood of liquefaction during a large earthquake. The slow strength gain of the CPB made with class C fly ash instead of PC needs to be considered when the CPB mix is designed.

4.4 Summary and Conclusions

1. class C fly ash can be used to replace a significant portion of Portland cement (PC) in CPB. The replacement of PC with class C fly ash is expected to result in a cheaper mix design as fly ash tends to be less expensive than PC. Fairly similar UCS values were obtained for 3%PC and 1.5%PC:3%FA specimens.
2. The replacement of PC with fly ash will increase the initial and final setting times of CPB. The reduction of PC to half and the addition of class C fly ash increased the initial and final setting times by approximately 3.5 times.

3. The contribution of fly ash to the CPB strength gain takes more time than the contribution of PC to the strength gain. The CPB specimens made with PC gained most of the strength in 28 days. When the PC content reduced to half and replaced with fly ash the specimens kept gaining strength between 28 days and 90 days.
4. The application of fly ash as a single binder agent to improve the geotechnical properties of tailings for the surface disposal method was evaluated. The addition of 10% class C fly ash to the thickened tailings (SC=70%) did not improve the geotechnical properties of the tailings.
5. The application of fly ash as a single binder agent to improve the geotechnical properties of tailings for the backfilling purposes was evaluated. The addition of 7% class C fly ash to the paste tailings (SC=78%) indicated improvement in the geotechnical properties of the tailings. The specimen made with 7% class C fly ash content yielded a 90-day UCS value of 109 kPa.

Chapter 5

Monotonic Triaxial Test Results

The main purpose of performing monotonic triaxial tests was to evaluate the critical state behavior of uncemented tailings and the CPB. The study of uncemented tailings and early-age CPB critical state behaviors would provide a basis to predict the early-age CPB field behavior. Conventional strain-controlled isotropically consolidated undrained (CU) and isotropically consolidated drained (CD) tests using uncemented and cemented specimens were performed to evaluate the critical state behavior of gold mine tailings and the CPB. The uncemented specimens were made at initially loose and dense conditions using moist tamp and slurry deposition methods. The laboratory test program was designed to evaluate the behavior of uncemented tailings for a range of initial positive and negative state parameters. The triaxial tests performed included specimens with initial void ratios lower than the critical void ratio (negative state parameter), higher than the critical void ratio (positive state parameter) as well as initial void ratios equal to the critical state void ratio (state parameter equal to zero). The state parameters of the CPB specimens tested were negative. The positive state parameter for the CPB specimens using the slurry deposition method could not be achieved due to the arrangement of mine tailings and binder particles in this method. A summary of triaxial tests were performed for this study is shown on Table 5-1. In this study the mean effective stress (p') and deviator stress (q) are defined as follows:

$$p' = \frac{\sigma_1' + 2 \times \sigma_3'}{3}$$

$$q = \sigma_1' - \sigma_3'$$

Where:

σ_1' and σ_3' = Major and minor principal stresses, respectively.

The back-saturation of CPB specimens and achieving a B parameter of 0.95 or higher completed in approximately four hours. The consolidation phase of the triaxial testing was started immediately after the saturation phase. There was no concern regarding the hydration of the CPB prior to consolidation since more than 98% of consolidations takes place in five minutes. To verify that the triaxial test procedure has no adverse impact on the strength gain of CPB, a trial triaxial specimen was made and subjected to UCS testing at 22 hours. The trial specimen (UCS test ID=78:1.5:3.0_0.9 TX) was made like the UMT-CU-0.99 specimen using the confining pressure of 100 kPa. The specimen was removed from the triaxial chamber and the latex membrane and was placed in the loading frame. The test yielded a UCS of 92 kPa, which confirmed that the triaxial test procedure has no adverse impact on the hydration and the initial setting time of CPB.

Table 5-1. Summary of monotonic triaxial tests performed for this study

Test ID.	Mode	Sample Preparation Method	Binder	Solid Content at Preparation (%)	Water Content at Preparation (%)	Pre-shear Void Ratio	Confining Stress (kPa)	Curing Time (Hours)
UMT-CU-1.03	Undrained	Moist Tamp	-	90	11	1.03	50	-
UMT-CU-0.99	Undrained	Moist Tamp	-	90	11	0.99	100	-
UMT-CU-0.94	Undrained	Moist Tamp	-	90	11	0.94	200	-
UMT-CU-0.86	Undrained	Moist Tamp	-	90	11	0.86	400	-
UMT-CU-0.79	Undrained	Moist Tamp	-	90	11	0.79	100	-
UMT-CU-0.87	Undrained	Moist Tamp	-	90	11	0.87	200	-
UMT-CU-0.84	Undrained	Moist Tamp	-	90	11	0.84	200	-
UMT-CU-0.70	Undrained	Slurry Deposition	-	78	28	0.7	100	-
UMT-CU-0.66	Undrained	Slurry Deposition	-	78	28	0.66	400	-
UMT-CU-0.86	Undrained	Moist Tamp	-	90	11	0.86	250	-
UMT-CD-0.99	Drained	Moist Tamp	-	90	11	0.99	100	-
UMT-CD-0.87	Drained	Moist Tamp	-	90	11	0.87	200	-
UMT-CD-0.76	Drained	Moist Tamp	-	90	11	0.76	100	-
UMT-CD-0.75	Drained	Moist Tamp	-	90	11	0.75	200	-
UMT-CD-0.77	Drained	Moist Tamp	-	90	11	0.77	300	-
UMT-CD-0.71	Drained	Slurry Deposition	-	78	28	0.71	100	-
CMT-CU-0.71	Undrained	Slurry Deposition	1.5%PC:3%FA	78	28	0.71	100	22
CMT-CU-0.69	Undrained	Slurry Deposition	1.5%PC:3%FA	78	28	0.69	400	22
CMT-CD-0.71	Drained	Slurry Deposition	1.5%PC:3%FA	78	28	0.71	100	22
CMT-CD-0.67	Drained	Slurry Deposition	1.5%PC:3%FA	78	28	0.67	300	22
CMT-CD-0.66	Drained	Slurry Deposition	1.5%PC:3%FA	78	28	0.66	400	22

Notes: UMT= uncemented mine tailings, CMT= cemented mine tailings, CU= consolidated undrained, CD= consolidated drained

5.1 Triaxial Test Results and Discussion for Mine Tailings Without Binder

Triaxial tests at various conditions were successfully performed to develop the critical state line (CSL) for gold mine tailings and the CPB. The summary of triaxial test results is shown on Table 5-2. Plots of stress-strain curves, stress paths, change in pore pressure versus axial strain, volumetric strain versus axial strain, and the critical state line in the e-log p' plane are shown in Figure 5-2 through Figure 5-6, respectively. The triaxial test results will be discussed in the following sections.

5.1.1 *Monotonic Behavior of the Mine Tailings Based on State Parameter*

Jefferies and Been (2006) suggested that coarse-grained ideal soils with a state parameter smaller than –0.05 tend to dilate at large strains when loaded in drained shear. Hence, coarse-grained saturated ideal soils with a state parameter smaller than –0.05 will tend to generate a reduction in pore pressure and increase in effective stress at larger strains in undrained shear and tend to be strain hardening.

In this study specimens with a state parameter of -0.05 or smaller experienced dilation at large strains resulting in strain hardening behavior, which is consistent with the Jefferies and Been's (2016) findings. UMT-CU-0.79, UMT-CU-0.70, UMT-CU-0.66, UMT-CD-0.76, UMT-CD-0.75, UMT-CD-0.77, and all CMT specimens had a state parameter smaller than -0.05 ($e<e_{cr}$) and indicated dilative behavior at large strains.

UMT-CU-1.03, UMT-CU-0.99, UMT-CU-0.94, UMT-CU-0.86, UMT-CD-0.99 and UMT-CD-0.87 with state parameters higher than 0.03 ($e>e_{cr}$) experienced contraction at large strains resulting in strain softening behavior. Loose specimens with $e>e_{cr}$ did not form shear planes and do not have the tendency to localization that is common in the dilative specimens as shown in Figure 5-1. The contractive specimens were made using the moist tamp preparation method. Despite several attempts, contractive specimens

could not be prepared using the slurry deposition method due to the arrangement of solid particles.

UMT-CU-0.87, UMT-CU-0.84, and UMT-CU-1.030 have a state parameter of zero or nearly zero ($e \approx e_{cr}$). The behavior of these three specimens was different from that of other loose specimens with state parameters higher than 0.03.

Based on the test results it is evident that the state parameter is a robust methodology to predict the behavior of silt-sized non-plastic mine tailings. In the following sections, the behavior of specimens at various state parameter conditions will be described.

UMT-CD-0.99 UMT-CD-0.76

Figure 5-1 Post-shear pictures of loose (UMT-CD-0.99) and dense (UMT-CD-0.76) specimen

Table 5-2. Summary of monotonic triaxial test results

Test ID.	Pre-shear void ratio (e_i)	Final void ratio (e_f)	p_i' [1] (kPa)	p_f' [2] (kPa)	q_f [3] (kPa)	Critical void ratio, e_{cr}	State Parameter, Ψ	Behavior at large strain	Initial State	Reached CSL?	Final Axial Strain
UMT-CU-1.03	1.03	1.03	50	0	0	0.90	0.13	Loose	$e>e_{cr}$	Yes	20%
UMT-CU-0.99	0.99	0.99	100	10	6	0.87	0.12	Loose	$e>e_{cr}$	Yes	20%
UMT-CU-0.94	0.94	0.94	200	25	13	0.84	0.10	Loose	$e>e_{cr}$	Yes	20%
UMT-CU-0.86	0.86	0.86	400	142	95	0.8	0.06	Loose	$e>e_{cr}$	Yes	24%
UMT-CU-0.79	0.79	0.79	100	405	289	0.87	-0.08	Dense	$e<e_{cr}$	Yes	20%
UMT-CU-0.87	0.87	0.87	200	118	87	0.84	0.03	~Critical	$e\approx e_{cr}$	Yes	20%
UMT-CU-0.84	0.84	0.84	200	180	128	0.84	0.00	~Critical	$e\approx e_{cr}$	Yes	20%
UMT-CU-0.70	0.70	0.70	100	384	287	0.87	-0.17	Dense	$e<<e_{cr}$	Unidentifiable	20%
UMT-CU-0.66	0.66	0.66	400	674	501	0.8	-0.14	Dense	$e<<e_{cr}$	Unidentifiable	20%
UMT-CU-0.86	0.86	0.86	250	142	99	0.84	0.02	~Critical	$e\approx e_{cr}$	Yes	20%
UMT-CD-0.99	0.99	0.86	100	171	110	0.87	0.12	Loose	$e<e_{cr}$	No	20%
UMT-CD-0.87	0.87	0.80	200	382	276	0.84	0.03	Loose	$e<e_{cr}$	Yes	20%
UMT-CD-0.76	0.76	0.79	100	204	155	0.87	-0.11	Dense	$e<e_{cr}$	Yes	20%
UMT-CD-0.75	0.75	0.76	200	393	289	0.84	-0.09	Dense	$e<e_{cr}$	No	20%
UMT-CD-0.77	0.77	0.75	300	588	432	0.82	-0.05	Dense	$e<e_{cr}$	No	20%
UMT-CD-0.71	0.71	0.72	100	207	320	0.87	-0.16	Dense	$e<e_{cr}$	No	20%
CMT-CU-0.71	0.71	0.71	100	476	355	0.87	-0.16	Dense	$e<<e_{cr}$	Unidentifiable	20%
CMT-CU-0.69	0.69	0.69	400	822	604	0.8	-0.11	Dense	$e<<e_{cr}$	Unidentifiable	20%
CMT-CD-0.71	0.71	0.77	100	211	162	0.87	-0.16	Dense	$e<e_{cr}$	No	20%
CMT-CD-0.67	0.67	0.68	300	555	381	0.82	-0.15	Dense	$e<e_{cr}$	No	30%
CMT-CD-0.66	0.66	0.66	400	782	572	0.8	-0.14	Dense	$e<e_{cr}$	No	26%

Notes: 1. pi' =initial mean effective stress

2. pf'= mean effective stress at critical state, or at maximum axial strain when critical state was not reached.

3. qf= deviator stress at critical state, or at maximum axial strain when critical state was not reached.

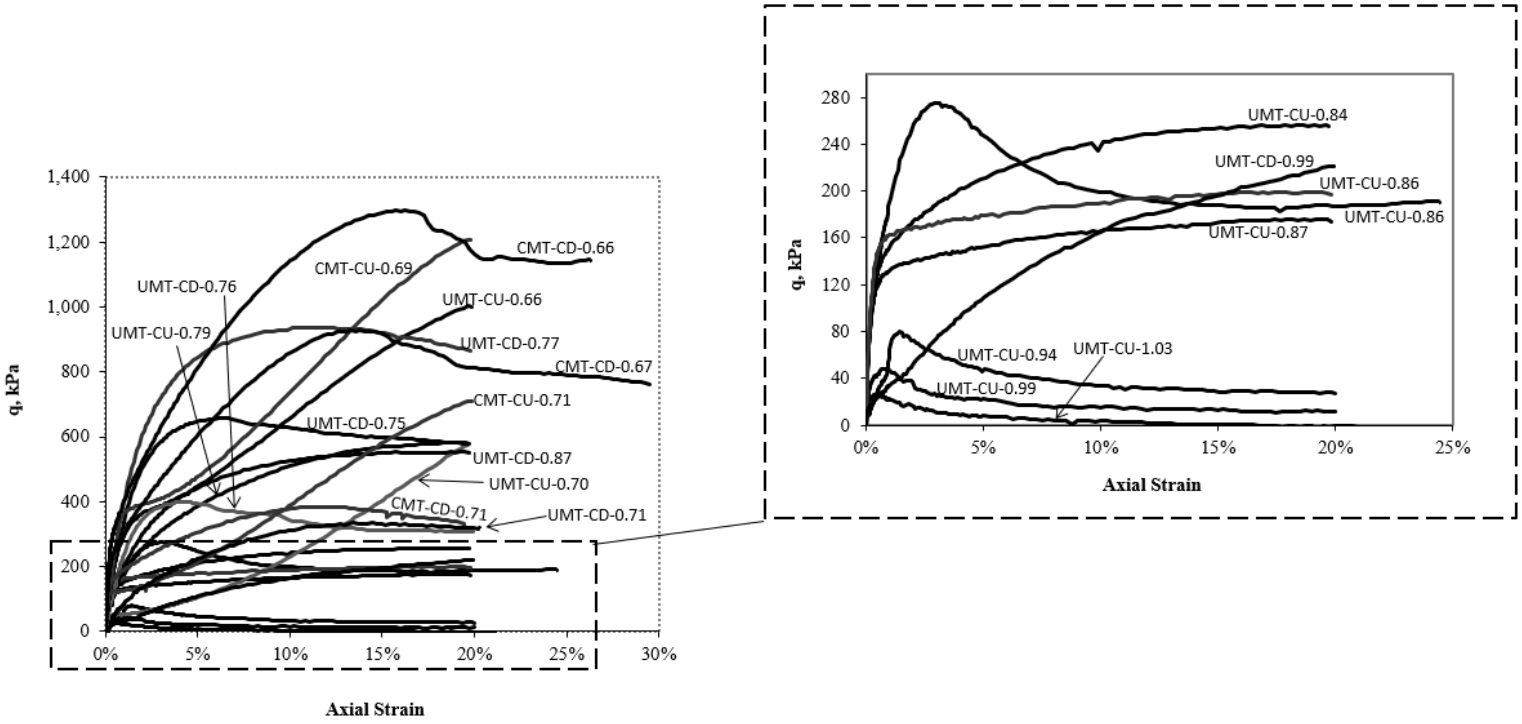

Figure 5-2 Stress-strain curves for all triaxial tests

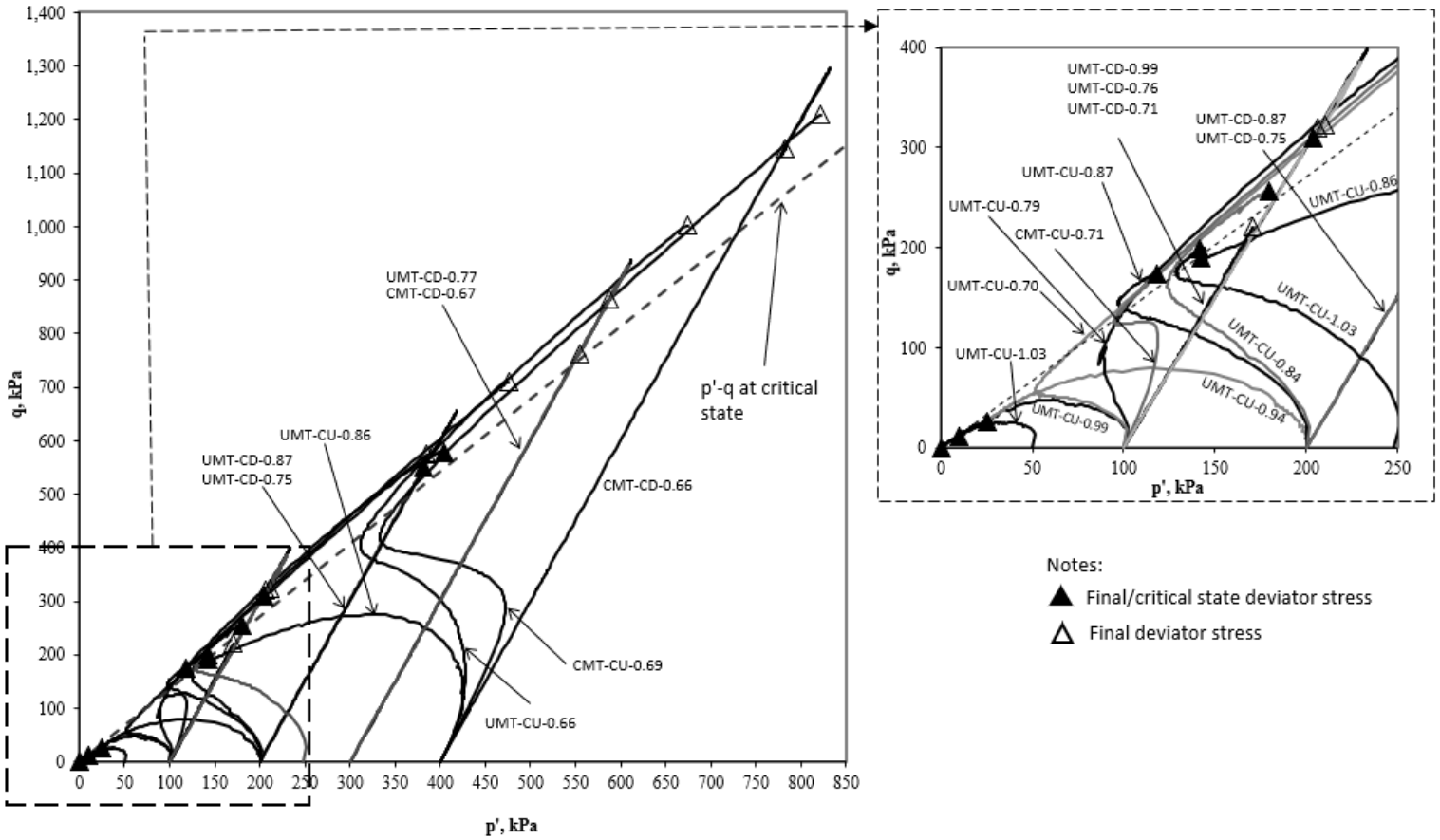

Figure 5-3 Stress paths for all triaxial tests

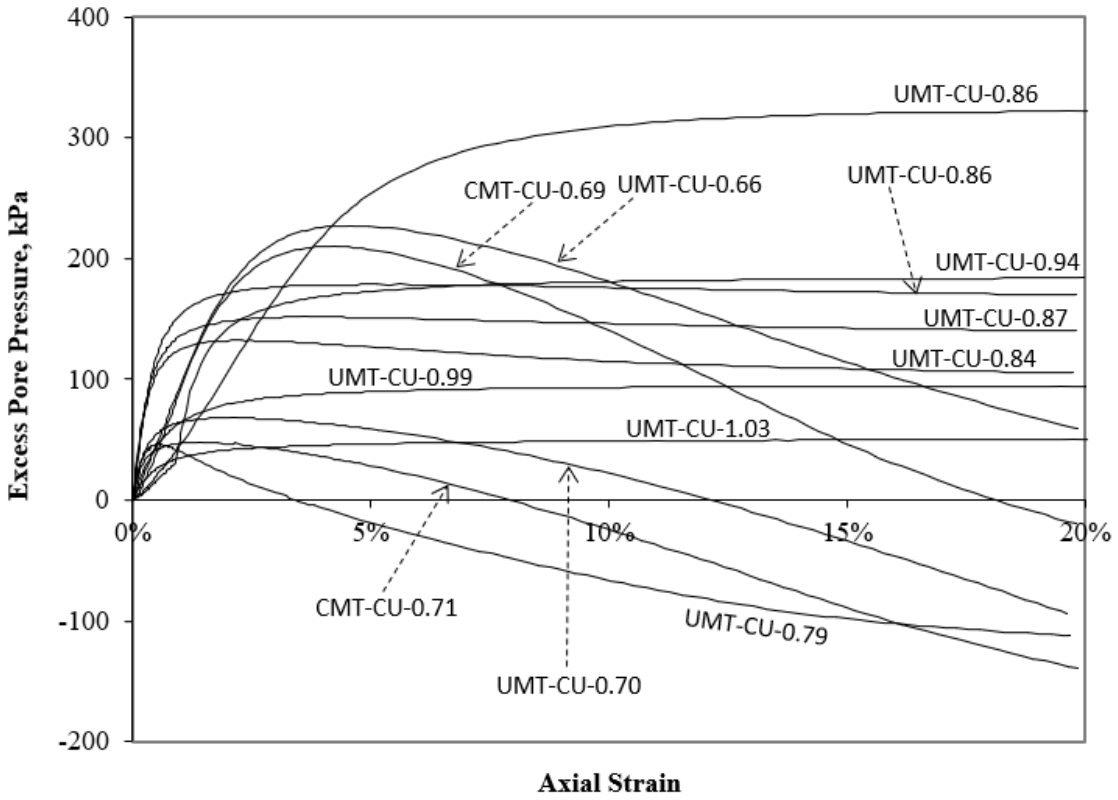

Figure 5-4 Change of porewater pressure versus axial strain for all triaxial tests

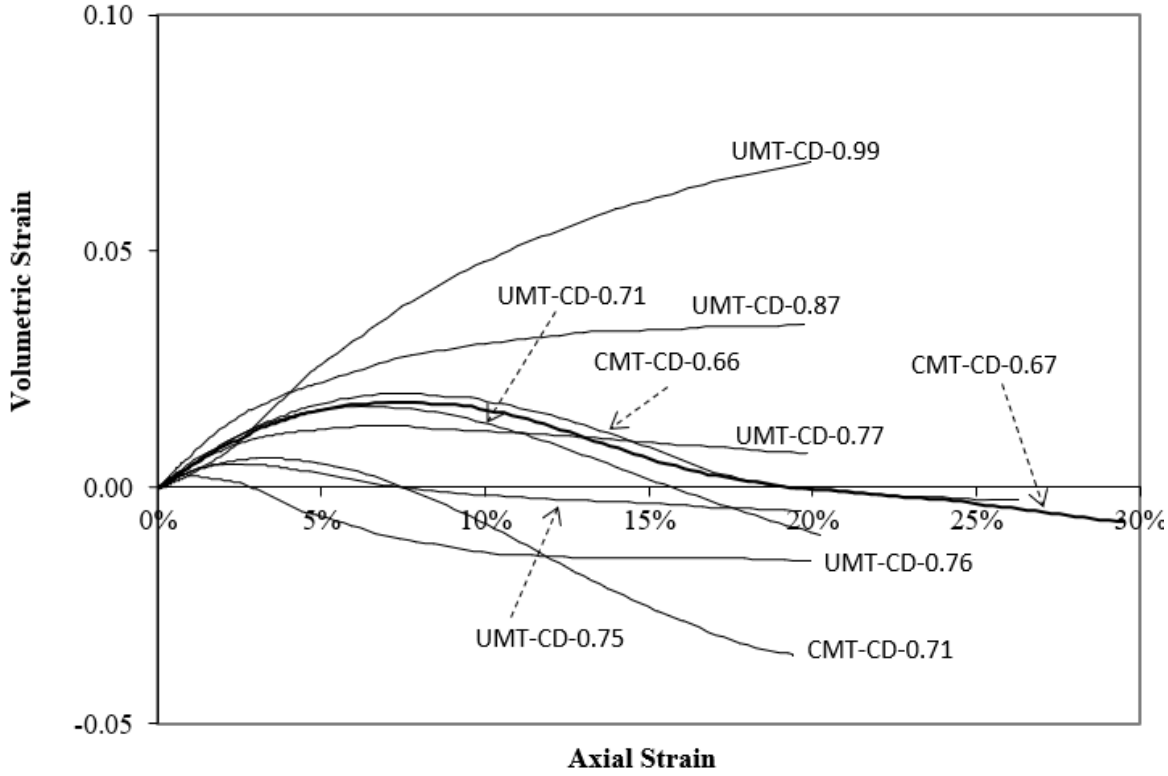

Figure 5-5 Volumetric strain versus axial strain for all triaxial tests

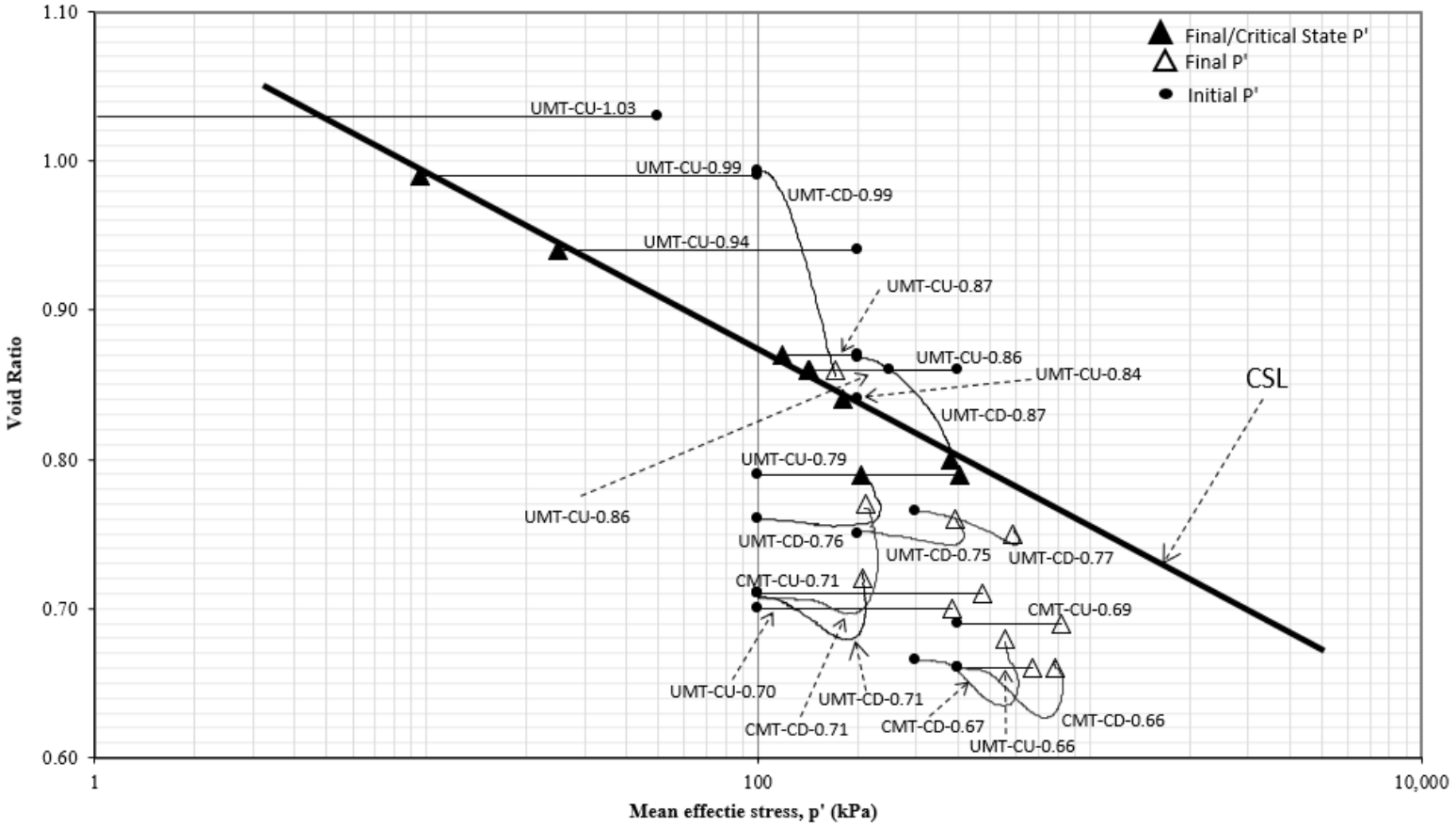

Figure 5-6 Critical state line plot

5.1.2 *Dilative Specimens with $e<e_{cr}$ – Undrained Loading*

UMT-CU-0.79, UMT-CU-0.70, UMT-CU-0.66, UMT-CD-0.76, UMT-CD-0.75, UMT-CD-0.77, and UMT-CD-0.71 specimens were “dense” of a critical state as shown in Figure 5-6 and indicated dilative behaviors at large strains. Two types of stress-strain curves were observed for the dilative specimens in undrained loading. The stress-strain curves and the graph of change in pore pressure versus axial strain for UMT-CU-0.79 and UMT-CU-0.70 are shown in Figure 5-7. Both specimens have void ratios smaller than the critical void ratio, however; the void ratio of UMT-CU-0.70 is much lower than the critical void ratio ($e<<e_{cr}$).

As shown in Figure 5-7, for the undrained specimens with $e<<e_{cr}$ (e.g. UMT-CU-0.70) the initial peak deviatoric stresses occur at about 0.5%–1.5% axial strain, and then a quasi-steady state is reached, which lasts for a short interval of strain, after which the shear stress increases again. For UMT-CU-0.79 with $e<e_{cr}$ the deviator stress steadily increases until it reaches a constant value when the specimen reaches the critical state. The dilative specimens at the start of undrained shearing indicated contractive behavior with positive changes of porewater pressure. With the increase of axial strain, a dilative trend occurs and the porewater pressures begin to de_{cr}ease, causing the increase of deviatoric stress. For all dense specimens except UMT-CU-0.79, it can be seen that the porewater pressures do not reach constant states, which means that these tests have not quite reached critical states. The effective stress path of the dilative specimens as shown in Figure 5-3 indicate that the effective stress of dilative specimens will increase monotonically and approach a constant stress ratio line (CSRL). The effective stresses at the critical state could not be identified under this strain hardening condition.

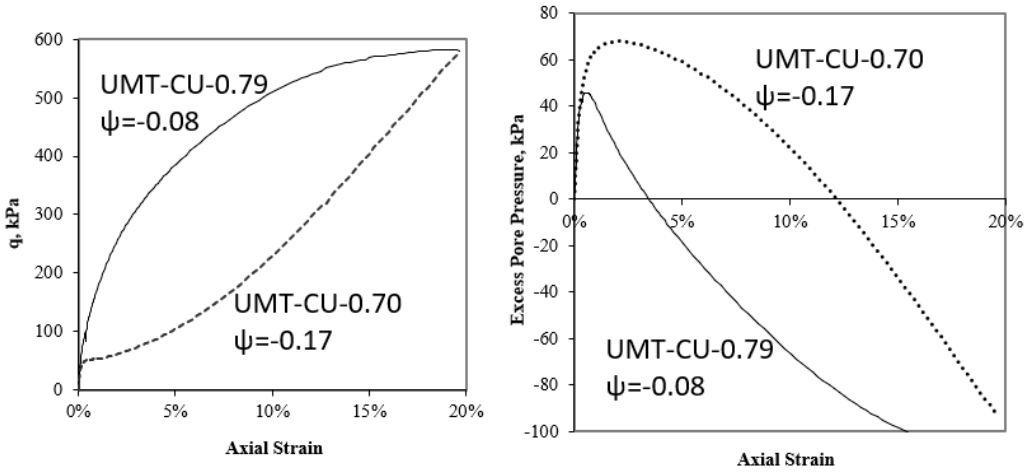

(a) (b)

Figure 5-7. UMT-CU-0.79 ($e<e_{cr}$) and UMT-CU-0.70 ($e<<e_{cr}$), a) stress-strain curves, b) change in pore pressure

5.1.3 *Contractive Specimens with $e>e_{cr}$ – Undrained Loading*

UMT-CU-1.03, UMT-CU-0.99, UMT-CU-0.94, and UMT-CU-0.86 had positive state parameters ($e>e_{cr}$) and exhibited contractive behavior. These specimens that were on the “loose” side of the critical state became unstable at the peak state and experienced static liquefaction. The flow liquefaction line as shown in Figure 5-8a is determined by a line connecting the peaks of effective stress paths obtained from the contractive specimens. Instability occurs when the stress path intercepts the instability line. Therefore, the instability line separates potentially unstable stress states from stable stress states.

Specimens that experience static liquefaction generate significate porewater pressure. UMT-CU-1.03 with ψ=0.13 and confining stress of 50 kPa experienced full liquefaction, or r_u=1.0, in which r_u is the ratio of generated pore pressure to the total stress. In other words, the effective stress of UMT-CU-1.03 at the critical state became

zero. Other contractive specimens (e.g. UMT-CU-0.99) experienced limited liquefaction (r_u<1.0) as shown in Figure 5-8.

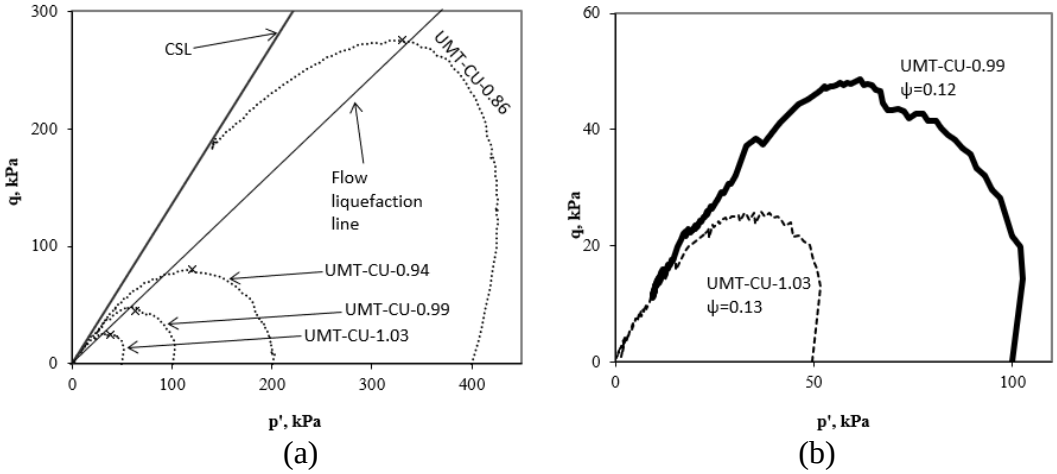

(a) (b)

Figure 5-8 Flow liquefaction of silt size gold mine tailings a) critical state line and flow liquefaction line, b) full liquefaction (UMT-CU-1.03) versus limited liquefaction (UMT-CU-0.99)

As it is shown in Figure 5-2, the contractive specimens in undrained loading reached the peak deviatoric stresses at approximately 1%–2% axial strain. The specimens exhibited strain-softening behavior due to significant porewater pressure generation after the peak stress. All contractive specimens reached critical state at about 15%–20% axial strain. The critical state can be easily identified for the contractive specimens since both deviatoric stress and change in pore pressure versus axial strain become constant.

5.1.4 *Specimens with $e \approx e_{cr}$ – Undrained Loading*

The void ratios of UMT-CU-0.87, UMT-CU-0.84, and UMT-CU-0.86 were equal or nearly equal to their corresponding critical void ratios. These specimens exhibited a different behavior from those of “loose” or “dense” of the critical state. For comparison, plots of stress-strain curves, change in pore pressure, and stress paths are shown in

Figure 5-9 for three specimens with $e \approx e_{cr}$, $e << e_{cr}$, and $e > e_{cr}$. UMT-CU-0.84 with $e \approx e_{cr}$ does not exhibit the strain-hardening, or the stress-softening behavior such as UMT-CU-0.70 and UMT-CU-0.86 do. The deviatoric stress increases with the increase in axial strain until it becomes stable. The same trend applies to the change in pore pressure. Pore pressure increases with an increase in axial strain until it becomes stable. The slight reduction in pore pressure from approximately 2% to 10% axial strain is likely because the initial void ratio of the specimen may have a small deviation from the critical void ratio.

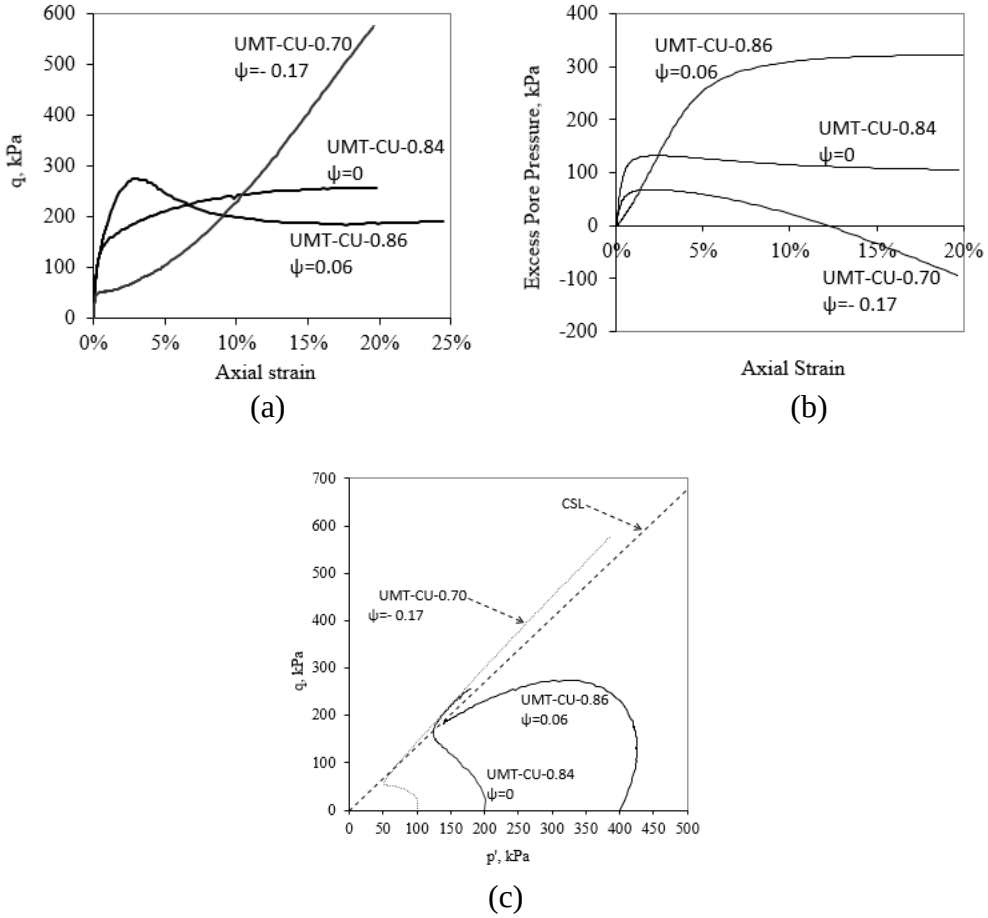

Figure 5-9 Behavior of gold mine tailings at various state parameters. a) stress-strain curves, b) change in pore pressure versus axial strain, and c) stress paths

Drained Specimens

Based on the volumetric strains shown in Figure 5-5, UMT-CD-0.99 and UMT-CD-0.87 which are “loose” of critical state (positive state parameter) exhibited contractive behavior while UMT-CD-0.76,UMT-CD-0.75, UMT-CD-0.77 and UMT-CD-0.71 which are “dense” of critical state (state parameter <-0.05) exhibited dilative behavior. UMT-CD-0.87 and UMT-CD-0.76 reached critical state after 15% axial strain based on stable volumetric strains as shown in Figure 5-5 while the rest of drained specimens did not reach the critical state when they sheared to 20% axial strain.

The dilative specimens exhibited strain-softening behavior after the peak deviatoric stresses at about 3%–15% axial strain. Conversely, the contractive specimens exhibited strain-hardening behavior. The volumetric strains are contractive initially for all specimens. For the specimens “loose” of critical state volumetric strains keep increasing until they stabilize at the critical state, while for the specimens “dense” of critical state (ψ<-0.05) they became dilative just before the peak shear stresses are reached.

5.1.5 *Development of Critical State Line*

The critical state line in the p-q’ plane and in e-log (p’) was drawn, as shown in Figure 5-3 and Figure 5-6, based on the individual triaxial test results. The CSL was represented using a conventional semi-log idealization in the form of a straight line. Although a curved critical state locus is a more accurate idealization of the CSL, a straight line is an acceptable approximation that has been used in many previous studies (Jefferies & Been, 2016).

In order to develop the CSL, the results of each triaxial test were separately evaluated to determine whether the sample reached the critical state during the shear. In Figure 5-2 through Figure 5-6, the solid triangles represent the post-shear data points for the samples that reached the critical state and the hollow triangles represent the post-

shear data points for the samples that did not reach the critical state. Cemented mine tailings, or CPB, samples did not reach the critical state; however, the q-p' graph as shown in Figure 5-3 suggests that the positions of the CSL for early-age CPB and uncemented tailings are fairly similar. The similarity or proximity of the CSL positions for uncemented and early-age CPB samples could not be established in the e-log p' plane as the CPB samples did not reach the critical state. The critical state line in the q-p' and e-log p' planes were developed using the best fit line through the solid data points that represent the critical state condition (UMT-CD-0.76 was an outlier and was not included). The specimens "loose" of critical state provided the most useful dataset to develop the critical state line since they reached the critical state at axial strains smaller than 20%. Specimens that did not achieve critical state could potentially be sheared to a higher axial strain to reach the critical sate; however, most specimens were sheared up to 20% because enough critical state data points were obtained during the experimental program.

5.2 Triaxial Test Results and Discussion for Cemented Paste Backfill

The CPB specimens all had state parameters smaller than -0.05, and thus exhibited dilative behavior at large strains as shown in Figure 5-2 and Figure 5-3. Adding binder to tailings slightly increased the initial void ratio of the CPB specimens; however, the addition of 4.5% binder to tailings did not cause a noticeable change in the position of CSL. This is likely due to the small percentage of the binder used to prepare the CPB specimens.

In general, cementation increased the secant shear stiffness of tailings at any given axial strain as shown in Figure 5-10. Also, cementation reduced the change in excess pore pressure by bonding particles during the contractive behavior at small strains before the phase transformation point (PTP) is reached. Additionally, the CPB

specimens resulted in a larger reduction in pore pressure during the dilation phase after the PTP as shown in Figure 5-11. Therefore, it can be concluded that cementation magnifies the dilative behavior of tailings.

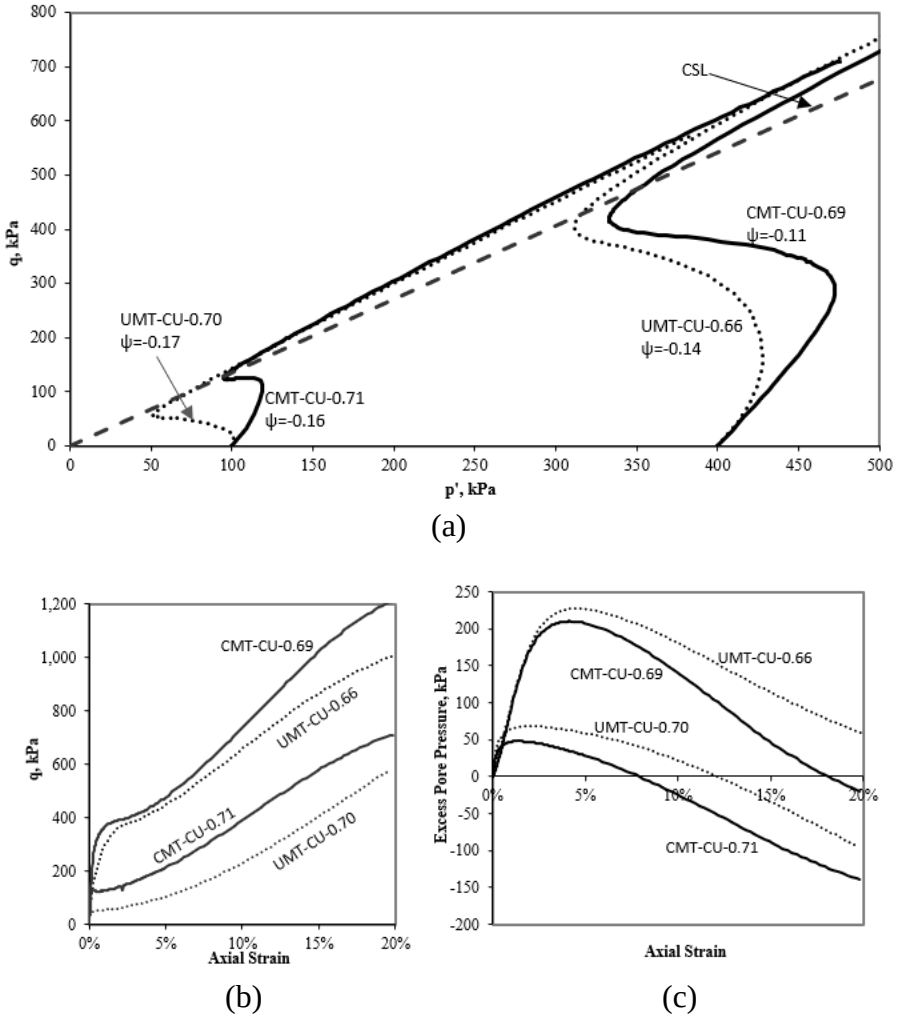

Figure 5-10 Comparison of CPB and uncemented tailings specimens in undrained loading, a) stress paths, b) stress-strain curves, and c) change in pore pressure versus axial strain

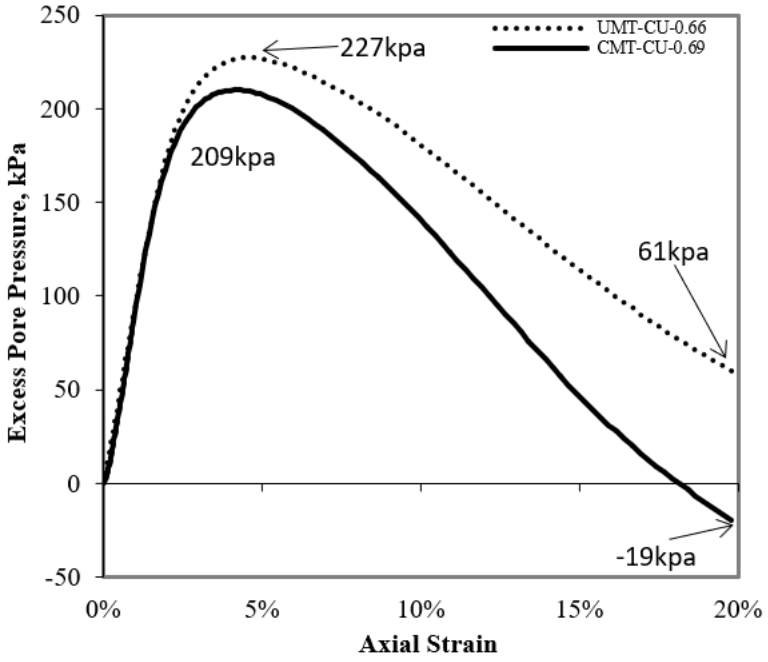

Figure 5-11 Magnitude of excess pore pressure for tailings with and without binder

5.3 Summary and Conclusions

1. The development of the critical state line and state parameters was a successful and robust technique to explain the behavior of silt-sized non-plastic mine tailings and the CPB. The comparison between the responses of cemented and uncemented samples in the q-p' plane suggests that the positions of the CSL for early-age CPB and uncemented tailings are fairly similar; however, the similarity or proximity of the CSL positions could not be established in the e-log p' plane as CPB samples did not reach the critical state.
2. Tailings specimens with an initial void ratio larger than their corresponding critical void ratio experienced static liquefaction in undrained loading. Two specimens at confining pressures of 50 kPa (Specimen ID) and 100 kPa (Specimen ID) with fairly similar initial state parameters (0.13 versus 0.12) resulted in full liquefaction and limited liquefaction, respectively.

3. Specimens prepared using the slurry deposition method resulted in state parameters smaller than -0.11, and therefore did not experience static liquefaction because of their dilative behavior at large strains.
4. The CPB specimens generated smaller excess pore pressures than the uncemented ones. They also indicated larger reductions in excess pore pressure after the phase transformation point, suggesting more dilative behavior than their corresponding uncemented specimens (control specimens).

Chapter 6

Cyclic Test Results

A total of eight cyclic direct simple shear tests (CDSS) were successfully conducted under undrained conditions to investigate the liquefaction potential of both CPB and uncemented mine tailings. This chapter summarizes the liquefaction investigation of CPB induced by seismic shear stress waves. The CDSS tests performed for this study are listed in Table 6-1. The normally consolidated specimens were tested at different cyclic stress ratios (CSRs) ranging from 0.05 to 0.5 at 100 kPa effective vertical pressure. The effective vertical pressure, 100 kPa, was selected to be similar to the historical cyclic response study of CPB made with Portland cement (Suazo et al., 2017). Note that for all CPB specimens, the binder ratio that was used is 1.5%PC:3%FA and the CPB specimens were cured for 22 hours (initial setting time). Uncemented specimens were tested to provide a data set for comparing the Cyclic Resistance Ratio (CRR)-N curves for uncemented and CPB tests. In the following section, cyclic resistance of materials will be evaluated and the overall liquefaction susceptibility will be investigated under cyclic loading.

Table 6-1 Summary of cyclic direct simple shear tests

Test No.	CSR	Effective Vertical Stress, σ'_{vc} (kPa)	Initial SC* (%)	Initial WC* (%)	Number of Cycles at 3.75% single amplitude shear strain	Type
UMT-0.05	0.05	100	78	28	>500	Uncemented
UMT-0.08	0.08	100	78	28	99	Uncemented
UMT-0.10	0.10	100	78	28	8	Uncemented
UMT-0.15	0.15	100	78	28	2	Uncemented
CMT-0.10	0.10	100	78	28	>500	22Hr-CPB
CMT-0.30	0.30	100	78	28	281	22Hr-CPB
CMT-0.40	0.40	100	78	28	60	22Hr-CPB
CMT-0.50	0.50	100	78	28	3	22Hr-CPB

Notes: *SC=solid content, WC=water content

6.1 Uncemented Mine Tailings (UMT)

The typical stress path, or the shear stress-effective vertical stress (τ-σ'_{vc}) plot, cyclic shear ratio versus number of cycles (N), pore pressure ratio ($\Delta u/\sigma'_{vc}$) versus number of cycles (N), and shear strain versus number of cycles (γ-N) for uncemented tailing specimens are shown in Figure 6-1. The UMT-0.10 test results are presented as an example in this section to discuss the response of uncemented specimens. Cyclic direct shear test results for all tests are provided in Appendix A.

All uncemented mine tailings indicate predominantly contractive response with the generation of positive pore pressure during cyclic loading. This response can also be referred to as a cyclic mobility type of response. The uncemented specimens experience

a cumulative increase in equivalent excess pore-water pressure and degradation of shear stiffness as the number of load cycles (N) increases.

The pore pressure ratio increase with a higher number of cycles in uncemented tailings will result in the stress paths moving from the initial effective stress (100 kPa) towards the origin of the plot. Figure 6-1c shows that the pore pressure ratio increases in a progressive manner with number of cycles, while the shear strain (Y) for the specimen does not considerably change in up to eight cycles, as shown in Figure 6-1d. The shear strain significantly increases in the 8th cycle. At the 8th cycle of uniform cyclic loading, the specimen reaches its 3.75% single amplitude (SA) shear strain, which is used as the criterion in this study to consider the initiation of liquefaction. The pore pressure ratio at this cycle is approximately 0.9.

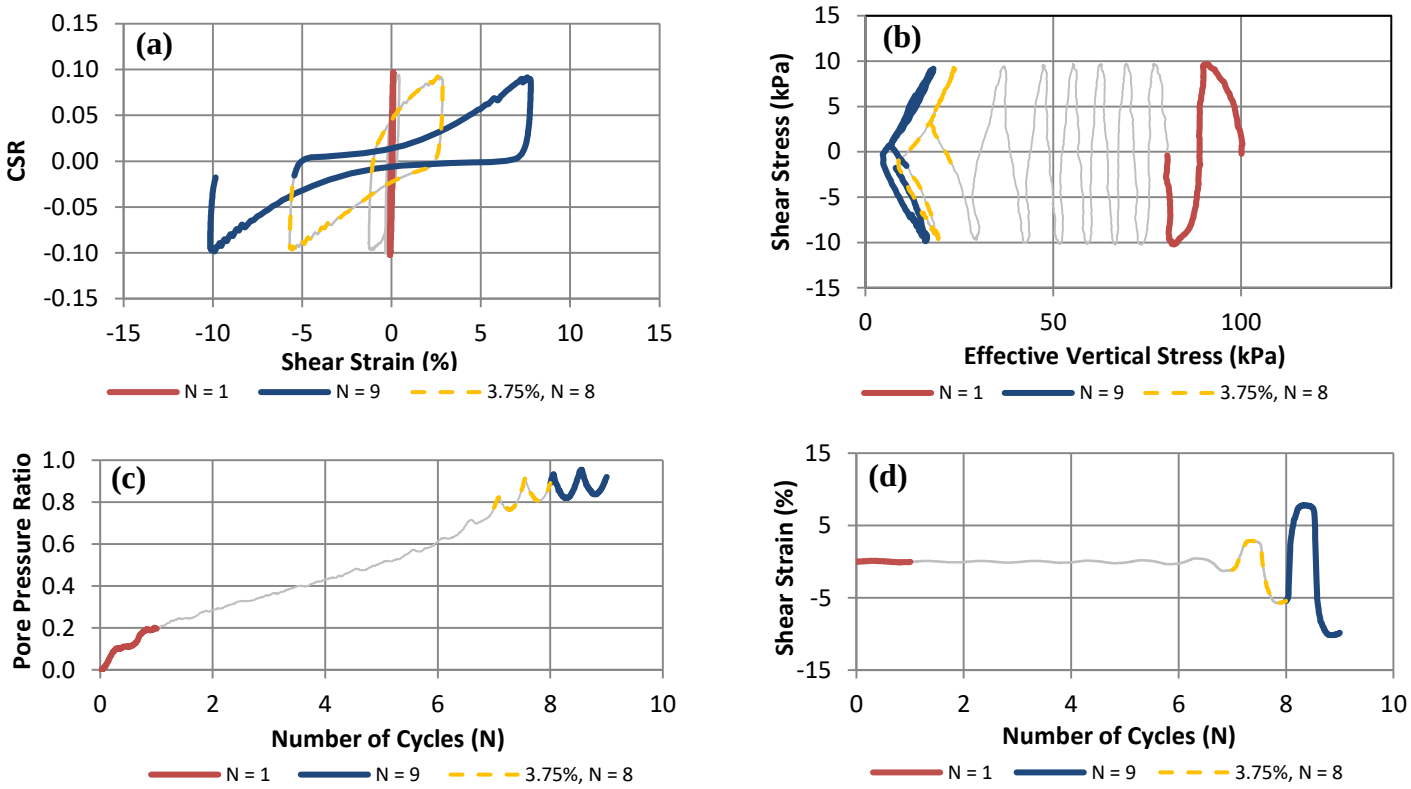

Figure 6-1. Response of uncemented tailings specimen UMT-0.10 tested at CSR = 0.10 and σ'_{vc}=100 kPa, a) cyclic stress ratio versus shear strain, b) stress path, c) pore pressure ratio versus number of cycles, and d) shear strain versus number of cycles response

6.2 Cemented Mine Tailings

6.2.1 *Cyclic Test Results for Cemented Paste Backfill with Fly Ash*

The test results for CMT-0.40 and CMT-0.10 as example responses of CPB specimen will be described in this section. All other cyclic test results are provided in Appendix B.

For the CPB samples that CSR was high enough to cause liquefaction, the stress path in the τ-σ'_{vc} plot as shown in Figure 6-2b moves from the initial effective stress (100 kPa) towards the origin of the plot as a result of an increase in pore pressure ratio. The progressive increase in pore pressure ratio with number of cycles for this specimen is shown in Figure 6-2c. For CMT-0.40, the maximum pore pressure ratio is more than 0.95 after 51 cycles, where 3.75% SA shear strain is reached, as shown in Figure 6-2d. The pore pressure ratio less than unity has been used by several previous researchers as an indication of cyclic mobility type of response versus flow liquefaction type of response (Suazo, 2017; Wijewickreme, 2005).

Specimen CMT-0.10 that was tested under CSR=0.1 did not experience liquefaction when the cyclic load was applied up to 500 number of cycles. The stress path as shown in Figure 6-3b moves toward the original of the plot as the number of cycles increases only to a limited degree. Figure 6-3c shows that there is no progressive excess porewater pressure such as the ones observed for uncemented specimens and CPB specimens tested at high CSR (>0.3). This indicates the resistance of the specimen to cyclic loading.

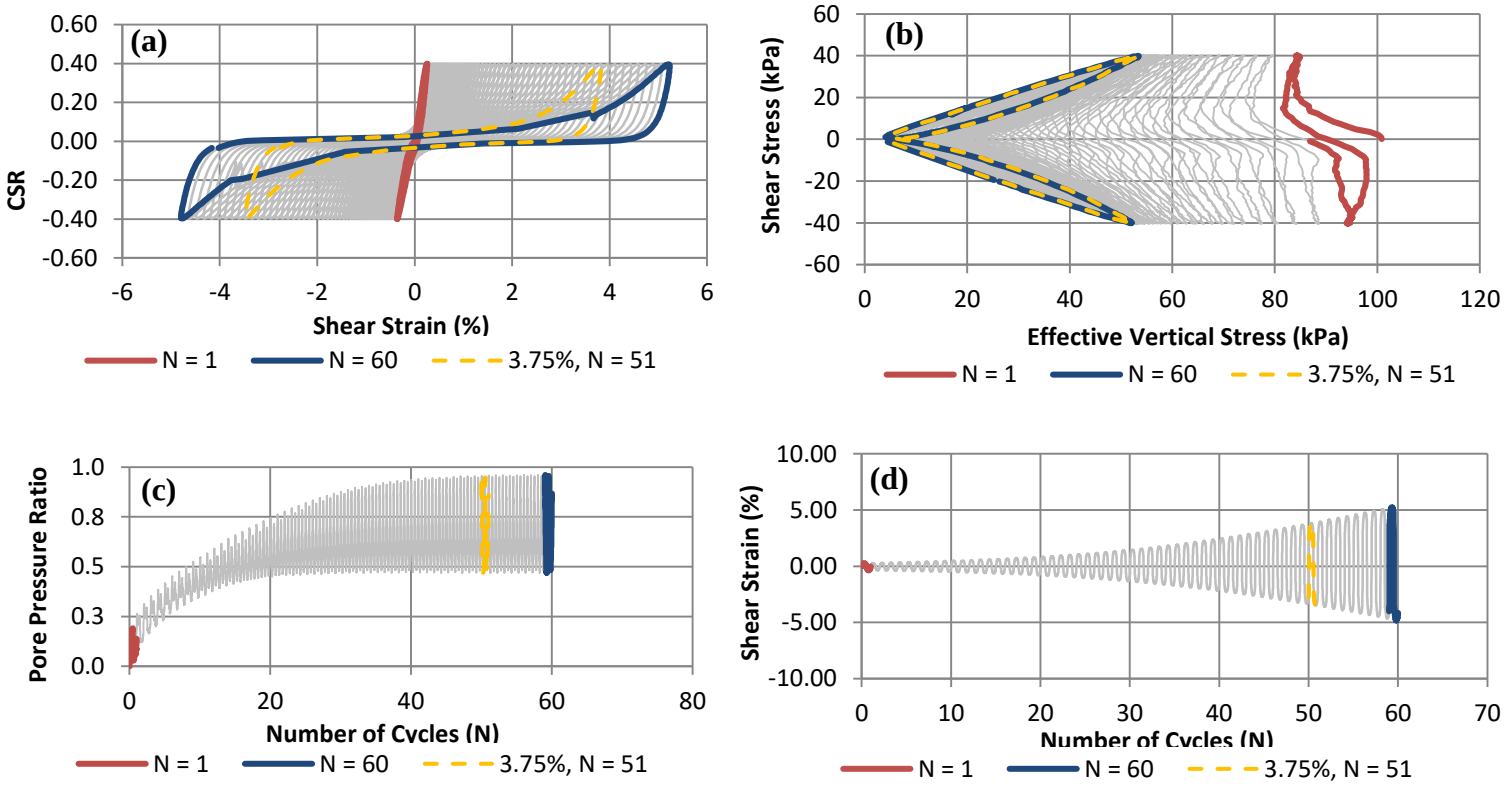

Figure 6-2 Response of uncemented tailings specimen CMT-0.40 tested at CSR = 0.40 and σ'_{vc}=100 kPa, a) cyclic stress ratio versus shear strain, b) stress path, c) pore pressure ratio versus number of cycles, and d) shear strain versus number of cycles response

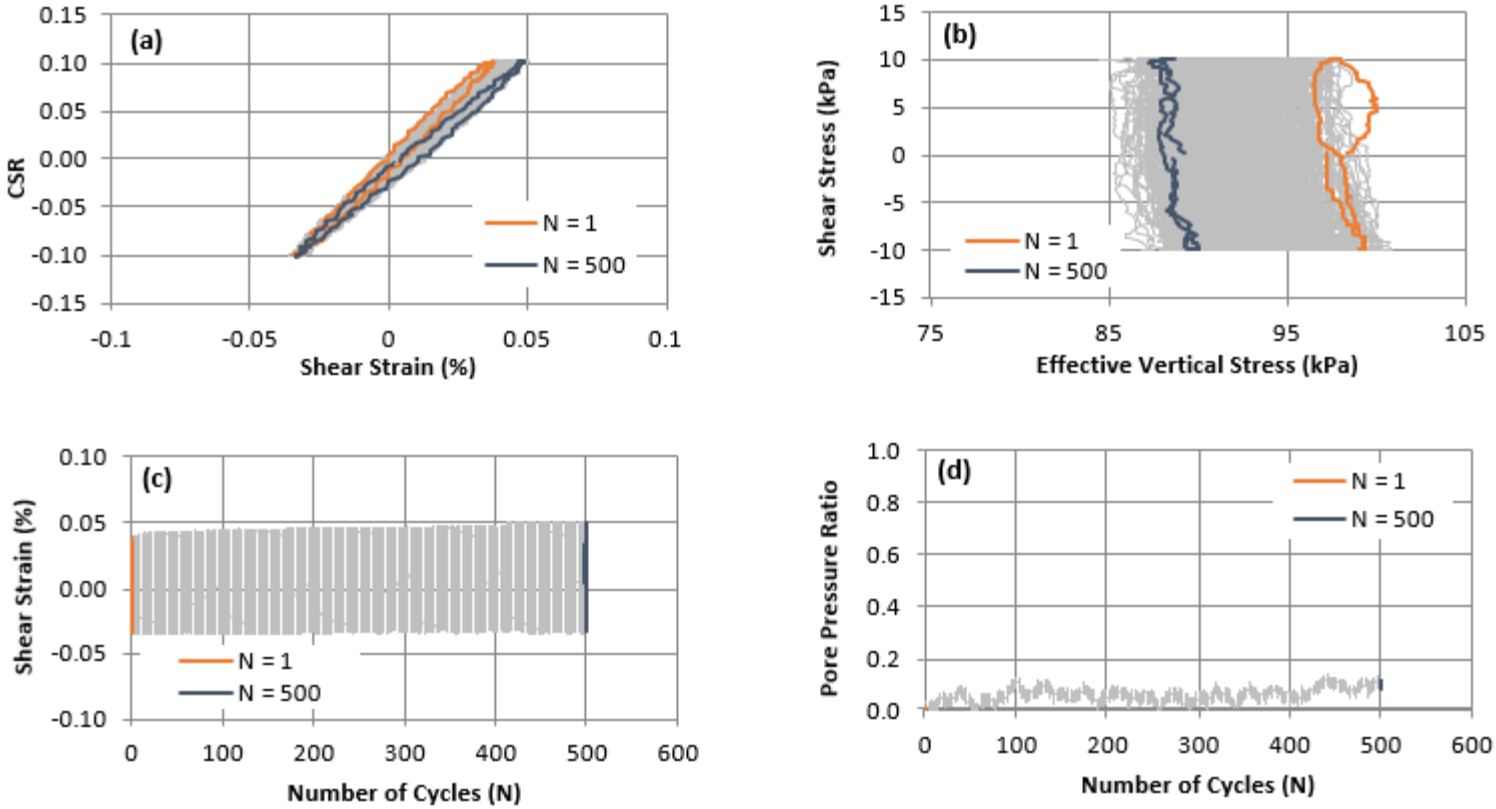

Figure 6-3 Response of uncemented tailings specimen CMT-0.10 tested at CSR = 0.10 and σ'_{vc}=100 kPa, a) cyclic stress ratio versus shear strain, b) stress path, c) pore pressure ratio versus the number of cycles, and d) shear strain versus the number of cycles response

6.2.2 *Discussion on Cyclic Resistance Ratio of Cemented Paste Backfill with Fly Ash*

The significant increment in the liquefaction resistance of CPB as curing progresses is reported by other authors (le Roux et al. 2004; Saebimoghaddam 2010; Suazo, 2017). Cemented mine tailings specimens were tested for cyclic mobility to evaluate the liquefaction resistance of CPB with fly ash. Based on the cyclic test results provided in this chapter, the replacement of Portland cement with fly ash was found to have no adverse impact on achieving significant liquefaction resistance at the early-age stage and thereafter.

The specimens tested during this study predominantly showed a cyclic mobility type of response. The shear stiffness of specimens degraded as the number of cycles increased. For CMT-0.40, the secant shear moduli were estimated to be 16000 kPa and 1066 kPa at N=1 and N=52, respectively. The pore pressure ratio had considerable increase only at the tests with high CSR (>0.3). This increase in the pore pressure ratio at high CSR values is caused by steady cumulative damage to cement bonds connecting tailings particles. Once the cement bonds break down the resistance to volumetric compression de$_{cr}$eases, causing excess pore pressure build-up, which eventually leads to liquefaction failure. At CSR=0.1 the cyclic load did not appear strong enough to significantly break the cement bonds. Thus, the pore pressure ratio did not rise significantly. The comparison of pore pressure ratios for cemented and uncemented specimens is shown in Figure 6-4.

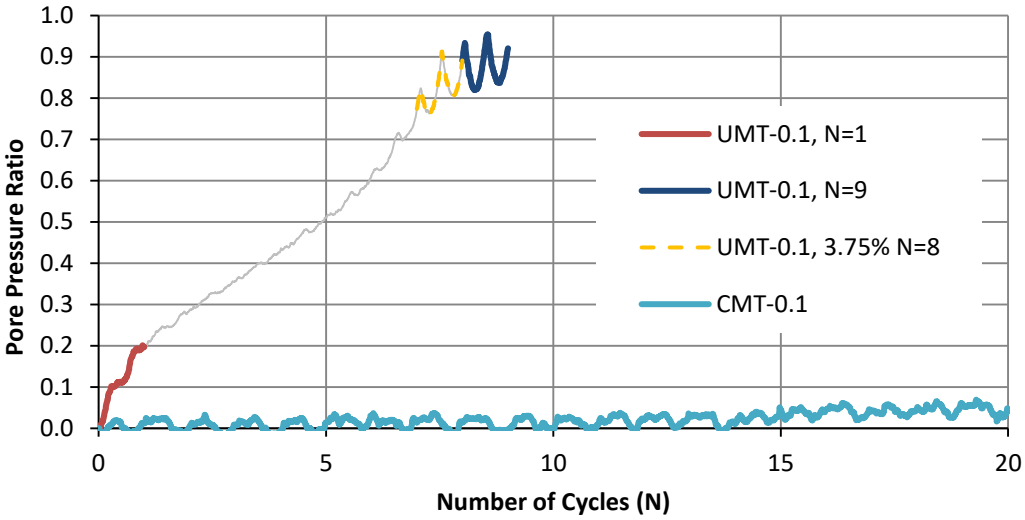

Figure 6-4 Pore pressure ratio comparison of uncemented tailings (UMT-0.10) and CPB (CMT-0.10) up to 20 number of cycles at CSR=0.1

All specimens showed an overall contractive behavior during shearing. However, after many cycles [e.g., from the eighth cycle in Figure 6-1c], a dilative response at the end of the loading phase was usually observed. This response was suppressed by a clear contractive tendency in the stress reversal path (or unloading phase). A similar cyclic shear response was reported for Fraser River silts (Wijewickreme and Sanin, 2004) and dense Fraser River sands (Sriskandakumar, 2004). The process of contraction followed by subsequently limited dilation likely resulted in a more accentuated fluctuation of the excess porewater pressures at each loading cycle, as shown in Figure 6-1c. Nevertheless, pore pressure curves steadily increased up to a maximum value and remained around this value beyond the failure (defined as 3.75% SA shear strain).

6.2.2.1 Liquefaction Resistance of CPB with Fly Ash

The CRR-N data points based on the cyclic test results are plotted and shown in Figure 6-5. The best-fit curves were developed to show the CRR-N relationship based on the following equation (Boulanger & Idriss, 2015) as discussed in Chapter 2:

$$CRR = aN^{-b}$$

The uncemented and cemented tailings show b values of 0.28 and 0.10, respectively. The b values for clean sand and clay can be assumed 0.337 and 0.135, respectively, based on the typical numbers used when deriving magnitude scaling factors (MSF) to adjust CRR to a common value of M (Boulanger and Idriss, 2004). The b value of 0.28 for tailings in this study lies between sand and clay, which appears reasonable considering the tailings classify as none plastic silt. The b value for uncemented tailings at this study is also consistent with the b value of 0.26 which was reported by Suazo et al. (2017) for low-plasticity silt.

For simplicity in comparing the CRR-N results under a unique criterion, 10 equivalent cycles (N=10) were selected in this study to simulate earthquakes with a magnitude of 7 as determined by Idriss (1999) for clean sands. The CSR=0.39 as determined from the simplified procedure proposed by Seed and Idriss (1971) was used as a criterion to compare the CRR's to a large earthquake assuming an equivalent maximum ground surface acceleration (a_{max}) of 0.3 and shear stress reduction factor (r_d) of unity.

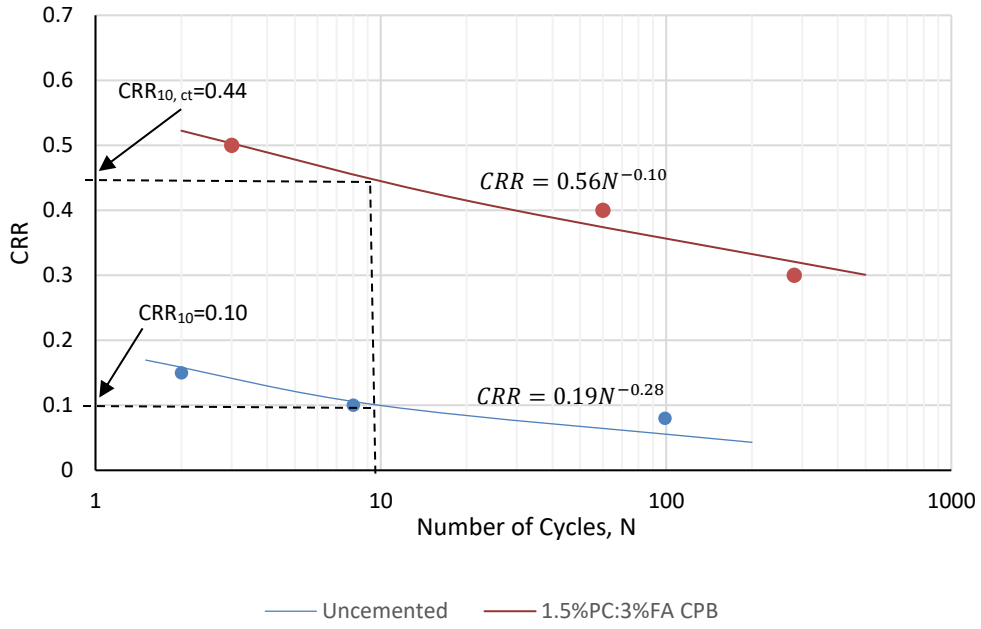

Figure 6-5 Cyclic stress ratio versus number of cycles (N) to reach single amplitude γ_{sa}=3.75% for uncemented tailings and the early-age CPB with fly ash (σ'_{vc}=100 kPa, α=0)

Based on the test results shown in Figure 6-5, the CRR values for the uncemented tailings and the CPB with fly ash at number of cycles equal to ten were estimated to be 0.1 and 0.44. The CRR value of 0.44 for the CPB is higher than 0.39 or the reasonably large value for most seismic regions (Australian Standard, 2007; Norma Chilena, 1966; Suazo, 2017). This indicates fly ash can successfully replace a significant portion of Portland cement in CPB without having an adverse impact on the liquefaction

resistance at the early-age as shown in Figure 6-6.

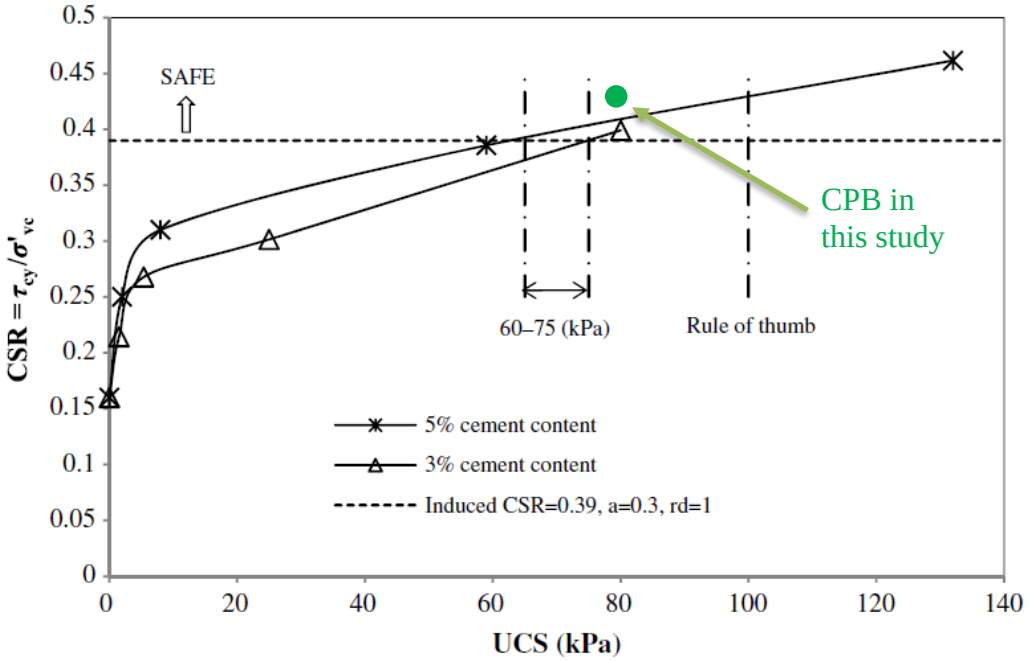

Figure 6-6 The evolution of liquefaction resistance versus unconfined compressive strength over time for CPB specimens (Suazo et al., 2017)

The correction factor (K_{ct}) for the cyclic resistance ratio of cemented samples proposed by Suazo et al. (2017) is shown in Figure 6-7. Based on Figure 6-5, the K_{ct} for the CPB at 22 hours (initial setting time) was tested to be 4.4. Based on Figure 6-7, the predicted K_{ct}'s developed by Suazo et al. (2017) for 1.5% PC and 3% PC at 22 hours was estimated to be 1.5 and 2.3. Both predicted values are considerably smaller than that of tested in this study. The difference between the predicted values and the tested value can be attributed to the tailings properties among other factors.

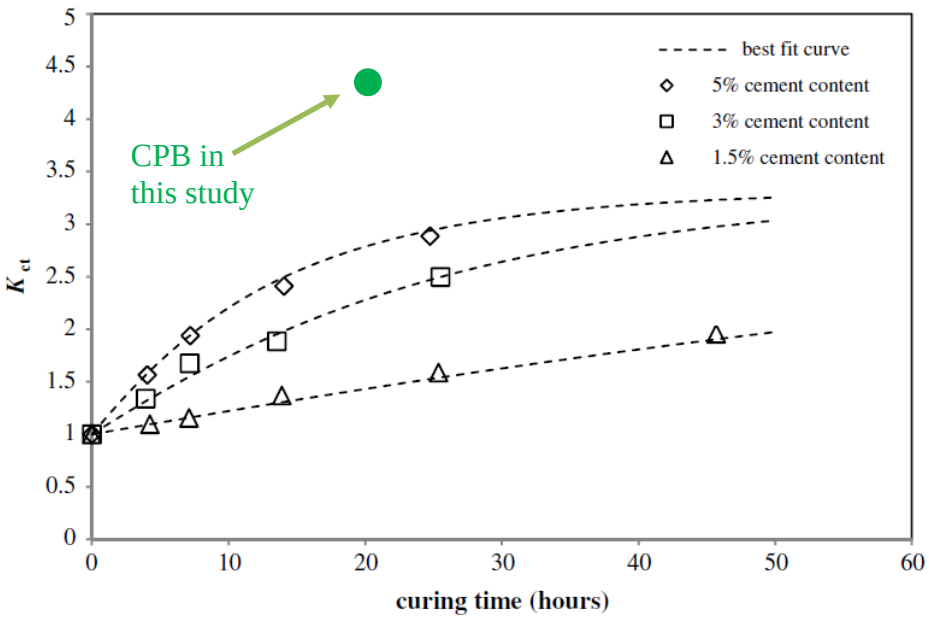

Figure 6-7 Evolution of K_{ct} correction factor versus curing time for CPB prepared using different cement content at σ'_{vc}=100 kPa (Suazo, 2017)

6.3 Summary and Conclusions

1. The CDSS test results indicated a cumulative increase in excess porewater pressure with progressive degradation of shear stiffness (cyclic mobility type response) for the CPB with fly ash. The behavior of the CPB with fly ash generally was found to be consistent with the behavior of CPB with no fly ash found in the previous studies.
2. Based on the cyclic test results, fly ash can be successfully used to replace a significant portion of Portland cement in CPB without an adverse impact on achieving significant liquefaction resistance at the early-age stage and thereafter.
3. The CPB prepared for this study with 50% replacement of PC with fly ash indicated adequate resistance against liquefaction at its initial setting time for a reasonable large earthquake in most seismic regions.

4. The correction factor (K_{ct}) for the CRR gain of early-age CPB proposed by Suazo et al. (2017) was found to be inaccurate to predict the CRR gain of CPB tested for this study. The CPB in this study gained significantly higher CRR comparing to the predicted value proposed by Suazo et al. (2017).
5. The UCS value at the initial setting time (22 hours) for to the CPB specimens tested under cyclic loading was obtained to be 78 kPa. This observation implies the proposed minimum UCS values of 60-75 kPa for the liquefaction resistance criterion under cyclic loading (Suazo et al., 2017) can be successfully used for CPB with fly ash.

Chapter 7

Constitutive Modeling of Early-Age CPB

This chapter presents the constitutive modeling of silt-sized mine tailings and early-age CPB. The constitutive modeling of silt-sized, non-plastic, gold mine tailings will provide information and insight into fundamental properties of the study tailings. Additionally, the constitute modeling of early-age CPB will provide insight on the impact of slight cementation on fundamental properties of silts and sands (i.e., study tailings). As mentioned in Chapter 6 specimens with positive state parameter ($e>e_{cr}$) could not be made using the slurry disposition method. All CPB specimens were prepared using the slurry deposition method and had a state parameter equal or smaller than -0.11. Based on the field in-situ stress and drainage conditions the state parameter of CPB can be larger than those of tested in the laboratory. One benefit of constative modeling is to predict the behavior of CPB at larger state parameters to evaluate the likelihood of static liquefaction before the final set of CPB.

NorSand as described in Chapter 2 is a proven constitutive model to simulate the monotonic behavior of sands and silts. NorSand was used in this study to simulate the actual triaxial tests and to develop the constitutive parameters. The Excel spreadsheet provided as part of the *Soil Liquefaction: A Critical State Approach* textbook (Jefferies and Been, 2016) was utilized to simulate the triaxial test results. The NorSand model successfully simulated the triaxial test results for the study tailings. For the early-age CPB simulation, NorSand appeared to be generally applicable particularly post-peak strength when cementitious bonds are broken down.

7.1 NorSand Simulation of Silt-Sized Mine Tailings

The critical state line (CSL) parameters, Γ and λ_{10}, were calculated based on the CSL developed in Chapter 5 as shown in Figure 7-1.

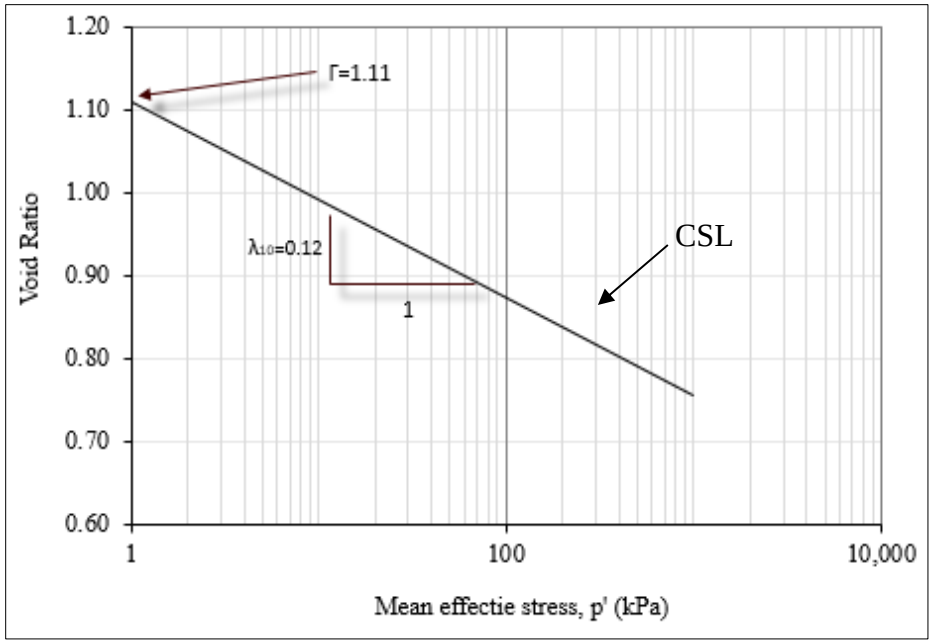

Figure 7-1 The CSL and NorSand parameters Γ and λ_{10}

The results of drained triaxial tests with dilative behavior at large strains were used to develop the peak dilatancy (D_{min}) versus peak stress ratio (η_{max}) and the state parameter (at η_{max}) relationships as shown in Figure 7-2 and Figure 7-3, respectively.

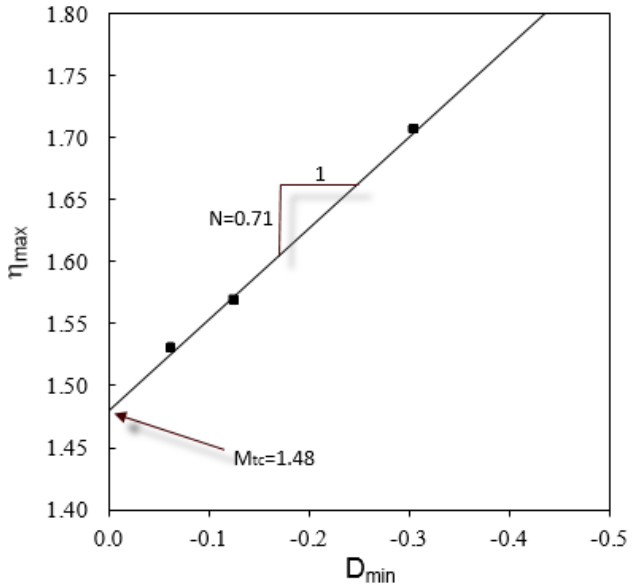

Figure 7-2 Peak dilatancy versus peak stress ratio from drained tests to determine "N"

Based on the triaxial tests results as shown in Figure 7-2, the "N" and "M_{tc}" parameters were calculated to be 0.71 and 1.48 , respectively. The "N" value is slightly greater than typical values for sands while the "M_{tc}" value is consistent with typical values for sands (Jefferies & Been, 2016). The "χ_{tc}" parameter was calculated to be 2.2, as shown in Figure 7-3. This value is consistent with typical values for sands (Jefferies & Been, 2016).

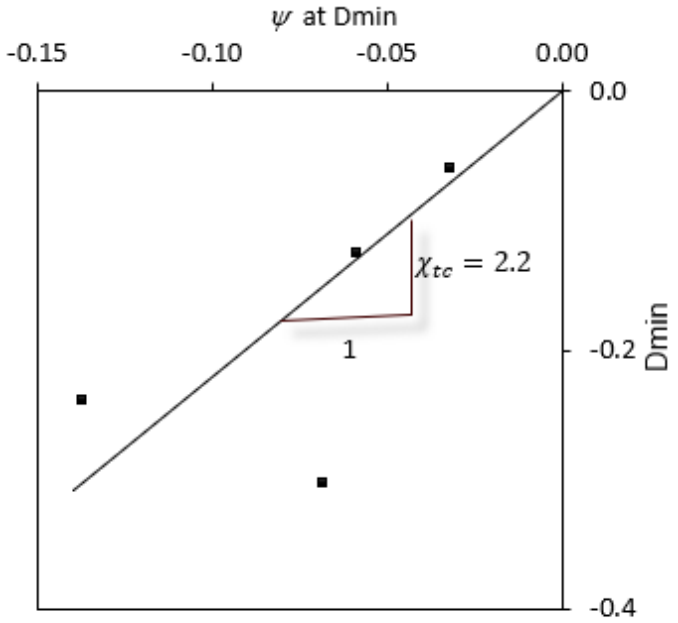

Figure 7-3 Peak dilatancy versus state parameter from drained tests to determine "χ_{tc}"

Elasticity parameters (G_{max} and G_{exp}) were first estimated from the triaxial test results. Later they were adjusted based on the NorSand models for a better fit. Generally, the calibrated G_{max} values are consistent with the test results. The G_{exp} parameter was obtained using the plot of calibrated G_{max} values and calibration through an iterative process. The plot of G_{max} versus initial effective confining stress is shown in Figure 7-4. The remaining parameters "H" was obtained through the calibration. The increase of plastic hardening modulus (H) with de$_{cr}$ease in the state parameter is shown in Figure 7-5. Input and calibration parameters for NorSand models are presented in Table 7-1. A Poisson's ratio of 0.3 was selected for the materials based on typical values for silts. Example comparisons between actual test results and NorSand simulations for the uncemented tailings are shown in Figure 7-6 through Figure 7-9.

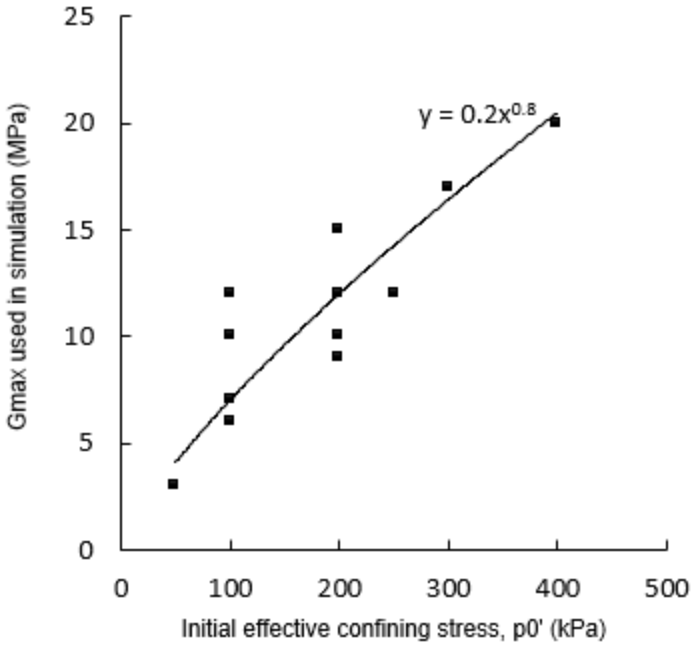

Figure 7-4 Plot of G_{max} versus initial effective confining stress

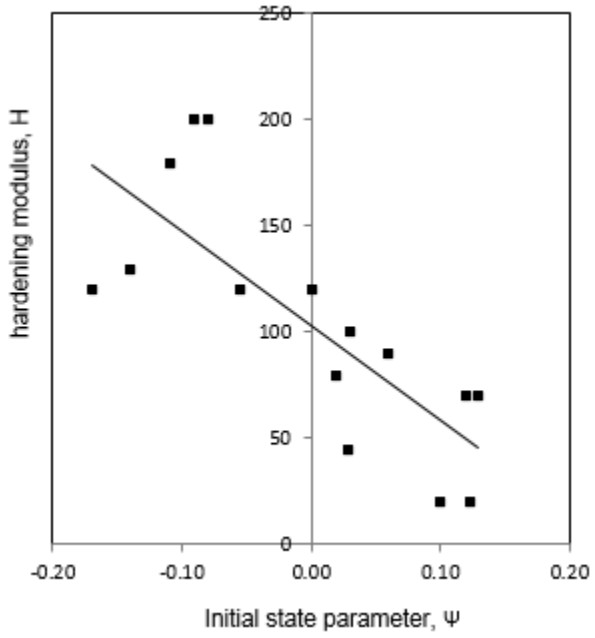

Figure 7-5 Plot of plastic hardening modulus versus initial state parameter

Table 7-1 NorSand parameters for the study mine tailings and CPB triaxial calibration

Materials	Test ID.	Prep. Method	P_0 (kPa)	Γ	λ_{10}	Ψ_0	M_{tc}	N	χ_{tc}	H	G_{max} (MPa)	G_{exp}	ν	I_r
Mine Tailings	UMT-CD-0.99	MT	100	1.11	0.12	0.12	1.49	0.71	2.2	20	6	0.8	0.3	60
	UMT-CD-0.87	MT	200	1.11	0.12	0.03	1.49	0.71	2.2	45	10	0.8	0.3	50
	UMT-CD-0.76	MT	100	1.11	0.12	-0.11	1.49	0.71	2.2	180	12	0.8	0.3	120
	UMT-CD-0.75	MT	200	1.11	0.12	-0.09	1.49	0.71	2.2	200	15	0.8	0.3	75
	UMT-CD-0.77	MT	300	1.11	0.12	-0.06	1.49	0.71	1.2	120	17	0.8	0.3	57
	UMT-CD-0.71	SD	100	1.11	0.12	-0.16	1.49	0.71	2.2	28	6	0.8	0.3	60
	UMT-CU-1.03	MT	50	1.11	0.12	0.13	1.49	0.71	2.2	70	3	0.8	0.3	60
	UMT-CU-0.99	MT	100	1.11	0.12	0.12	1.49	0.71	2.2	50	6	0.8	0.3	60
	UMT-CU-0.94	MT	200	1.11	0.12	0.1	1.49	0.71	2.2	20	9	0.8	0.3	45
	UMT-CU-0.86	MT	400	1.11	0.12	0.06	1.49	0.71	2.2	90	20	0.8	0.3	50
	UMT-CU-0.79	MT	100	1.11	0.12	-0.08	1.49	0.71	2.2	200	7	0.8	0.3	70
	UMT-CU-0.87	MT	200	1.11	0.12	0.03	1.49	0.71	2.2	100	12	0.8	0.3	60
	UMT-CU-0.84	MT	200	1.11	0.12	0	1.3	0.71	2.2	120	15	0.8	0.3	75
	UMT-CU-0.70	SD	100	1.11	0.12	-0.17	1.49	0.71	0.4	120	10	0.8	0.3	100
	UMT-CU-0.66	SD	400	1.11	0.12	-0.14	1.49	0.71	0.4	130	20	0.3	0.3	50
	UMT-CU-1.030	MT	250	1.11	0.12	0.02	1.22	0.71	2.2	80	12	0.8	0.3	48
Early-age CPB	CMT-CD-0.71	SD	100	1.11	0.12	-0.16	1.5	0.5	2.5	60	22	0.4	0.3	220
	CMT-CD-0.67	SD	300	1.11	0.12	-0.16	1.4	0.4	1.1	50	25	0.4	0.3	83
	CMT-CD-0.66	SD	400	1.11	0.12	-0.14	1.4	0.4	2.5	20	30	0.4	0.3	75
	CMT-CU-0.71	SD	100	1.11	0.12	-0.16	1.4	0.75	0.4	600	15	0.4	0.3	150
	CMT-CU-0.69	SD	400	1.11	0.12	-0.11	1.4	0.75	0.4	300	32	0.4	0.3	80

Note: MT: Moist tamp, SD: Slurry deposition

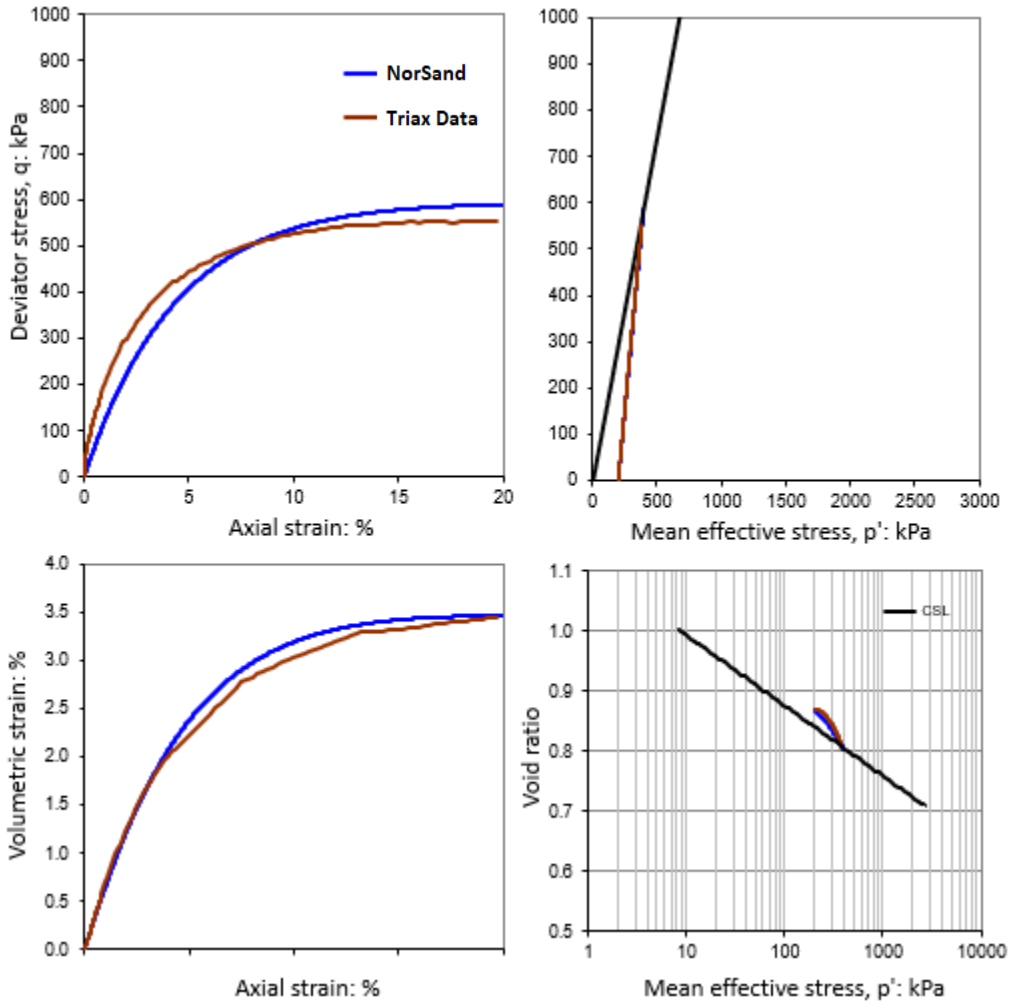

Figure 7-6 Comparison of UMT-CD-0.87 actual test results versus NorSand simulation

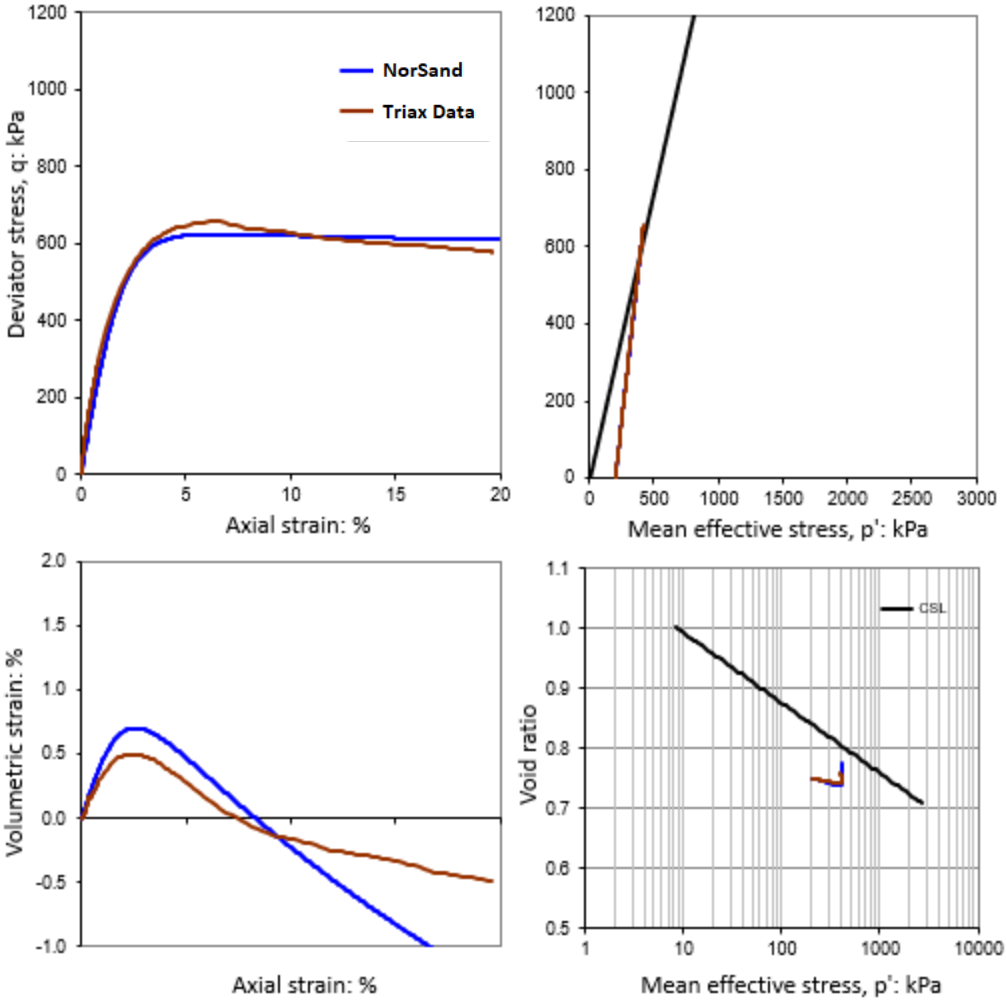

Figure 7-7 Comparison of UMT-CD-0.75 actual test results versus NorSand simulation

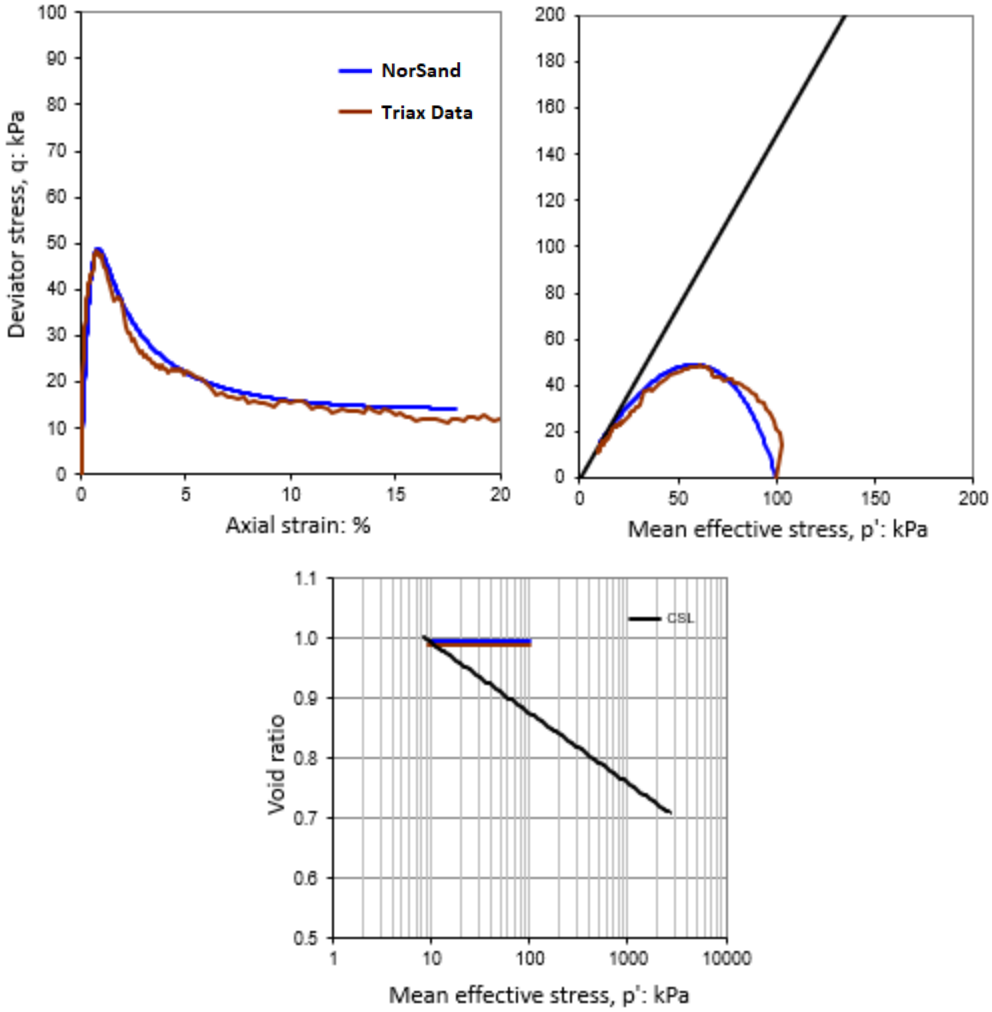

Figure 7-8 Comparison of UMT-CU-0.99 actual test results versus NorSand simulation

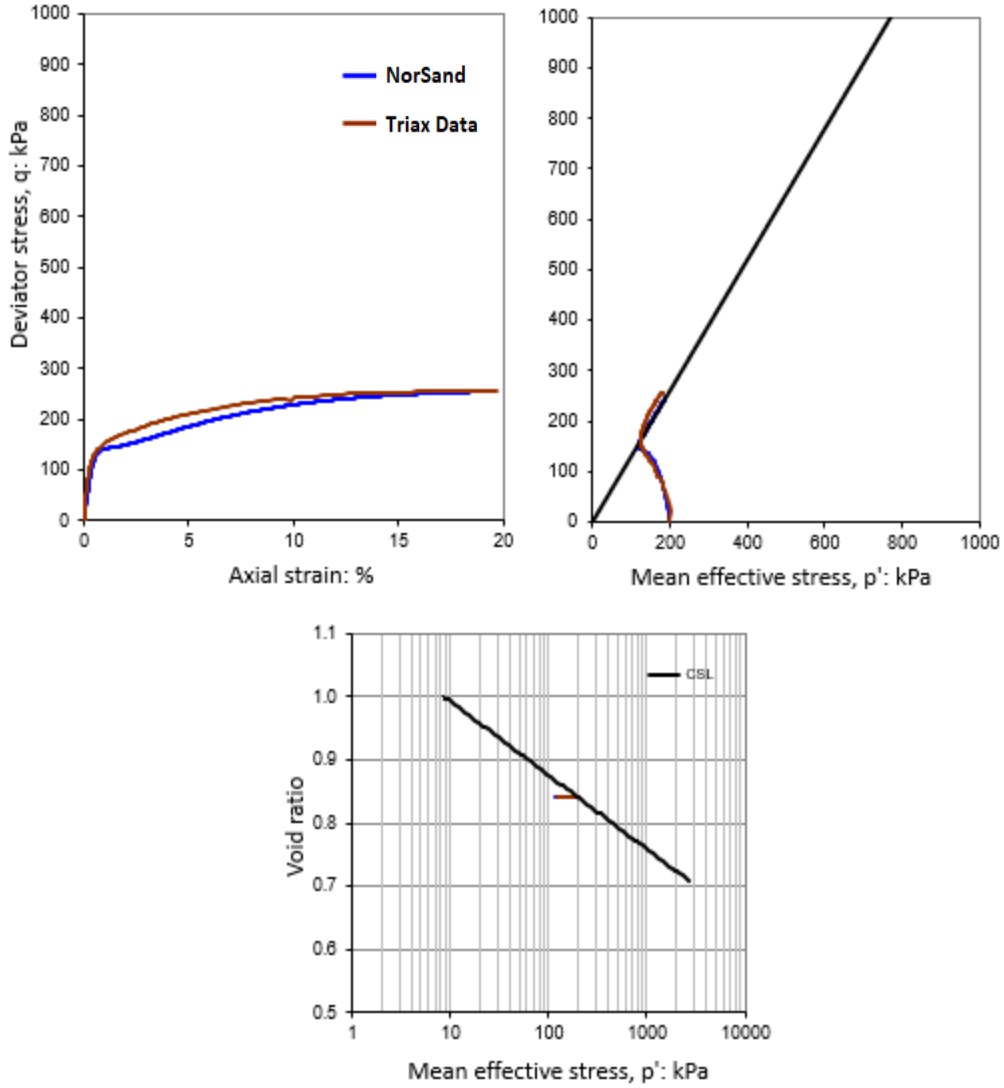

Figure 7-9 Comparison of UMT-CU-0.84 actual test results versus NorSand simulation

7.2 NorSand Simulation of Early-Age CPB

Similar critical state line (CSL) parameters, Γ and λ_{10}, were selected for early-age CPB based on the stress paths for uncemented and cemented specimens shown in Figure 5-3 provided in Chapter 5. The stress paths for CPB specimens at large strain suggest that the location of the CSL does not noticeably deviate from the location of the CSL for uncemented specimens. This is a reasonable observation since the amount of

binders used is 4.5% of the total solids. Additionally, the binders are fine-grained and their particle size distributions are not significantly different from the mine tailings. The slight cementitious bonds developed during the early-age curing time are not expected to impact the location of the CSL either as the soil fabric is destroyed at small strains. Large strains are required for specimens to reach the critical state.

The results of drained triaxial tests with dilative behavior at large strains were used to develop the peak dilatancy (D_{min}) versus peak stress ratio (η_{max}) and the state parameter (at η_{max}) relationships as shown in Figure 7-10 and Figure 7-11, respectively.

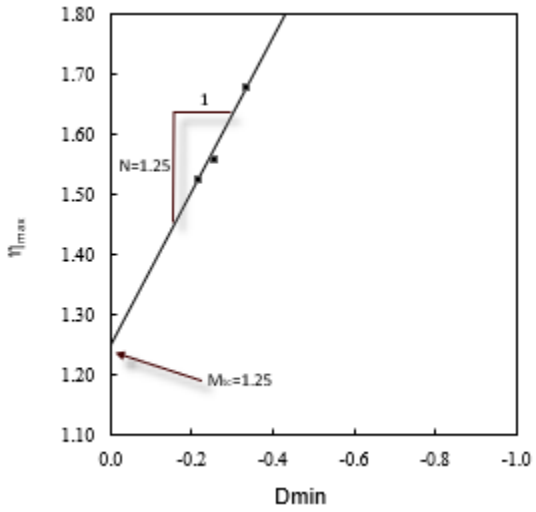

Figure 7-10. Peak dilatancy versus state parameter from drained tests to determine "χtc" for early-age CPB

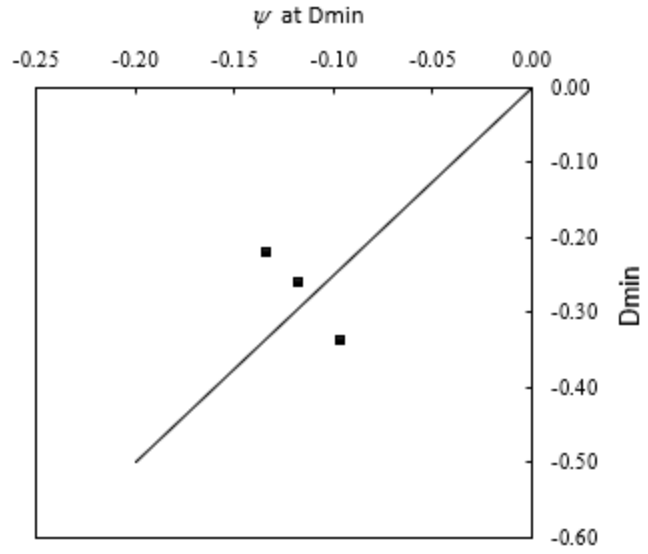

Figure 7-11. Peak dilatancy versus state parameter from drained tests to determine "χtc" for early-age CPB

Based on the triaxial test results as shown in Figure 7-10, the "N" and "M_{tc}" parameters were calculated to be 1.25. The "N" value is slightly greater than typical values for sands while the "M_{tc}" value is consistent with typical values for sands (Jefferies & Been, 2016). The "χ_{tc}" parameter was calculated to be 2.66, as shown in Figure 7-3. This value is consistent with typical values for sands (Jefferies & Been, 2016). The peak dilatancy (D_{min}) versus the state parameter (at η_{max}) graph indicated no predictable relationship between these two parameters for the early-age CPB. This is likely because for the early-age CPB specimens the dilatancy is governed by the cementitious bonds in addition to the initial density of the specimen. Calibrated "N", "M_{tc}", and "χ_{tc}" parameters based on the individual test results are shown on Table 7-1.

The G_{exp} parameter was obtained using the plot of calibrated G_{max} values and calibration through an iterative process as shown in Figure 7-12. The remaining parameters "H" was obtained through the calibration. Input and calibration parameters for

NorSand models are presented in Table 7-1. The cementitious bonds increased the plastic hardening modulus during an undrained loading as expected. Example comparisons between actual test results and NorSand simulations for the uncemented tailings are shown in Figure 7-13.

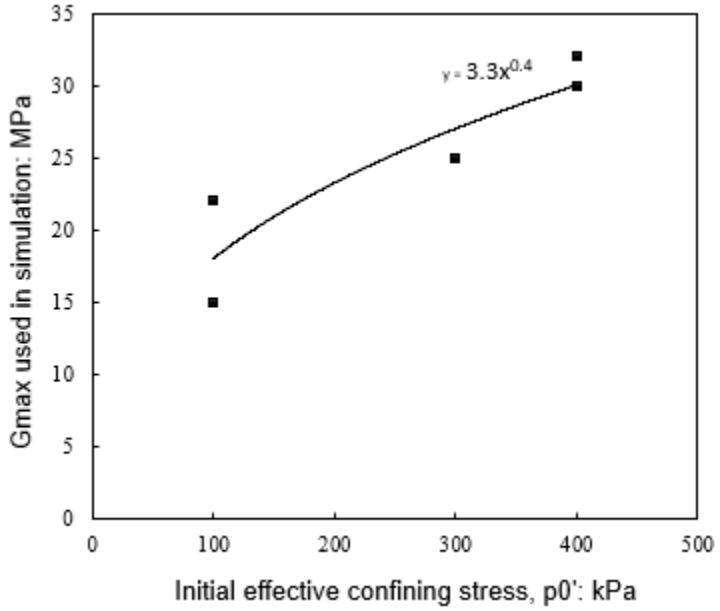

Figure 7-12. Plot of Gmax versus initial effective confining stress for early-age CPB

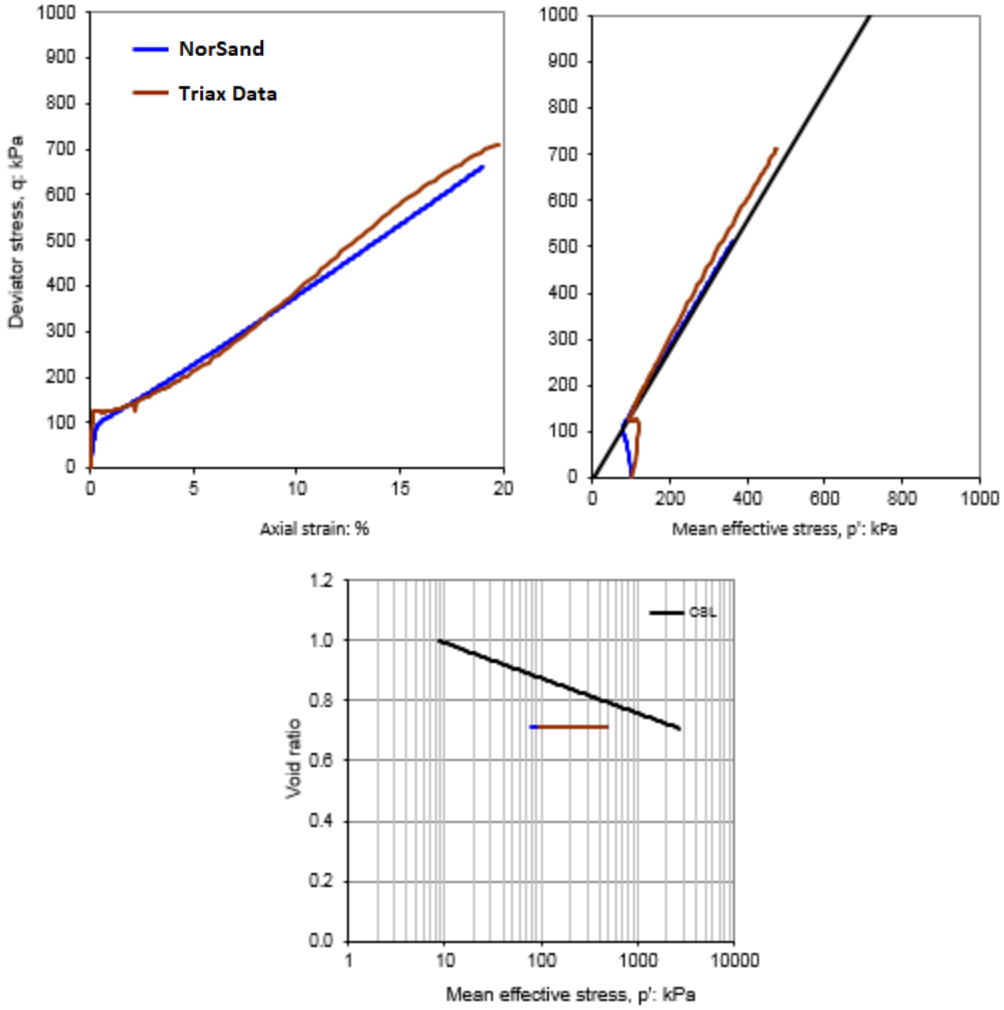

Figure 7-13 Comparison of CMT-CU-0.71 actual test results versus NorSand simulation.

7.3 Summary and Conclusions

1. NorSand was successfully used to model the behavior of non-plastic silt-sized mine tailings for a range of state parameters in drained and undrained loading.
2. In undrained loading, the CPB specimens (CMT-CU-0.71 and CMT-CU-0.69) indicated higher plastic hardening modulus comparing to the uncemented control specimens (UMT-CU-0.70 and UMT-CU-0.66).
3. NorSand was found to be applicable to early-age CPB particularly post-peak strength, approximately after 1% axial strain, due to breakage of cementitious bonds. The influence of cementation at small strains less than 1% was not fully captured by NorSand.

Chapter 8

Conclusions and Recommendations

The main objectives of this thesis were to: i) investigate the application of fly ash in preparation of CPB, ii) evaluate the mechanics of silt-sized mine tailings and early-age CPB through a framework of critical state soil mechanics, and iii) assess the applicability of constitutive modes to predict the behavior of early-age CPB.

The conclusions and recommendations are based on the experiments conducted and the material used in this study, and may only be applicable for similar material and type of experiments. However, the general framework of investigation can be applied to other mines' materials and geo-mechanical parameters.

8.1 Conclusions

8.2 Application of Fly Ash in CPB Preparation

1. class C fly ash can be used to replace a significant portion of Portland cement (PC) in CPB. The replacement of PC with class C fly ash is expected to result in a cheaper mix design since fly ash is usually much cheaper than PC.
2. The replacement of PC with fly ash will increase the initial and final setting times of CPB. The reduction of PC to half and addition of class C fly ash increased the initial and final setting times by approximately 3.5 times.
3. The application of fly ash as a single binder agent to improve the geotechnical properties of tailings for the surface disposal method was evaluated. The addition of 10% class C fly ash to the thickened tailings (SC=70%) did not improve the geotechnical properties of the tailings.
4. The application of fly ash as a single binder agent to improve the geotechnical properties of tailings for the backfilling purposes was evaluated. The addition of

7% class C fly ash to the paste tailings (SC=78%) indicated improvement in the geotechnical properties of the tailings.

8.3 Monotonic Response

1. The development of the critical state line and state parameters was a successful and robust technique to explain the behavior of silt-sized non-plastic mine tailings and the early-age CPB. The comparison between the responses of cemented and uncemented samples in the q-p' plane suggests that the positions of the CSL for early-age CPB and uncemented tailings are fairly similar; however, the similarity or proximity of the CSL positions could not be established in the e-log p' plane as CPB samples did not reach the critical state. The field void ratios can be used along with the CSL to predict the liquefaction susceptibility of early-age CPB.
2. Tailings specimens with an initial void ratio larger than their corresponding critical void ratio experienced static liquefaction in undrained loading. Two specimens at confining pressures of 50 kPa and 100 kPa with fairly similar initial state parameters (0.13 versus 0.12) resulted in full liquefaction and limited liquefaction, respectively.
3. Specimens prepared using the slurry deposition method resulted in state parameters smaller than -0.11, and therefore did not experience static liquefaction due to their dilative behavior at large strains. The dense state of specimens can be attributed to the consolidation process in the triaxial setup. However, the CPB may not consolidate in the field if no drainage is present. Therefore, it is important to use the field void ratios to assess the liquefaction susceptibility of early-age CPB.

4. The CPB specimens generated smaller excess pore pressures than the uncemented ones. They also indicated larger reductions in excess pore pressure after the phase transformation point suggesting more dilative behavior than their corresponding uncemented specimens (control specimens).

8.4 Cyclic Response

1. The CDSS test results indicated the cyclic mobility type of response for the CPB with fly ash. The behavior of the CPB with fly ash generally was found to be consistent with the behavior of CPB with no fly ash in previous studies.
2. Based on the cyclic test results, the addition of fly ash was found to have no adverse impact on achieving significant liquefaction resistance as CPB cures.
3. The CPB prepared for this study with 50% replacement of PC with fly ash indicated adequate resistance against liquefaction at its initial setting time for a reasonable large earthquake in most seismic regions.
4. The UCS value at the initial setting time (22 hours) for to the CPB specimens tested under cyclic loading was obtained to be 78 kPa. This observation implies the proposed minimum UCS values of 60-75 kPa for the liquefaction resistance criterion under cyclic loading (Suazo et al., 2017) can be successfully used for CPB with fly ash.

8.5 Constitutive Model of CPB

1. NorSand was successfully used to model the behavior of silt-sized non-plastic mine tailings for a range of state parameters in drained and undrained loading.
2. In undrained loading, the CPB specimens (CMT-CU-0.71 and CMT-CU-0.69) indicated higher plastic hardening modulus compared to the uncemented control specimens (UMT-CU-0.70 and UMT-CU-0.66).

3. NorSand was found to be applicable to early-age CPB particularly post peak strength, approximately after 1% axial strain, due to breakage of cementitious bonds. The influence of cementation at small strains less than 1% was not fully captured by NorSand.

8.6 Recommendations and Future works

1. The application of class F fly ash in the CPB preparation needs to be studied.
2. Higher dosages of class C fly ash may have potential applications to improve the mechanical properties of thickened tailings. High fly ash content mix designs can be studied for a fly ash and mine tailings co-disposal scenario.
3. The consolidation of the slurry deposition specimens results a dense state of tailings. Innovative techniques need to be used to make slurry deposition specimens with positive state parameter (loose specimens).

Appendix A

Cyclic Direct Simple Shear Test Results

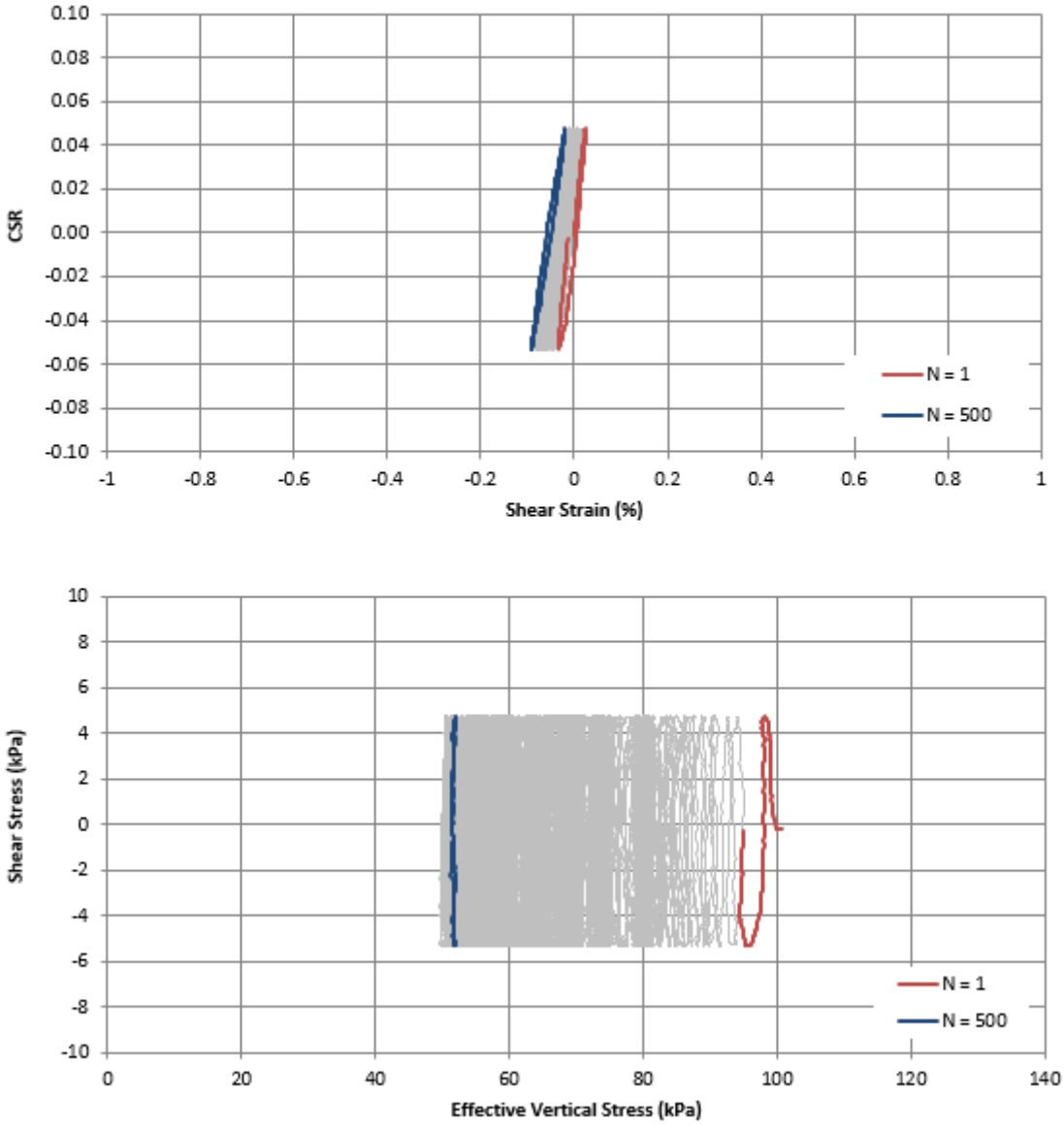

Figure A.1. Response of uncemented tailings specimen UMT-0.05 tested at CSR = 0.05 and σvc'=100 kPa, cyclic stress ratio versus shear strain (top), stress path (bottom).

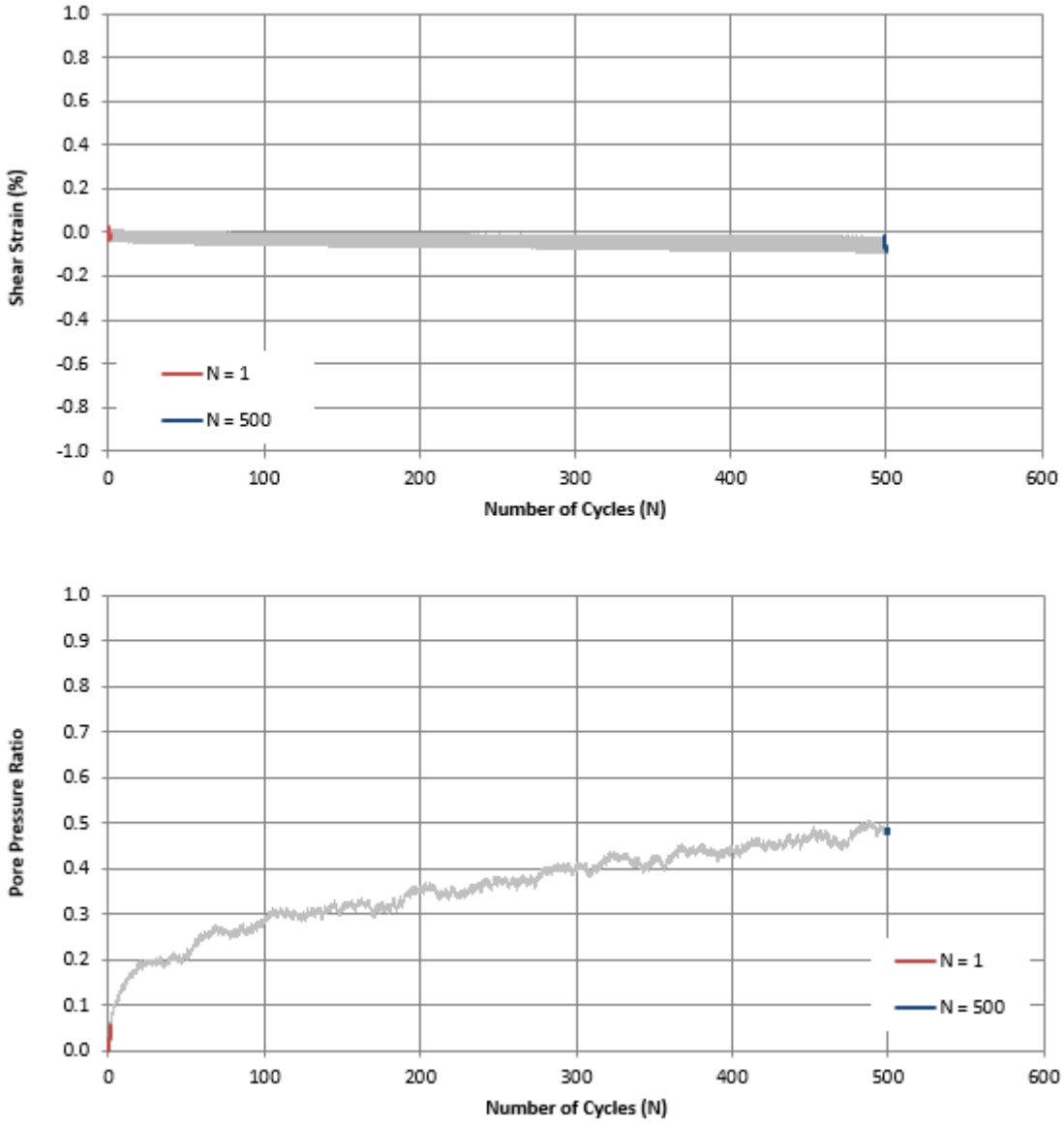

Figure A.2. Response of uncemented tailings specimen UMT-0.05 tested at CSR = 0.05 and σvc'=100 kPa, shear strain versus number of cycles response (top), pore pressure ratio versus number of cycles (bottom).

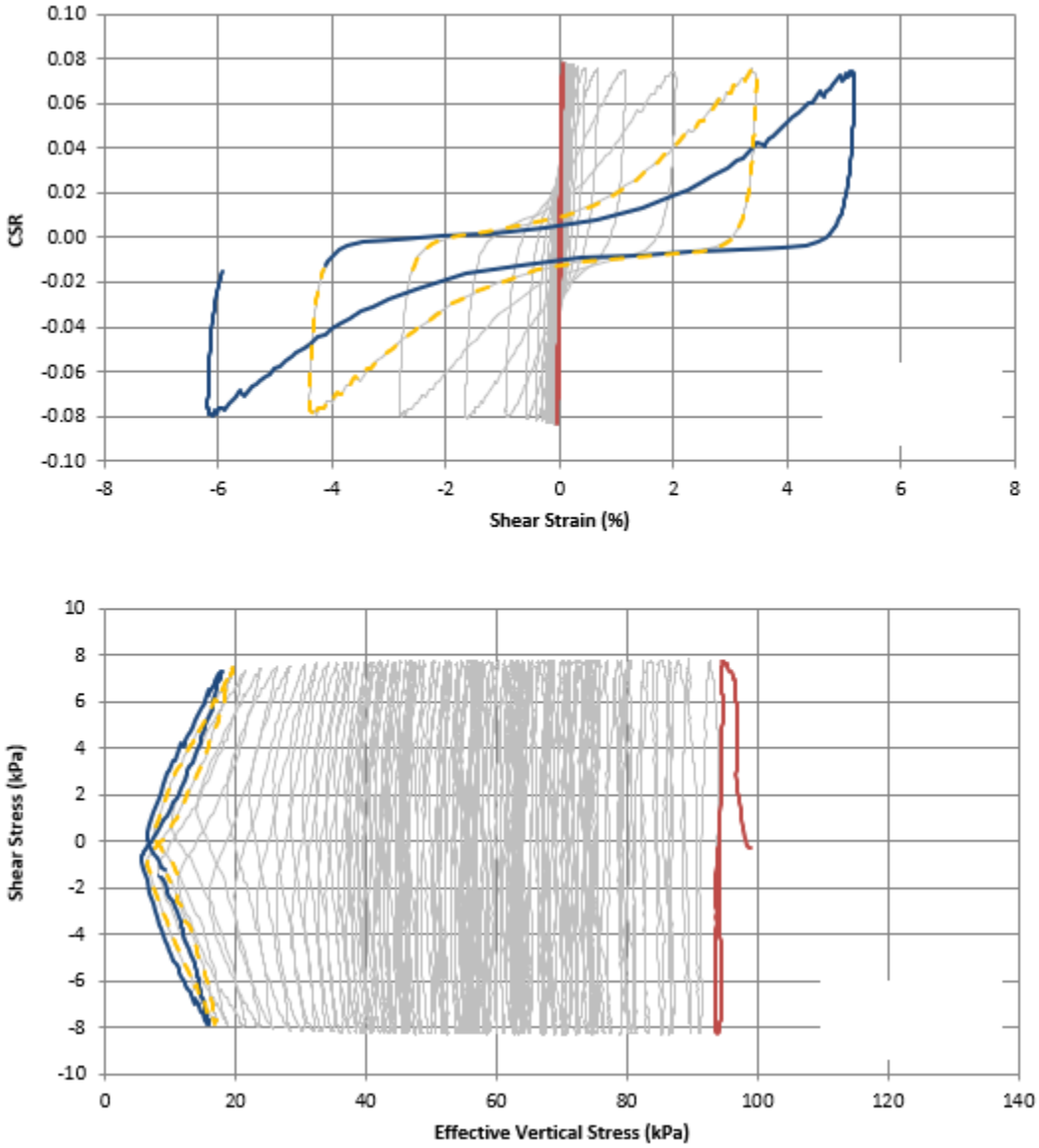

Figure A.3. Response of uncemented tailings specimen UMT-0.08 tested at CSR = 0.08 and σvc'=100 kPa, cyclic stress ratio versus shear strain (top), stress path (bottom).

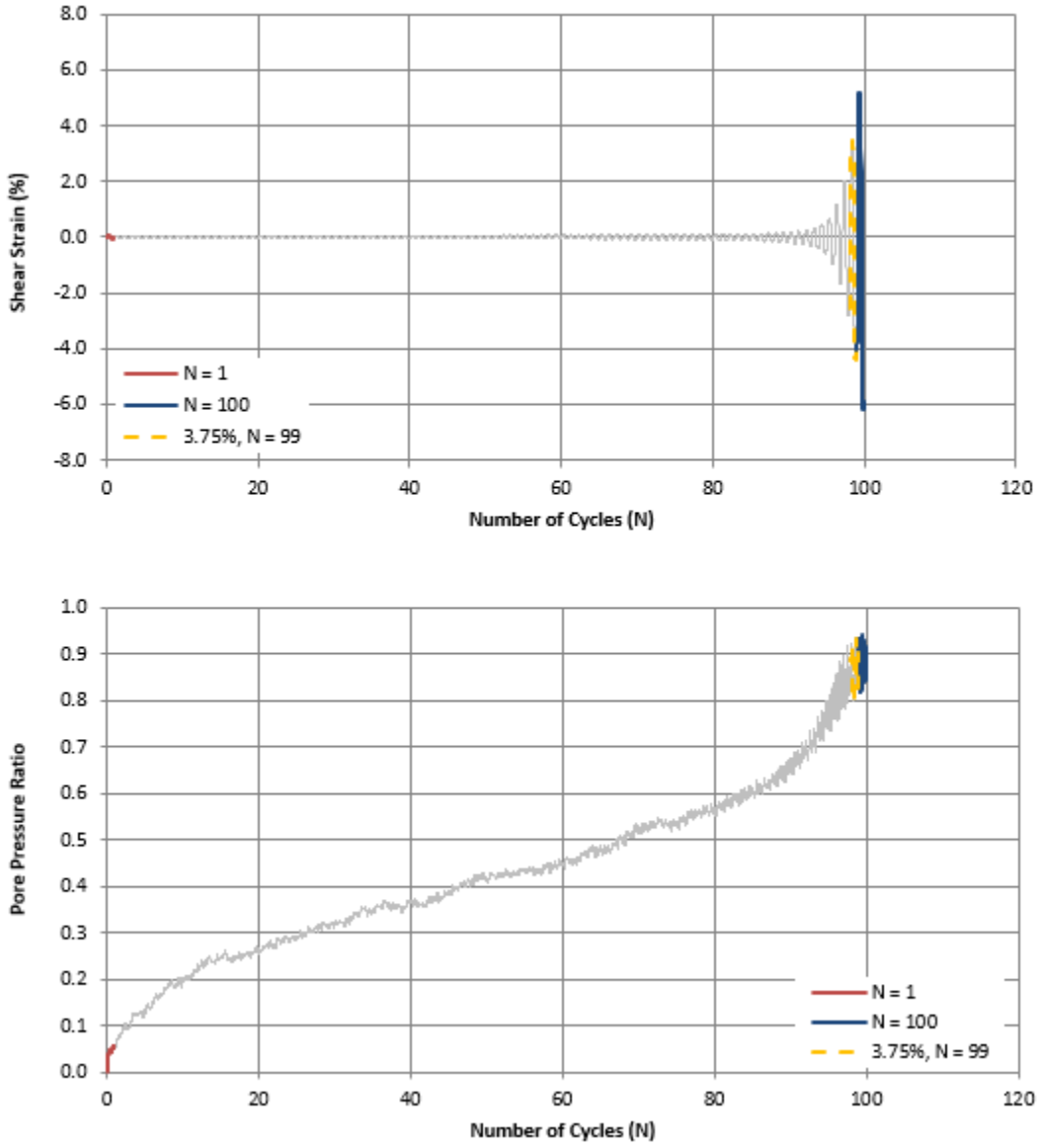

Figure A.4. Response of uncemented tailings specimen UMT-0.08 tested at CSR = 0.08 and σvc'=100 kPa, shear strain versus number of cycles response (top), pore pressure ratio versus number of cycles (bottom).

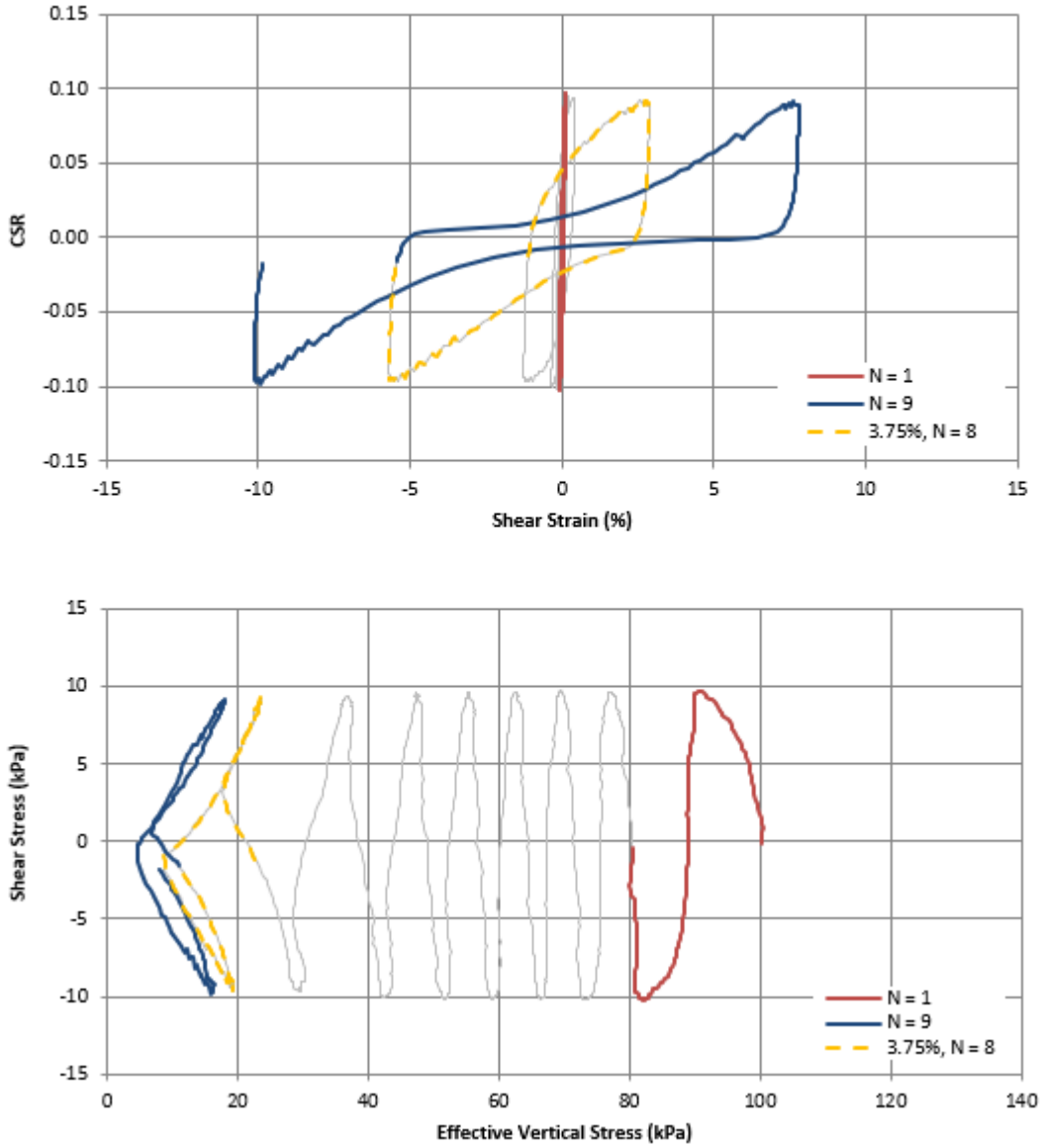

Figure A.5. Response of uncemented tailings specimen UMT-0.10 tested at CSR = 0.10 and σvc'=100 kPa, cyclic stress ratio versus shear strain (top), stress path (bottom).

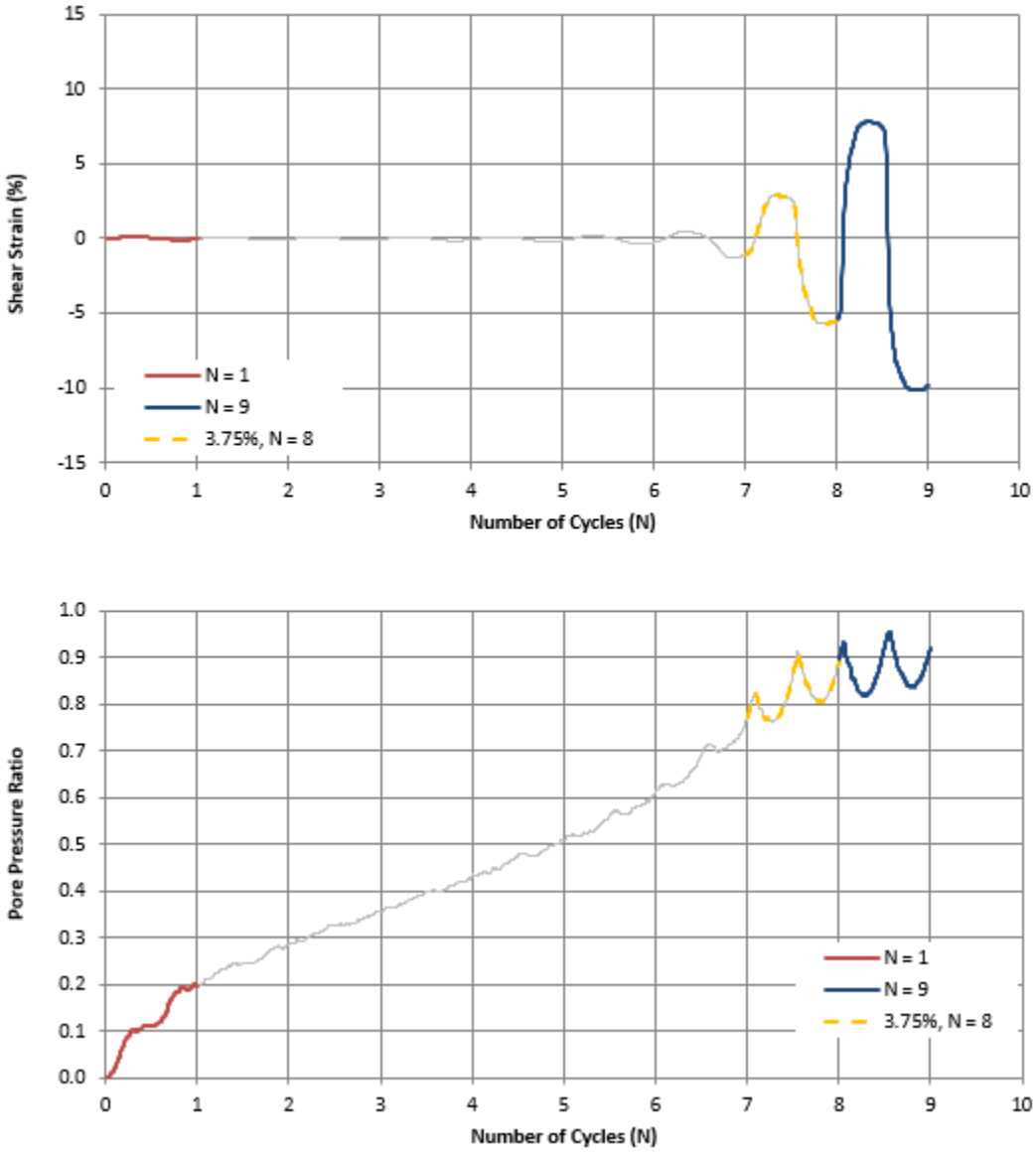

Figure A.6. Response of uncemented tailings specimen UMT-0.10 tested at CSR = 0.10 and σvc'=100 kPa, shear strain versus number of cycles response (top), pore pressure ratio versus number of cycles (bottom).

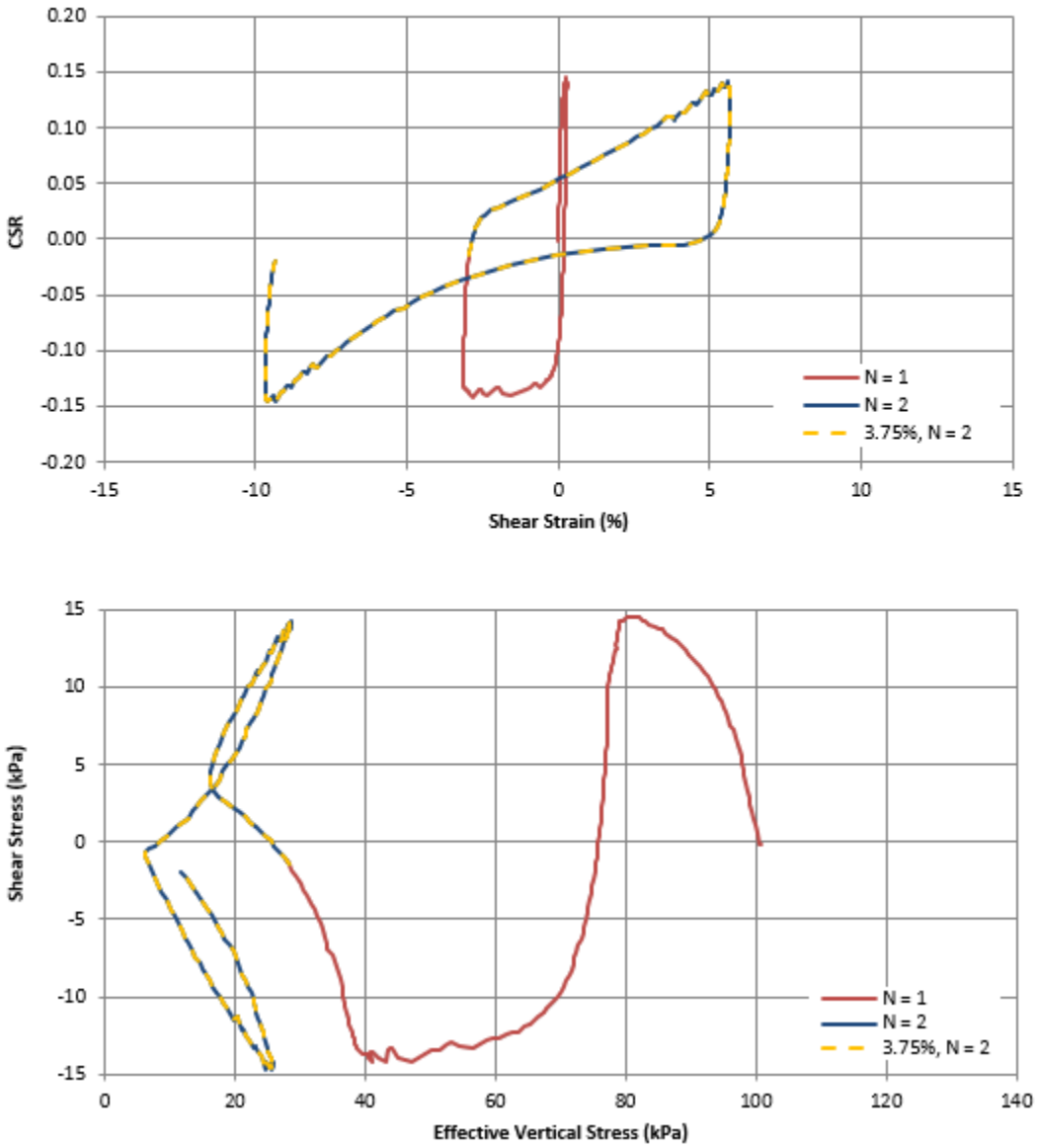

Figure A.7. Response of uncemented tailings specimen UMT-0.15 tested at CSR = 0.15 and σvc'=100 kPa, cyclic stress ratio versus shear strain (top), stress path (bottom).

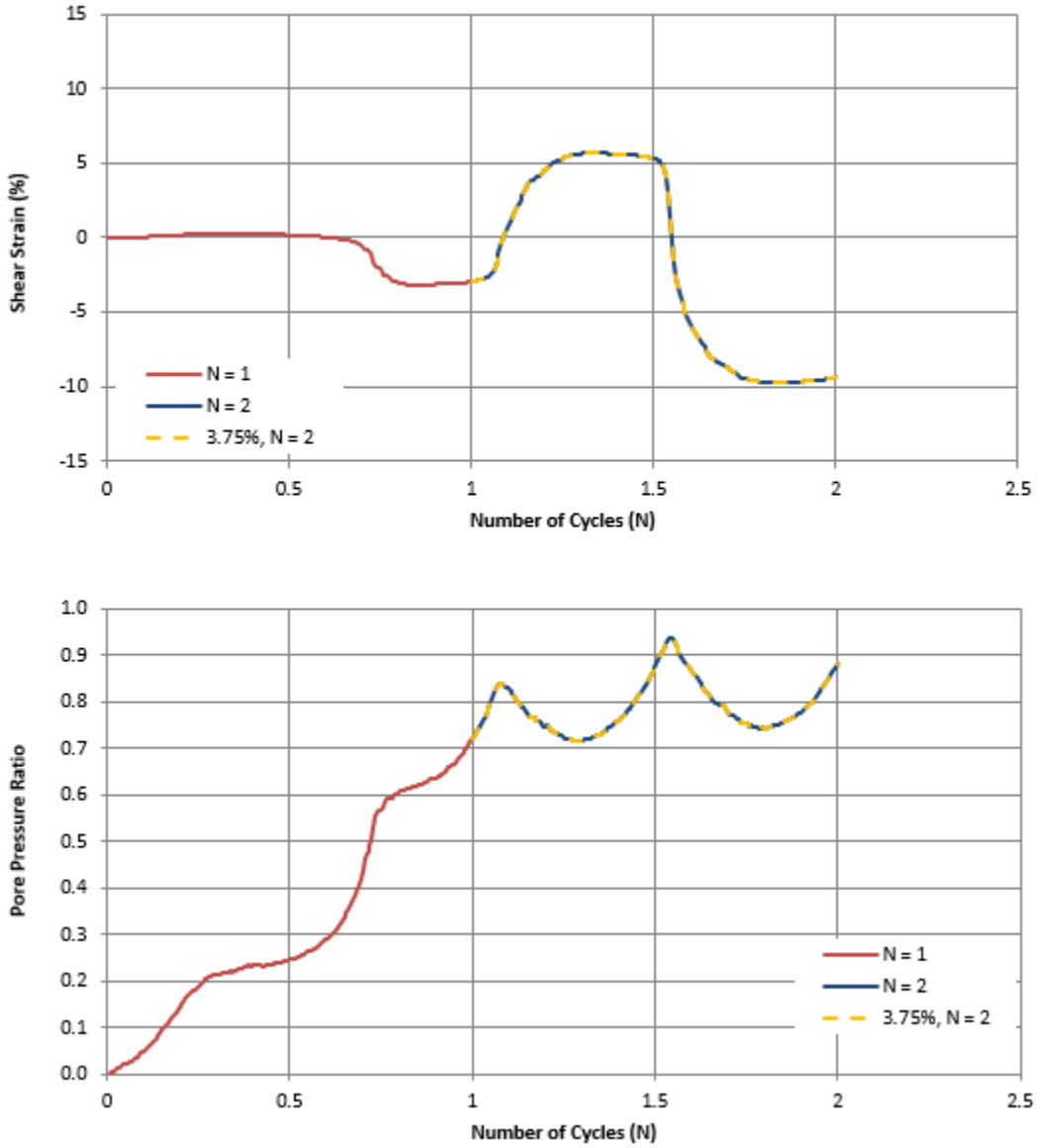

Figure A.8. Response of uncemented tailings specimen UMT-0.15 tested at CSR = 0.15 and σvc'=100 kPa, shear strain versus number of cycles response (top), pore pressure ratio versus number of cycles (bottom).

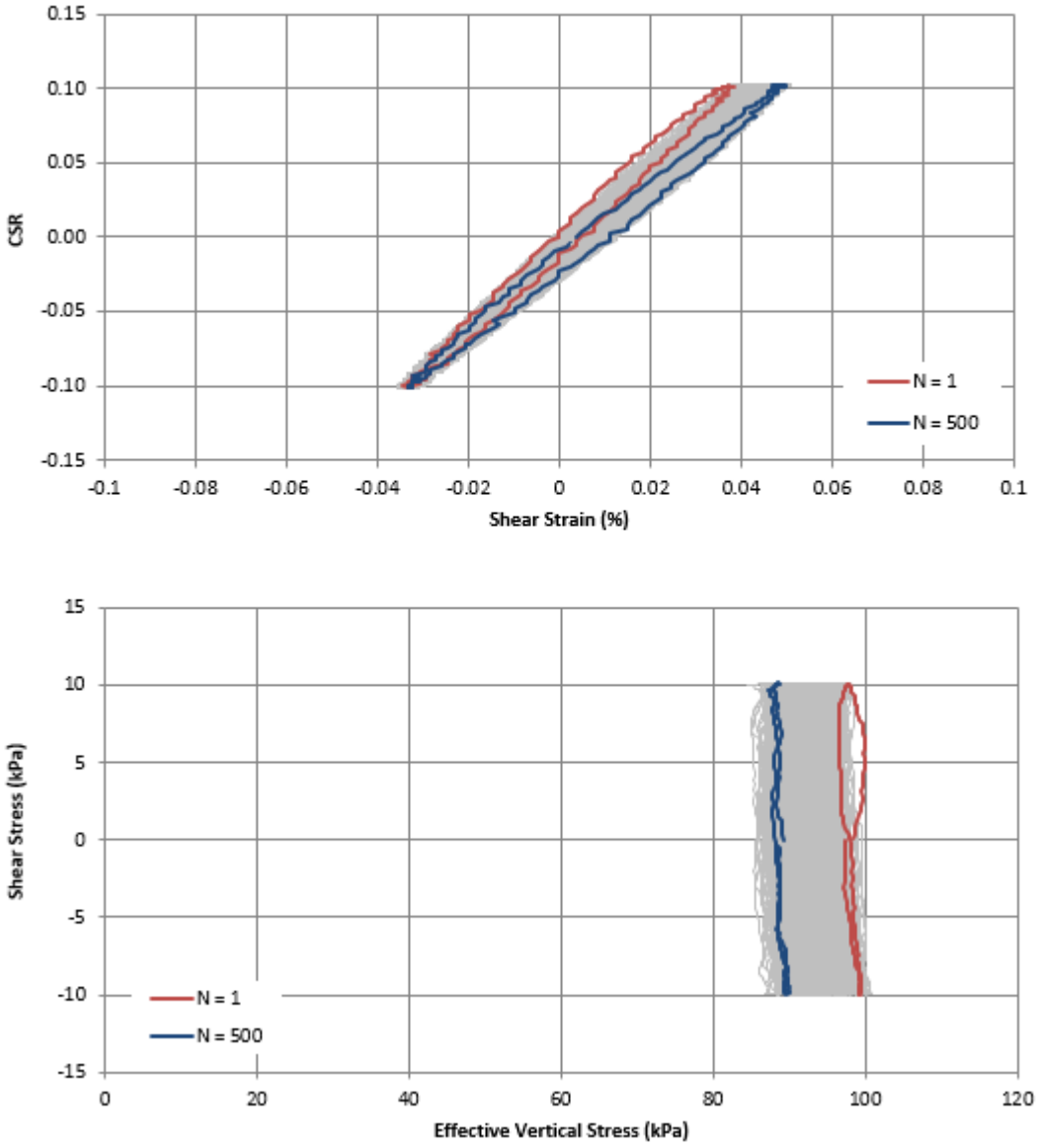

Figure A.9. Response of CPB specimen CMT-0.10 tested at CSR = 0.10 and σvc'=100 kPa, cyclic stress ratio versus shear strain (top), stress path (bottom).

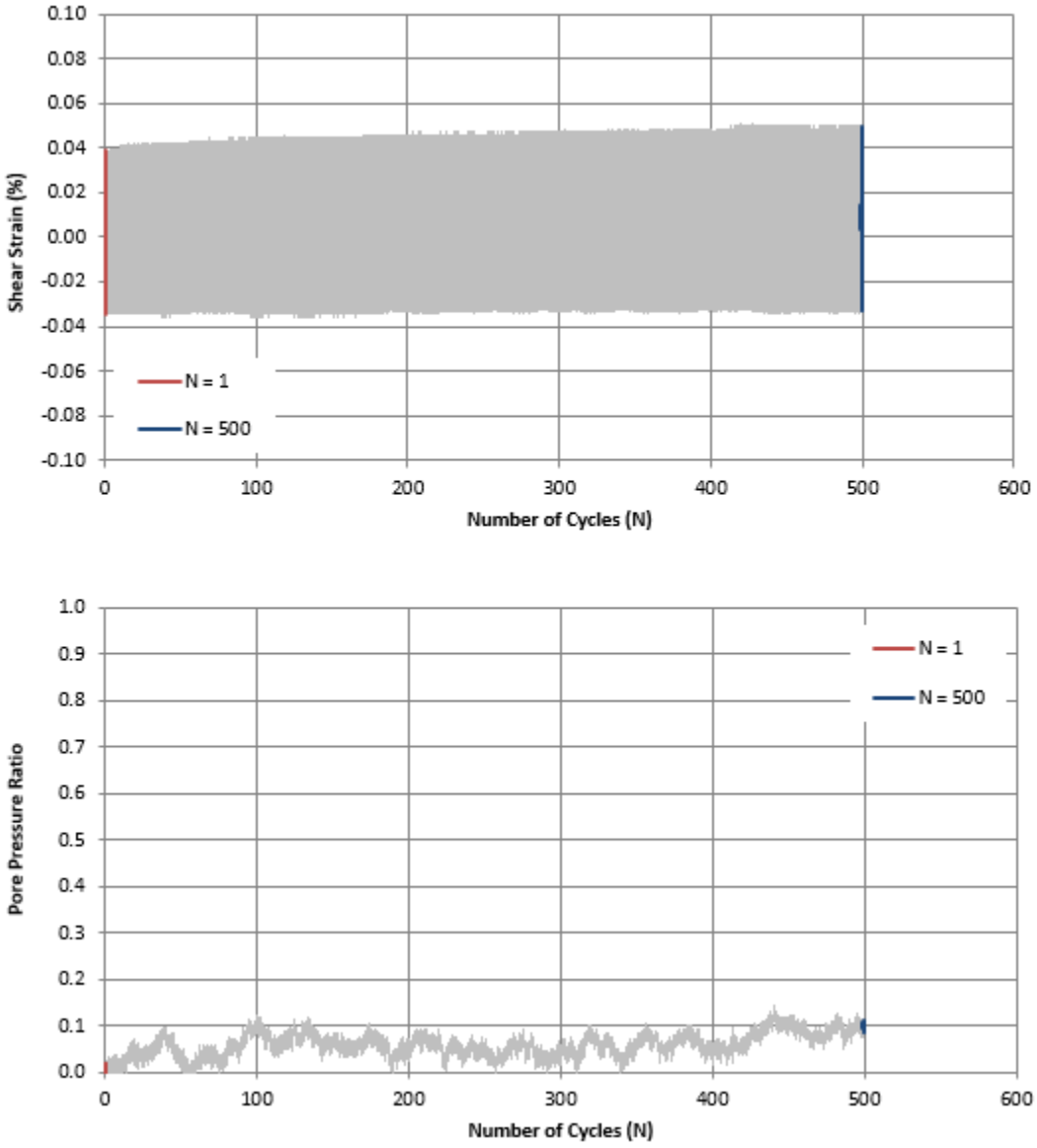

Figure A.10. Response of uncemented tailings specimen CMT-0.10 tested at CSR = 0.10 and σvc'=100 kPa, shear strain versus number of cycles response (top), pore pressure ratio versus number of cycles (bottom).

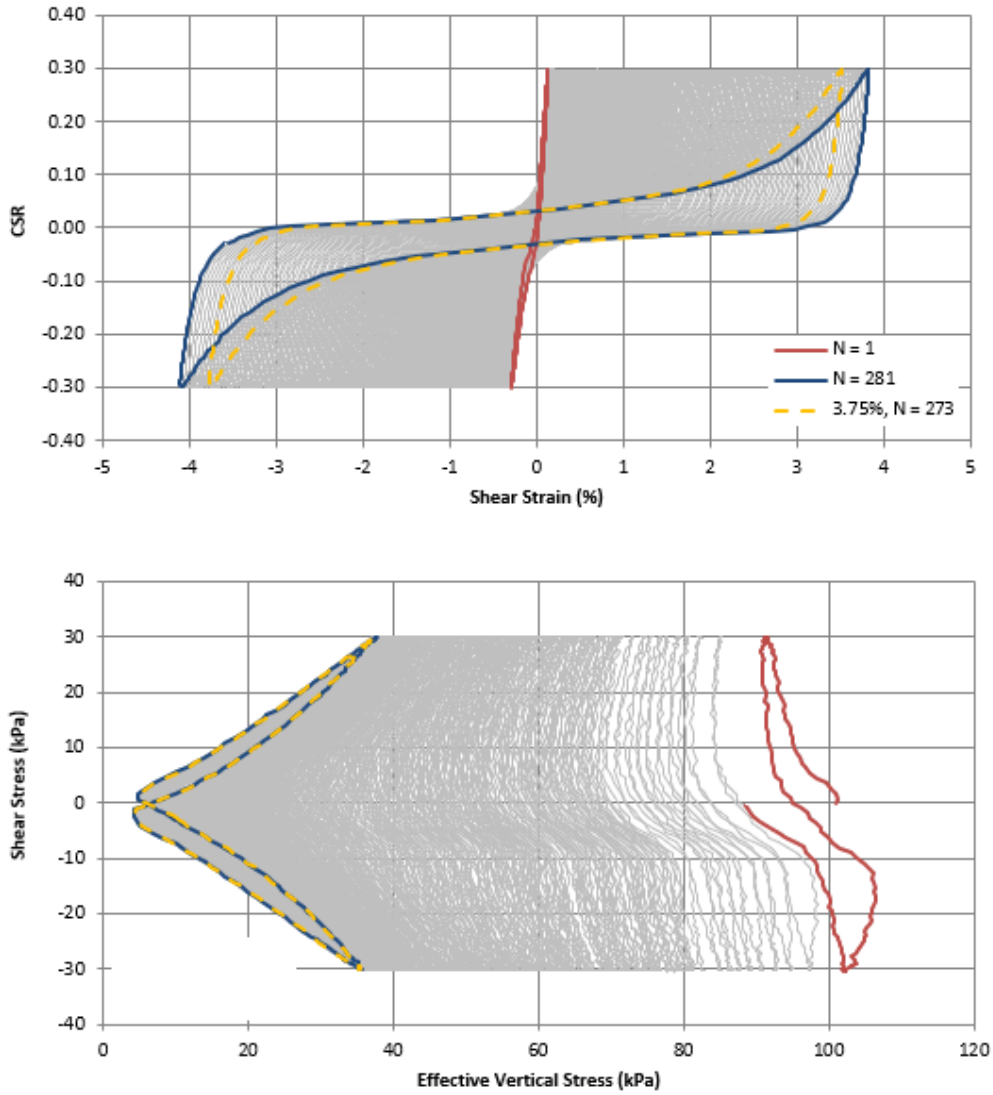

Figure A.11. Response of CPB specimen CMT-0.30 tested at CSR = 0.30 and σvc'=100 kPa, cyclic stress ratio versus shear strain (top), stress path (bottom).

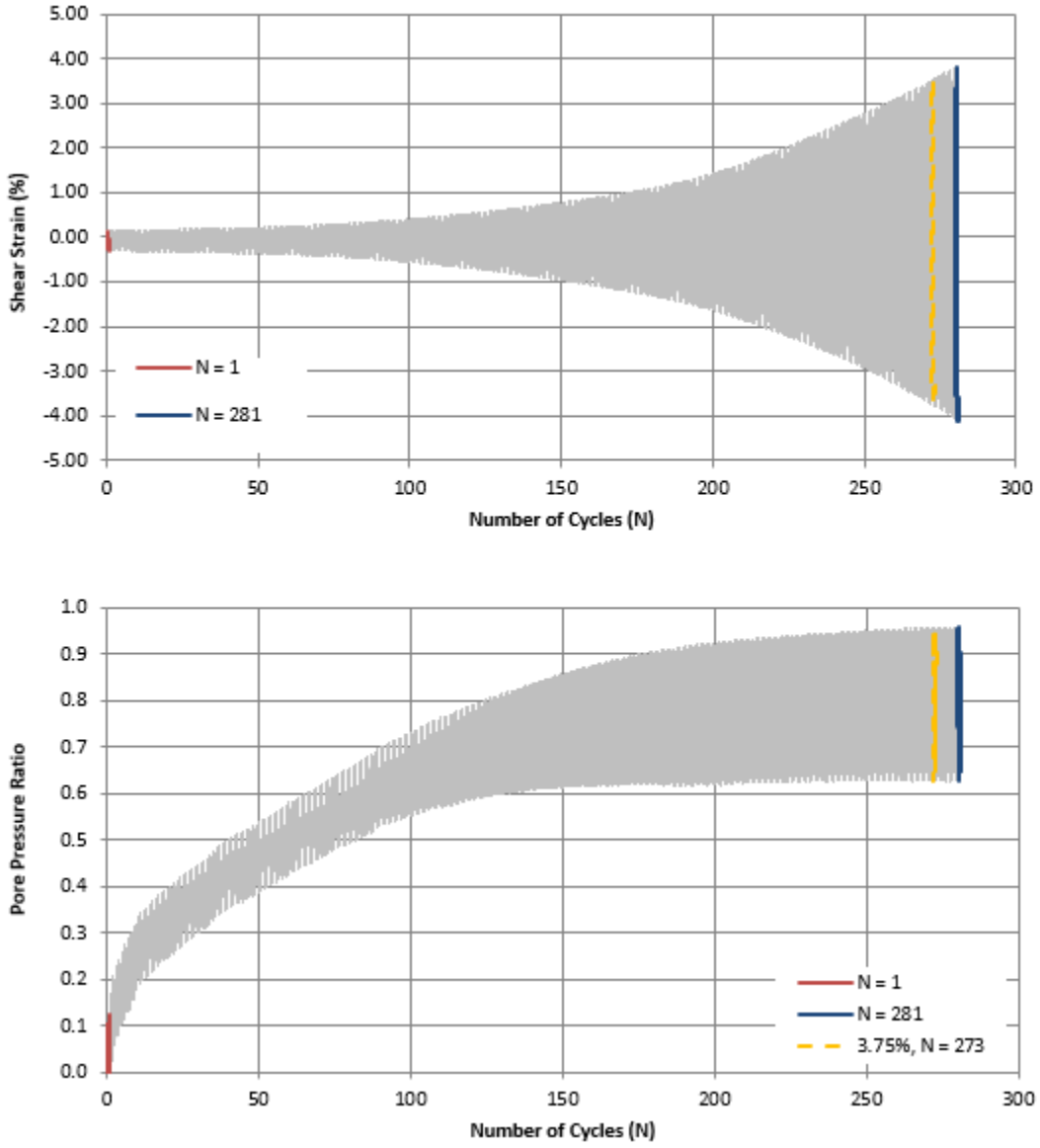

Figure A.12. Response of uncemented tailings specimen CMT-0.30 tested at CSR = 0.30 and σvc'=100 kPa, shear strain versus number of cycles response (top), pore pressure ratio versus number of cycles (bottom).

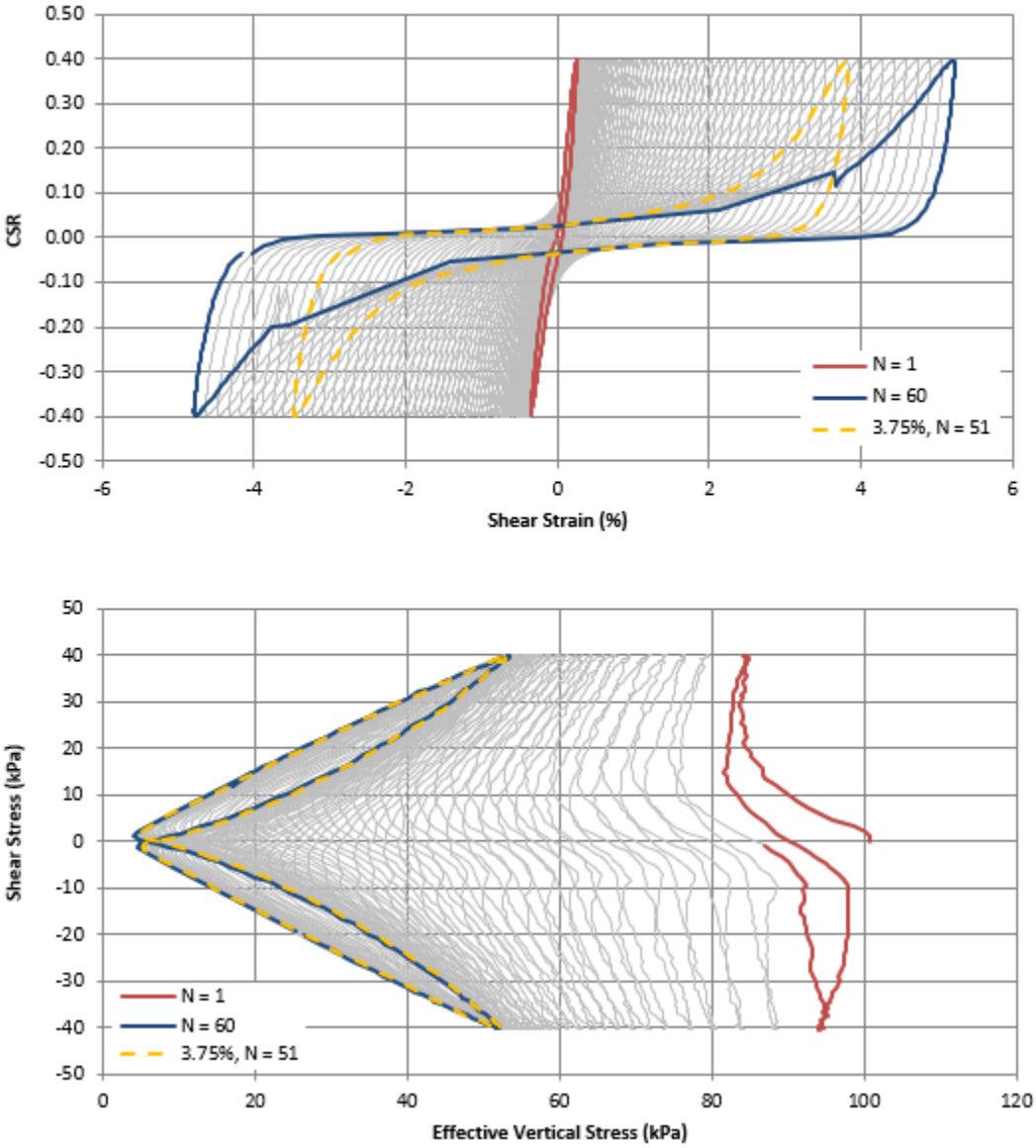

Figure A.13. Response of CPB specimen CMT-0.40 tested at CSR = 0.40 and σvc'=100 kPa, cyclic stress ratio versus shear strain (top), stress path (bottom).

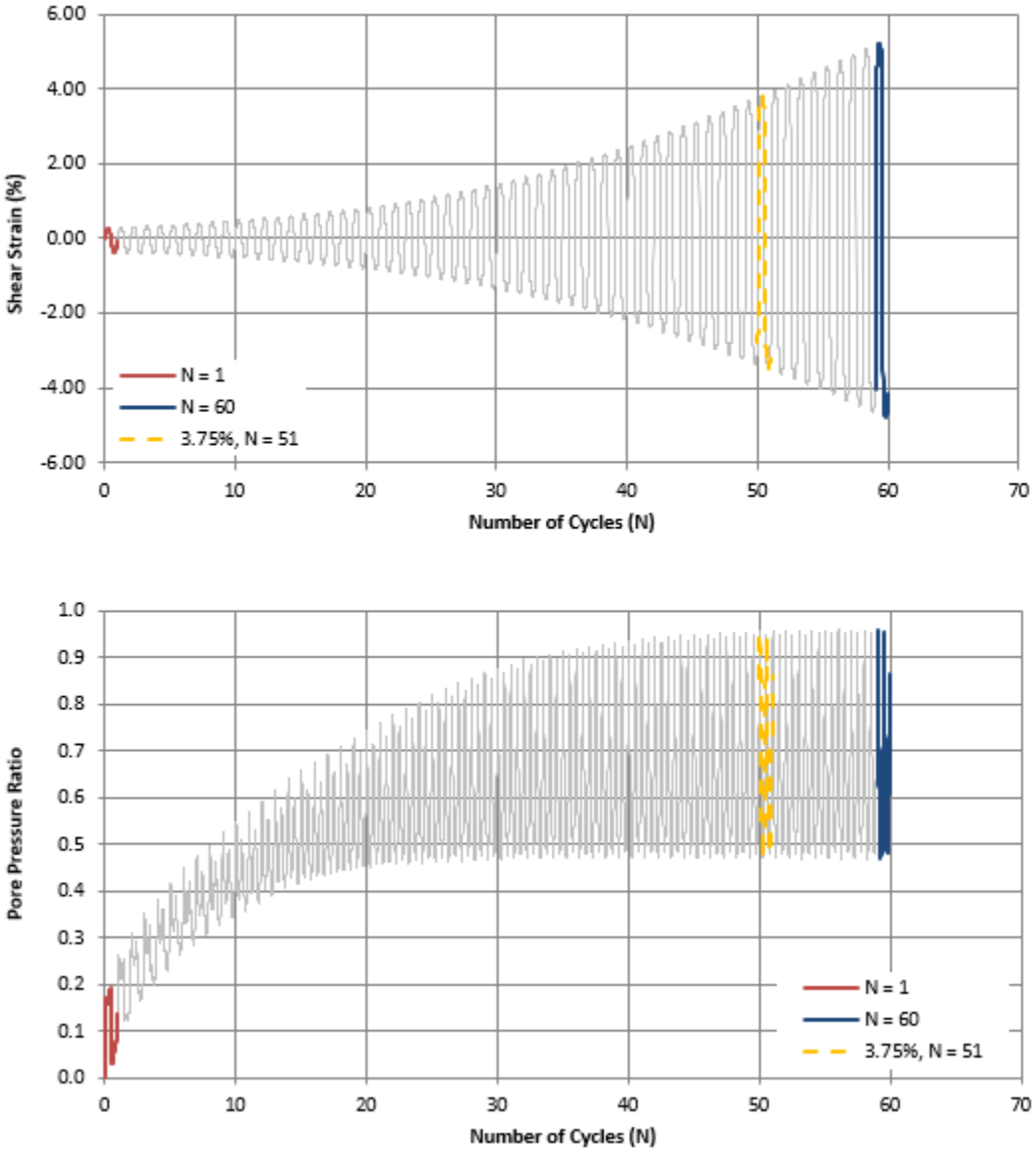

Figure A.14. Response of uncemented tailings specimen CMT-0.40 tested at CSR = 0.40 and σvc'=100 kPa, shear strain versus number of cycles response (top), pore pressure ratio versus number of cycles (bottom).

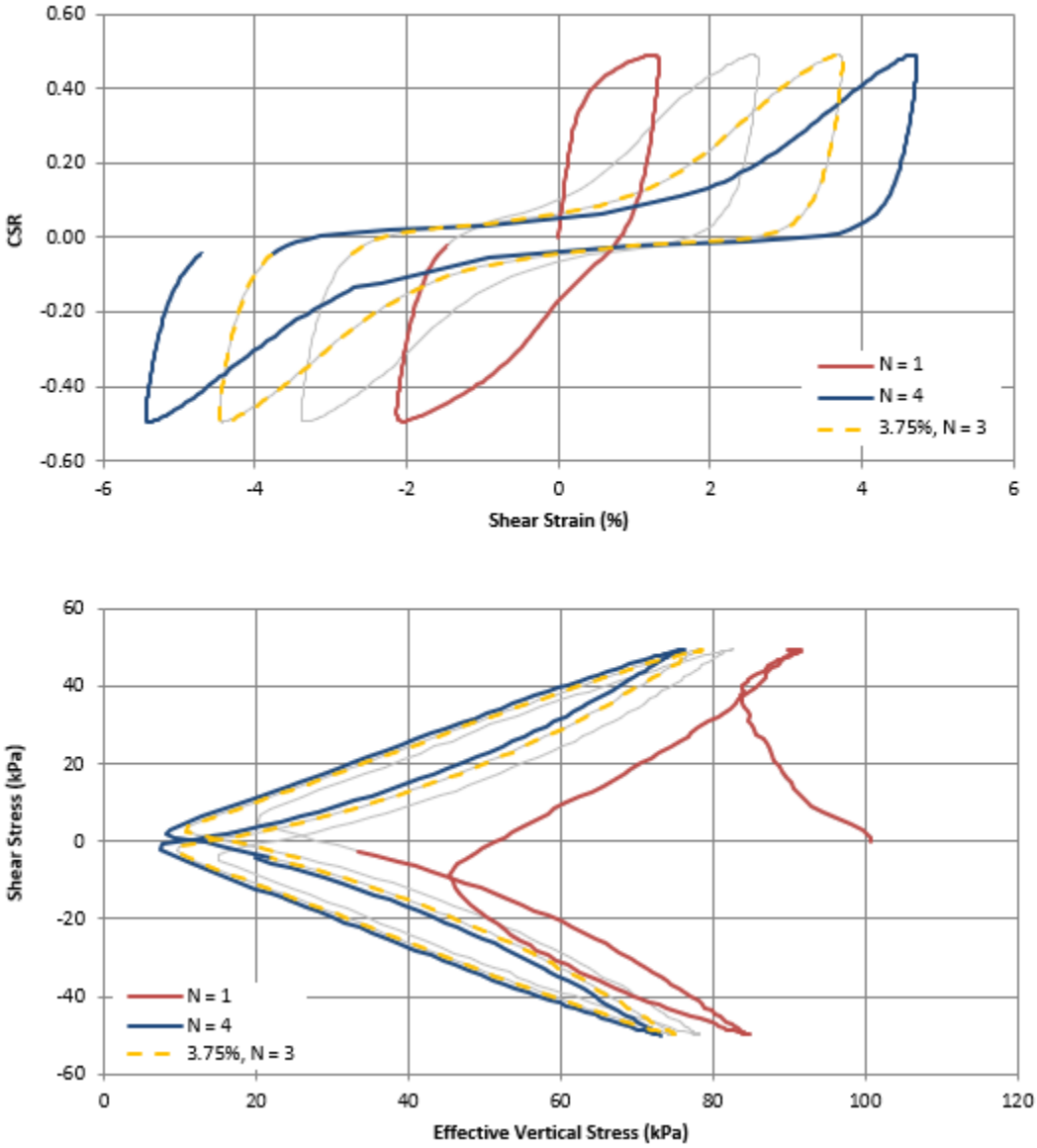

Figure A.15. Response of CPB specimen CMT-0.50 tested at CSR = 0.50 and σvc'=100 kPa, cyclic stress ratio versus shear strain (top), stress path (bottom).

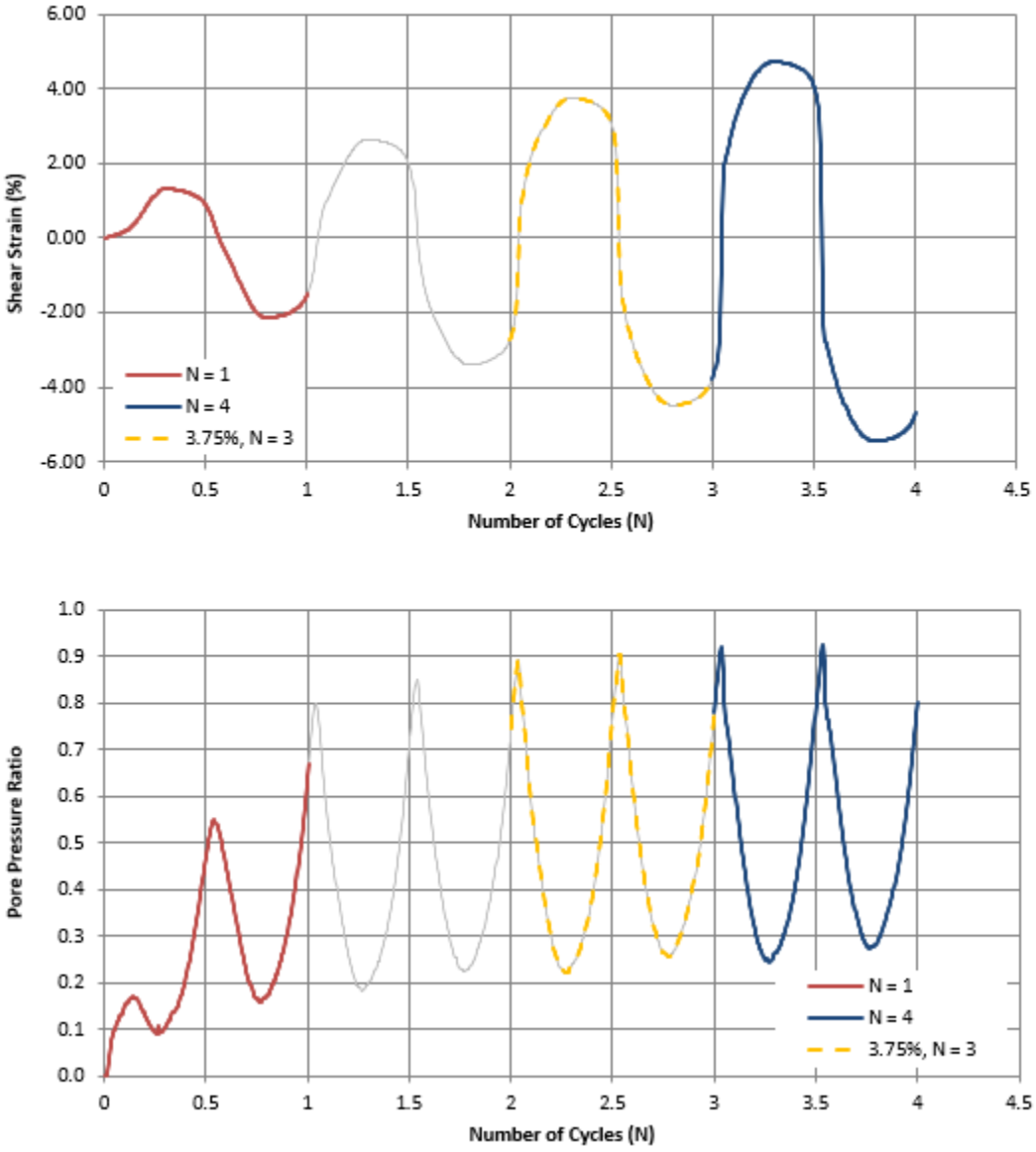

Figure A.16. Response of uncemented tailings specimen CMT-0.50 tested at CSR = 0.50 and σvc'=100 kPa, shear strain versus number of cycles response (top), pore pressure ratio versus number of cycles (bottom).

Appendix B

NorSand Simulations

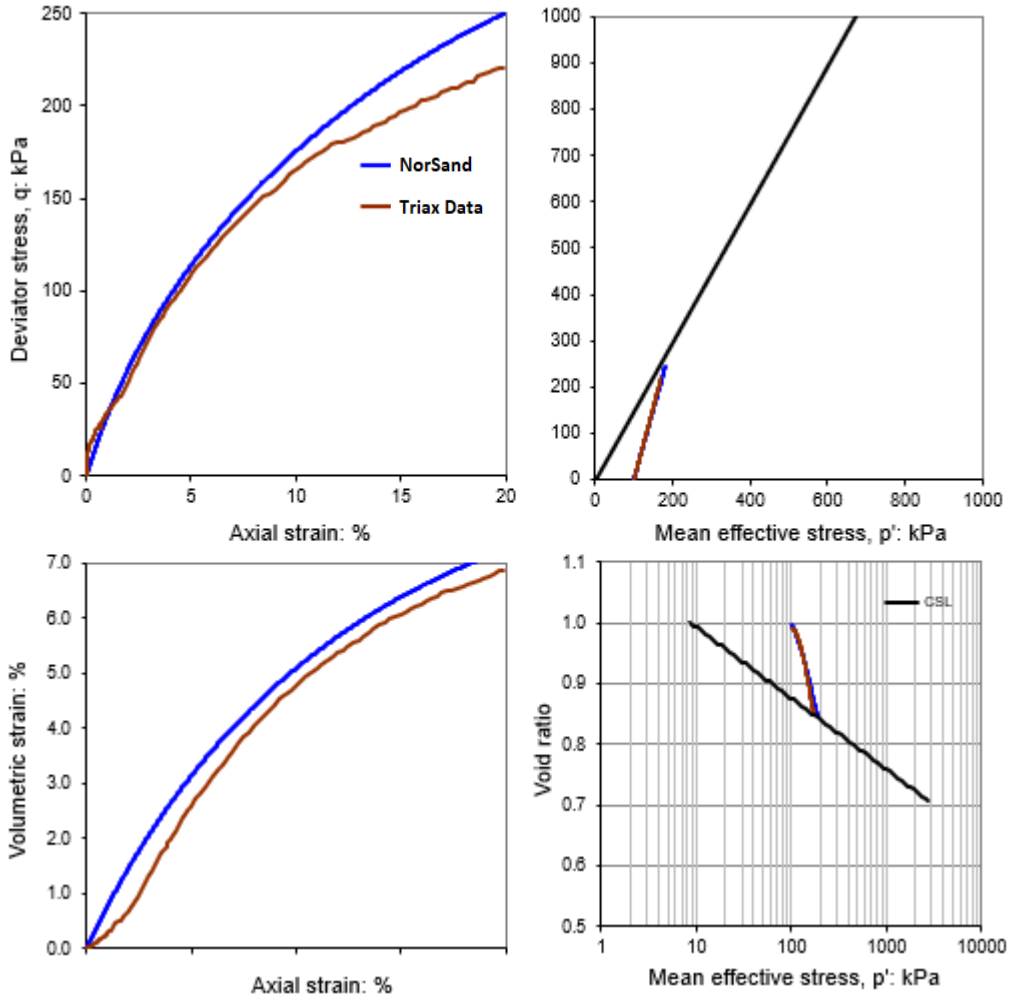

Figure B.1. Comparison of UMT-CD-0.99 actual test results versus NorSand simulation.

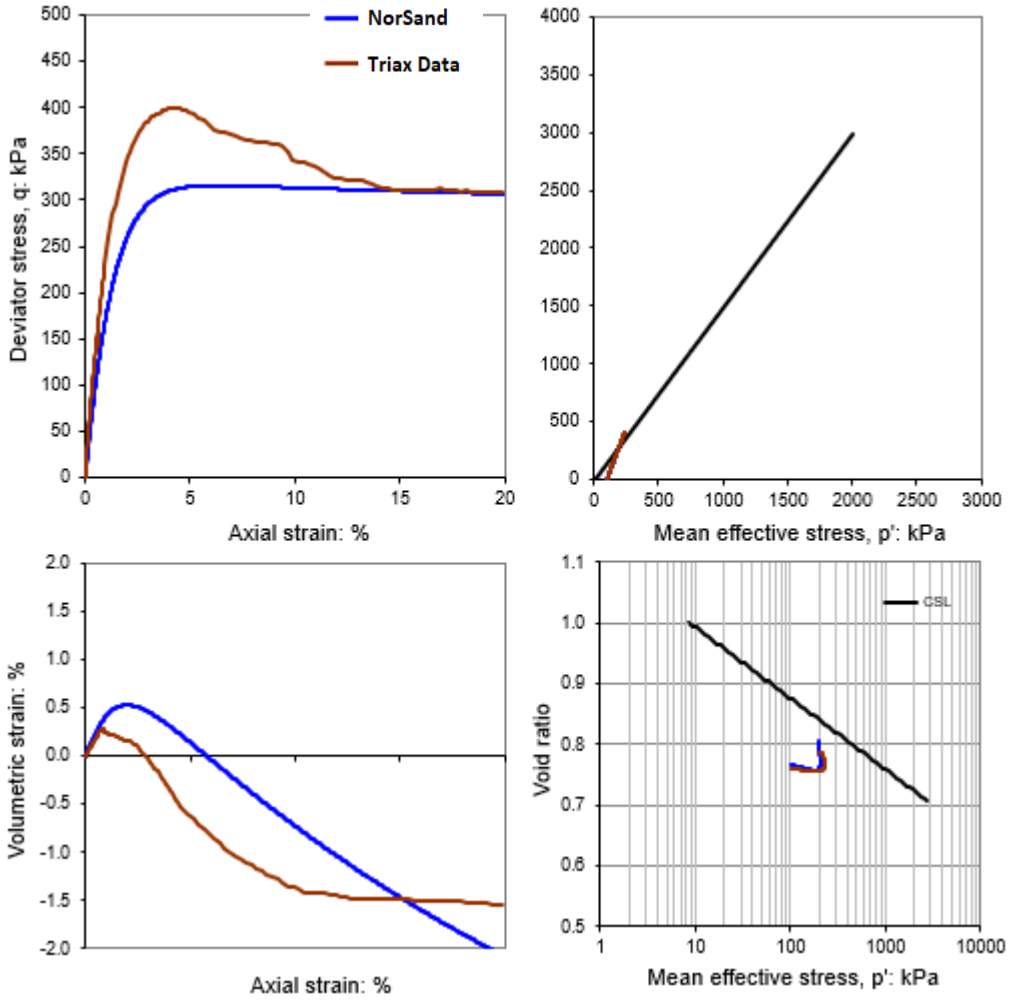

Figure B.2. Comparison of UMT-CD-0.76 actual test results versus NorSand simulation.

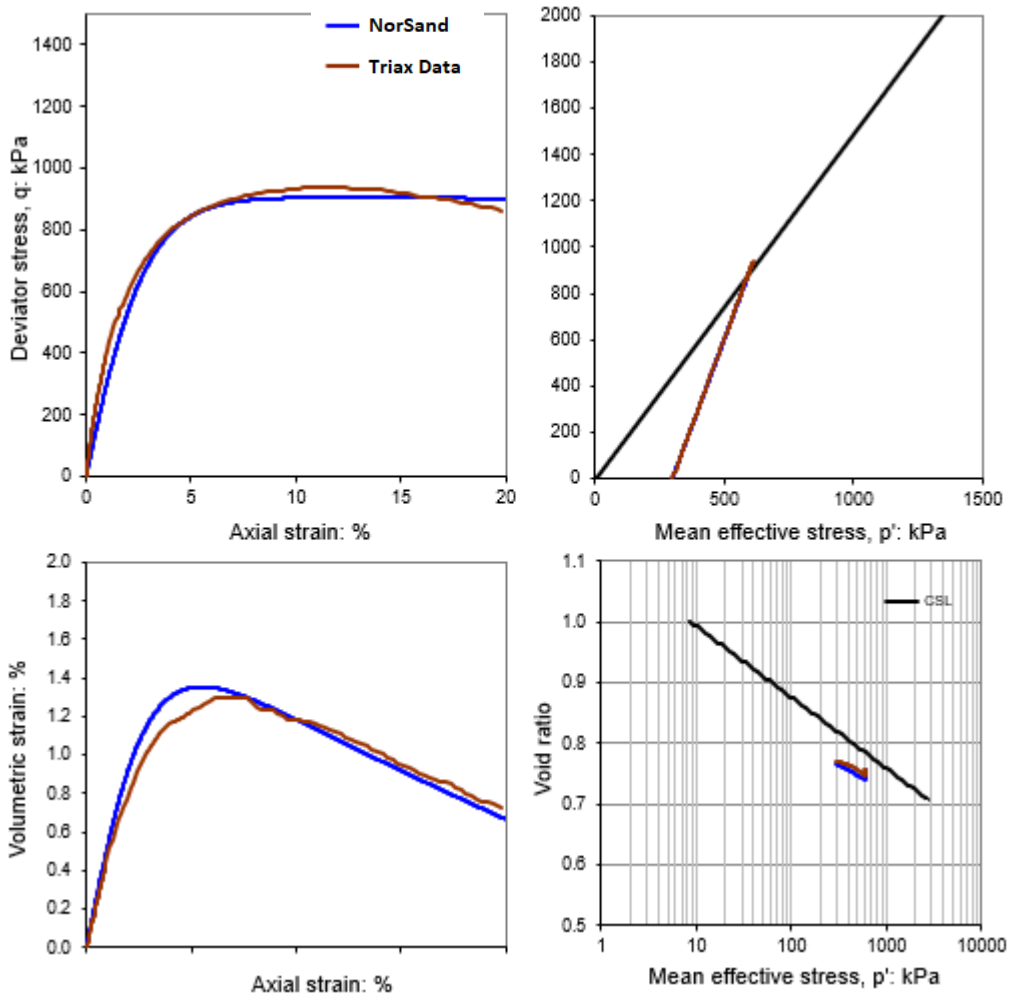

Figure B.3. Comparison of UMT-CD-0.77 actual test results versus NorSand simulation.

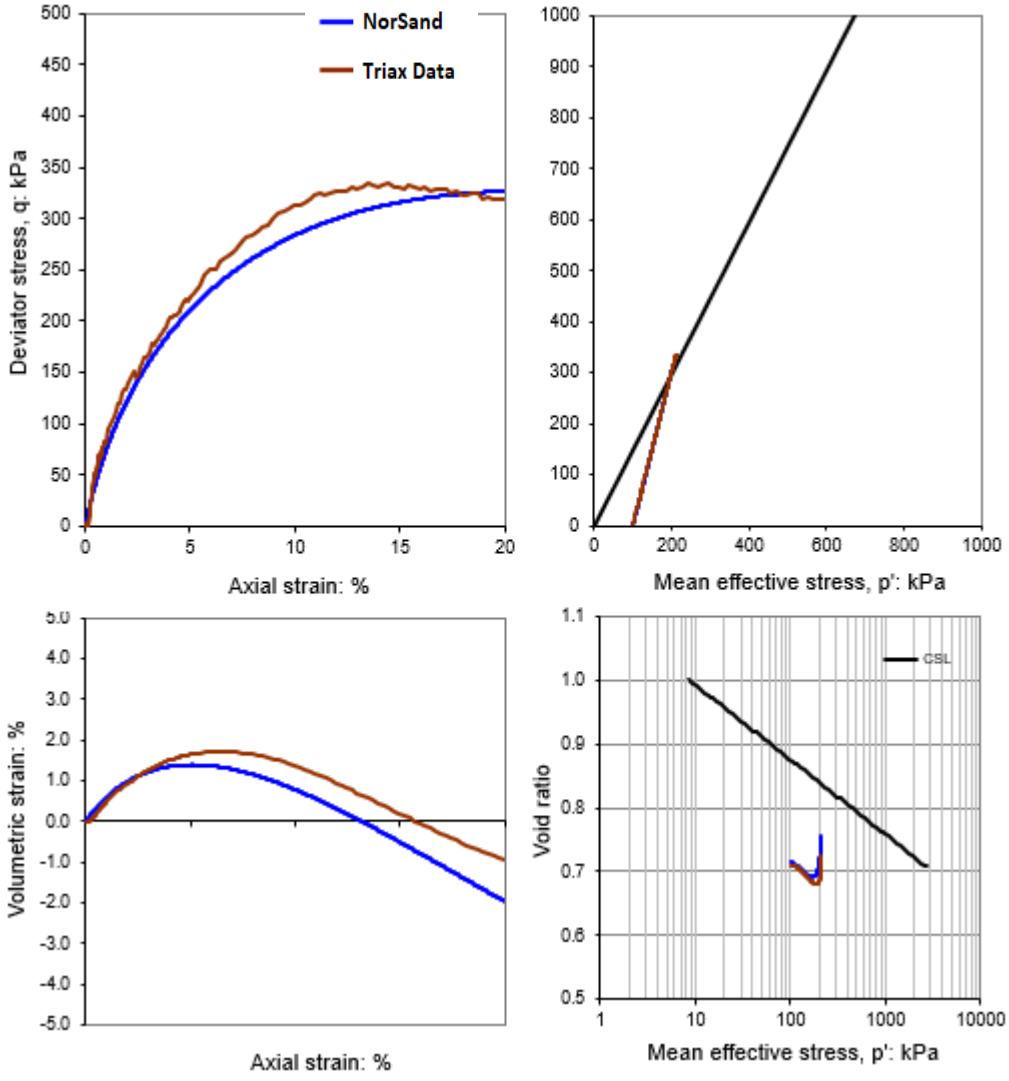

Figure B.4. Comparison of UMT-CD-0.71 actual test results versus NorSand simulation.

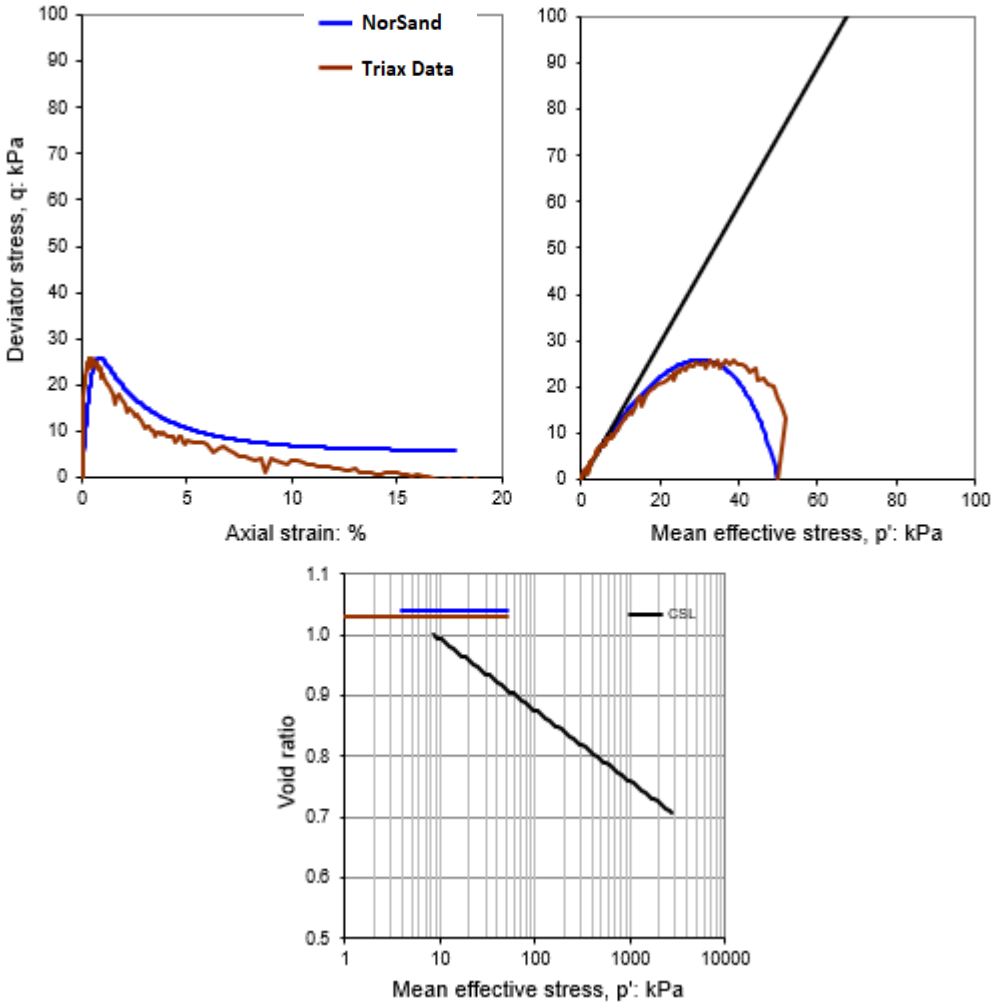

Figure B.5. Comparison of UMT-CU-1.03 actual test results versus NorSand simulation.

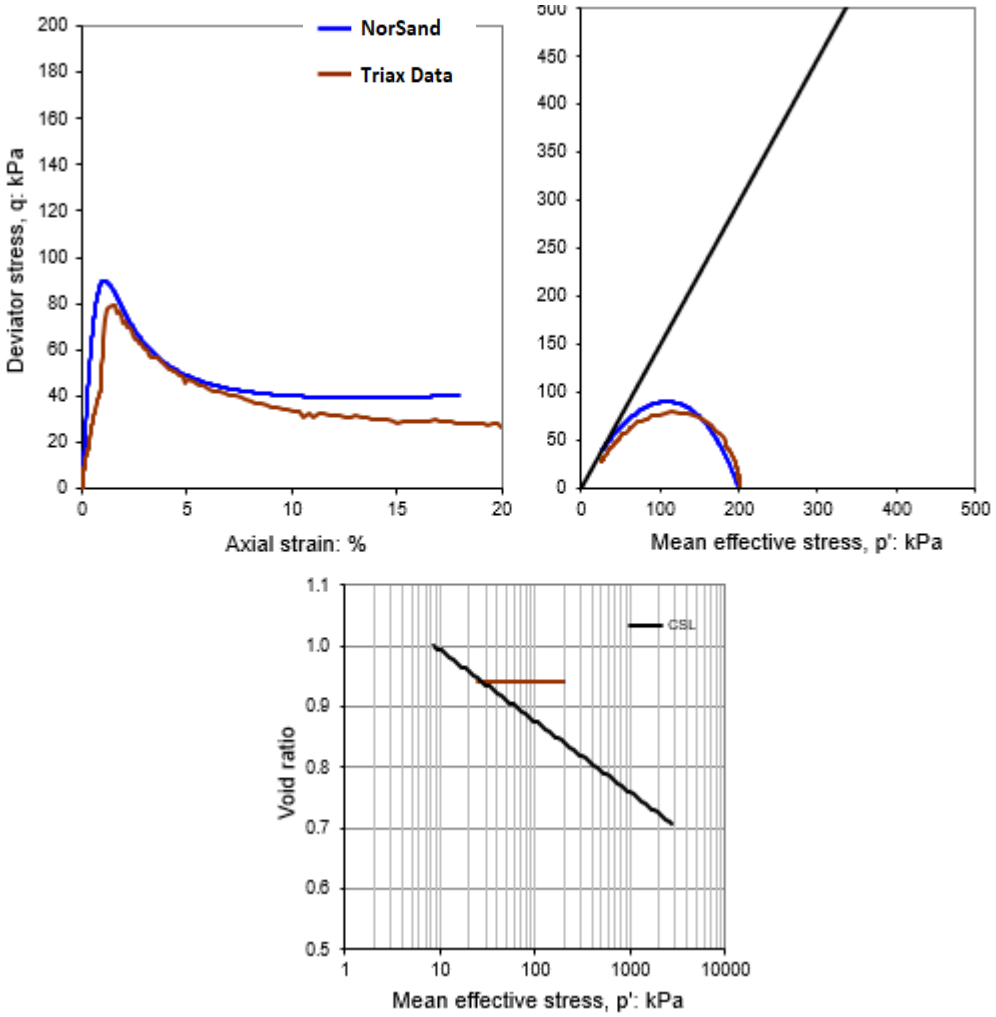

Figure B.6. Comparison of UMT-CU-0.94 actual test results versus NorSand simulation.

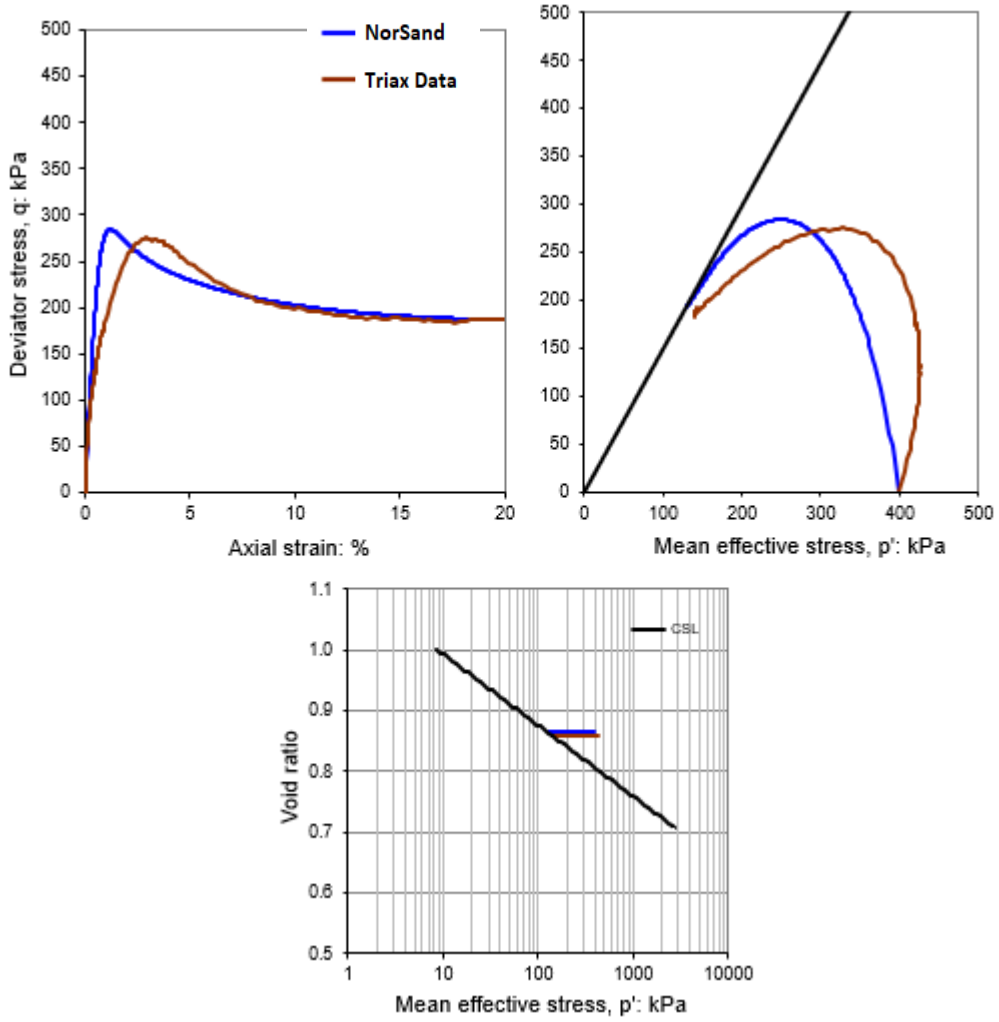

Figure B.7. Comparison of UMT-CU-0.86 actual test results versus NorSand simulation.

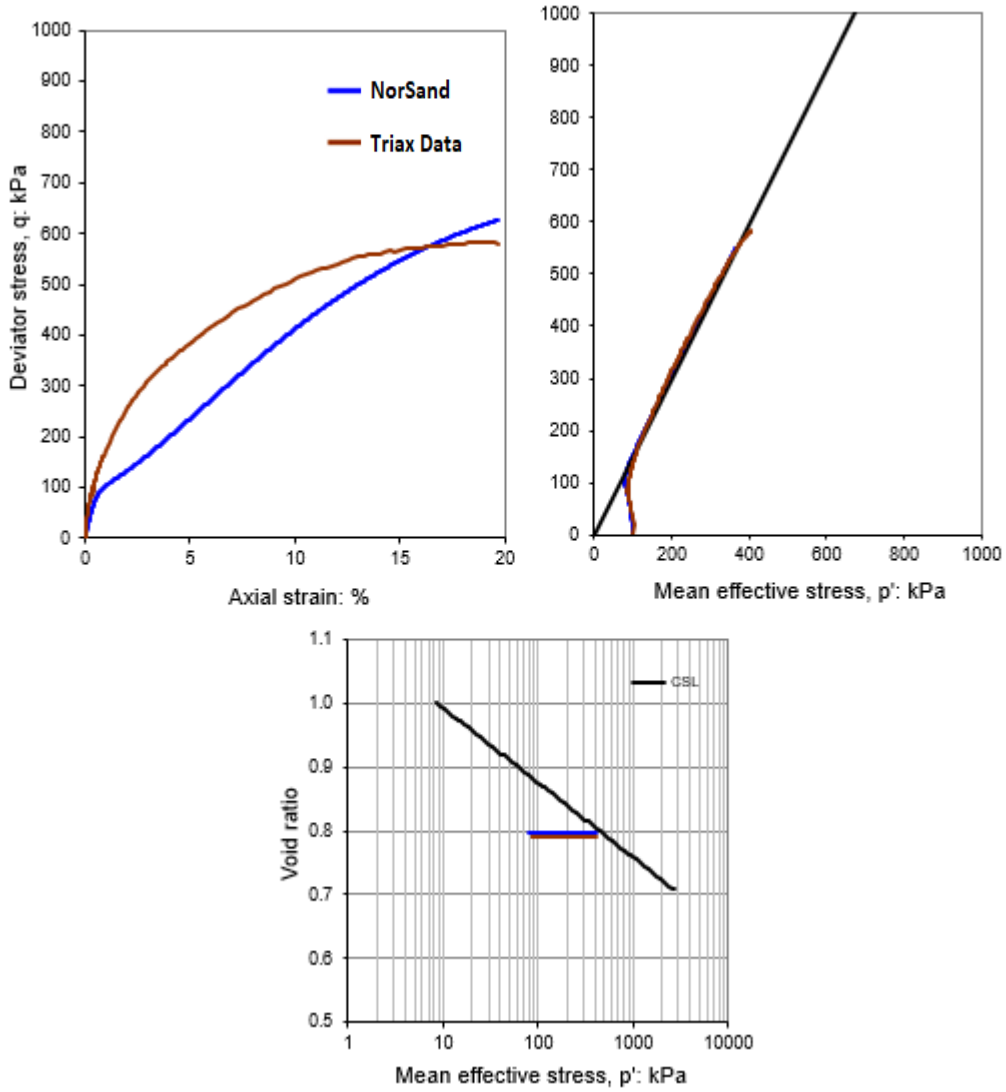

Figure B.8. Comparison of UMT-CU-0.79 actual test results versus NorSand simulation.

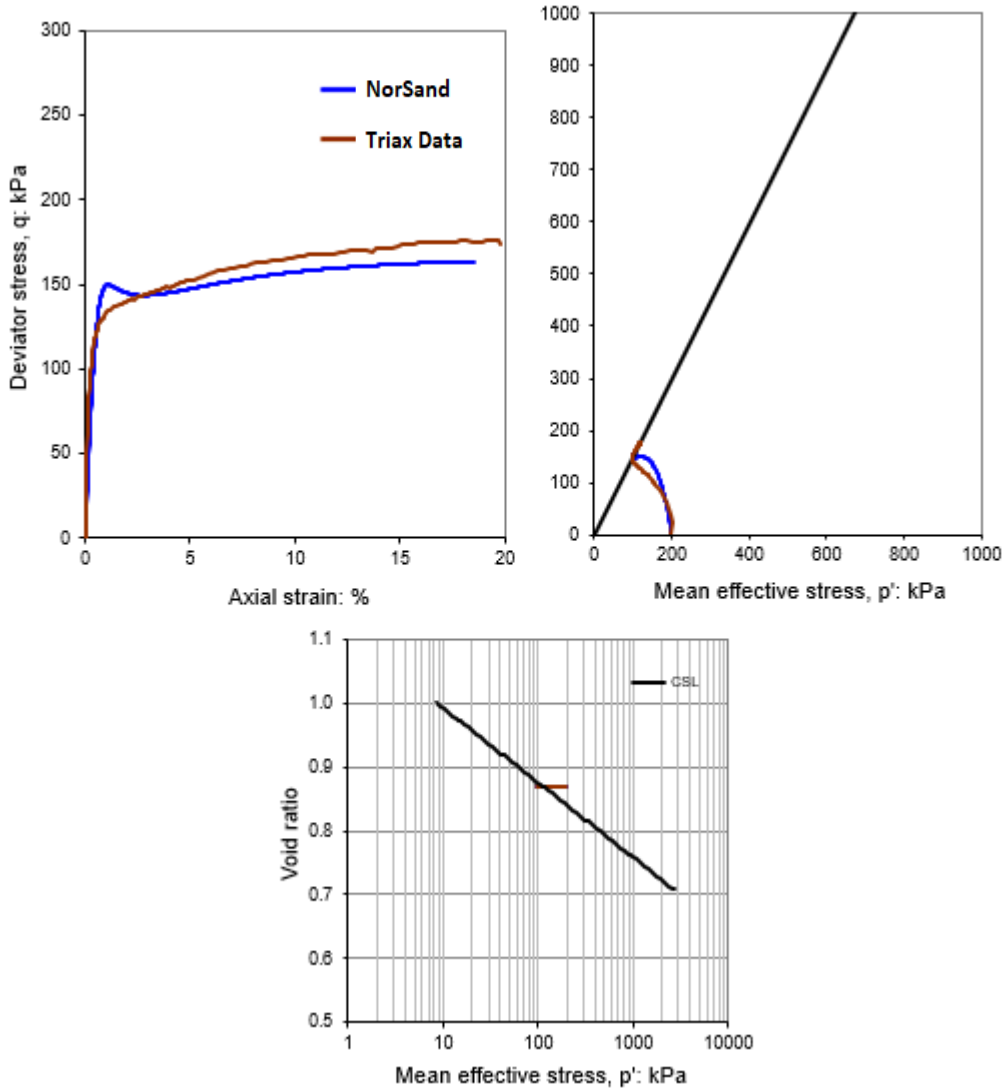

Figure B.9. Comparison of UMT-CU-0.87 actual test results versus NorSand simulation.

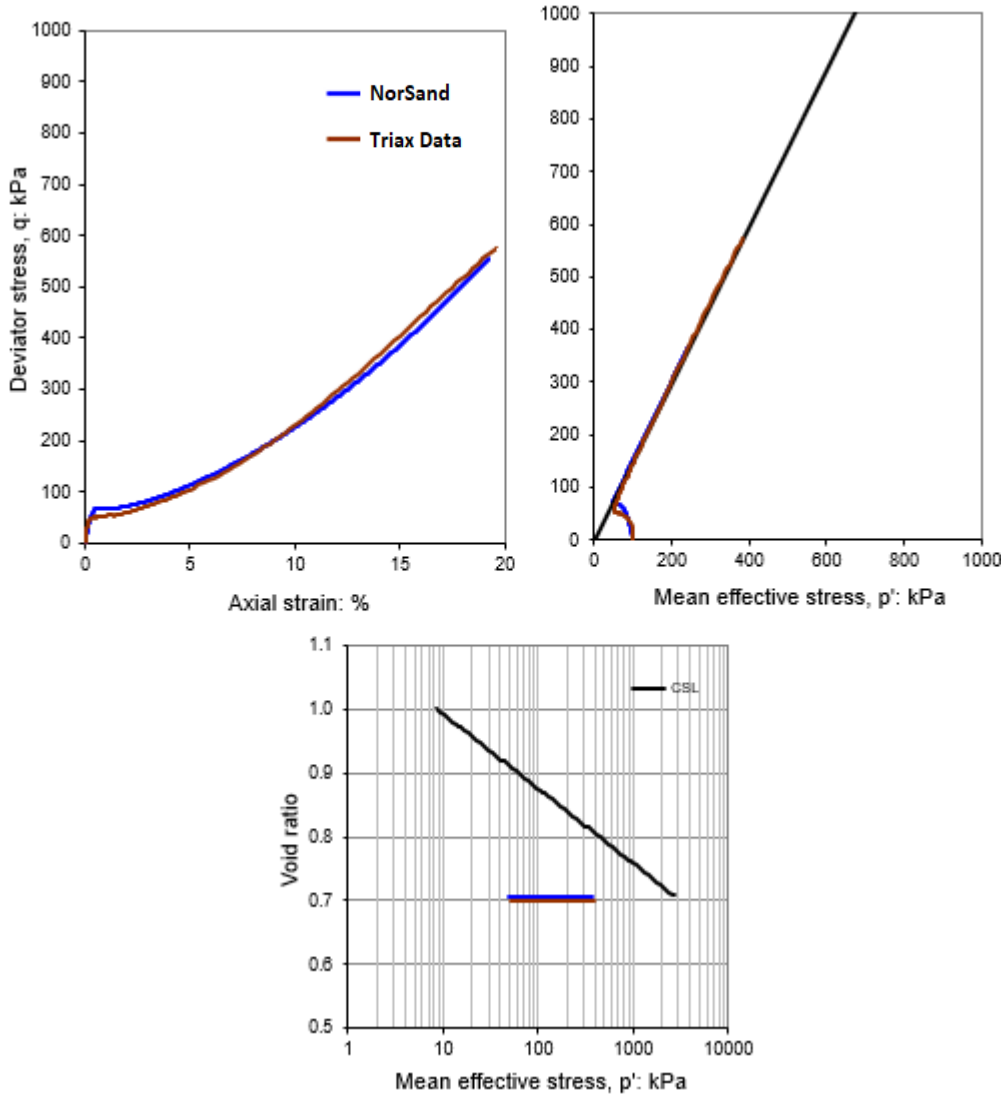

`

Figure B.10. Comparison of UMT-CU-0.70 actual test results versus NorSand simulation.

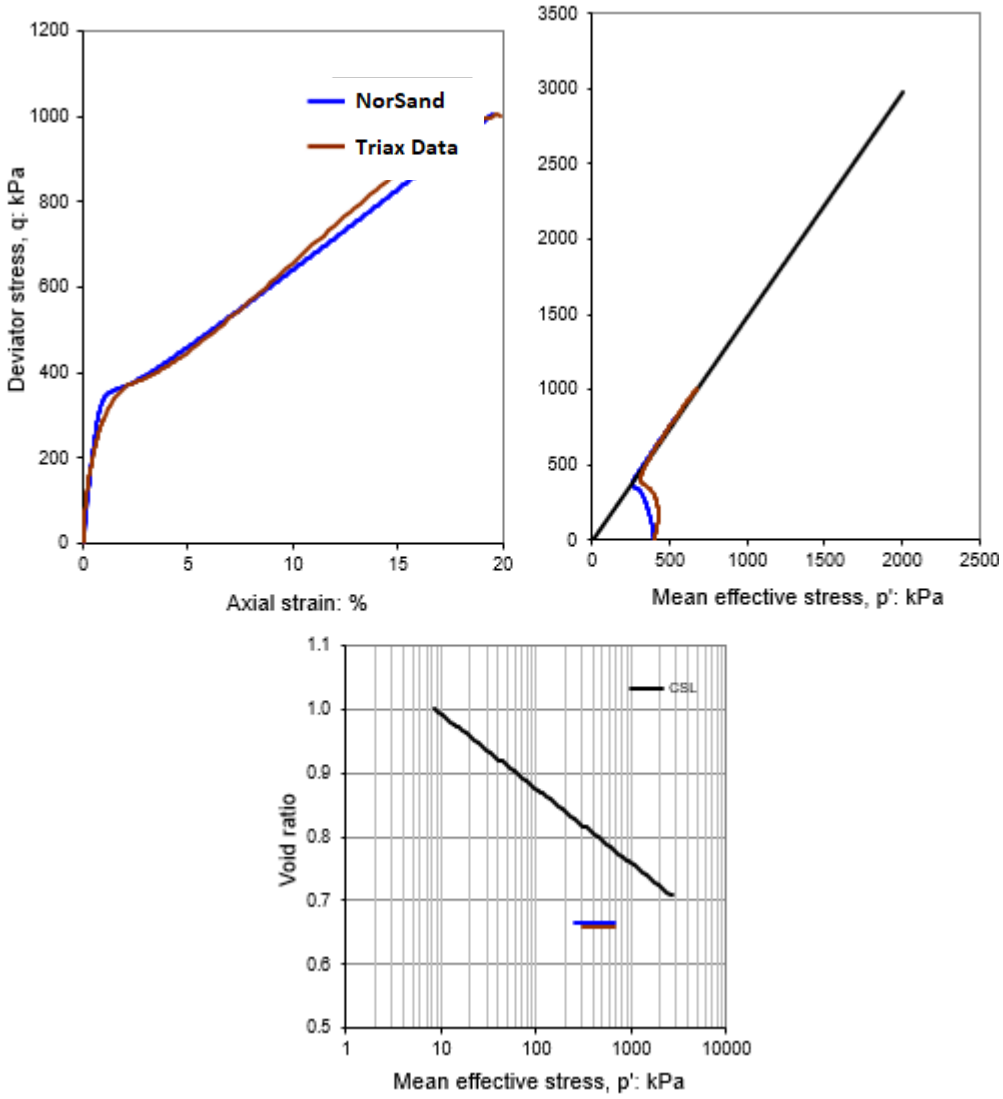

Figure B.11. Comparison of UMT-CU-0.66 actual test results versus NorSand simulation.

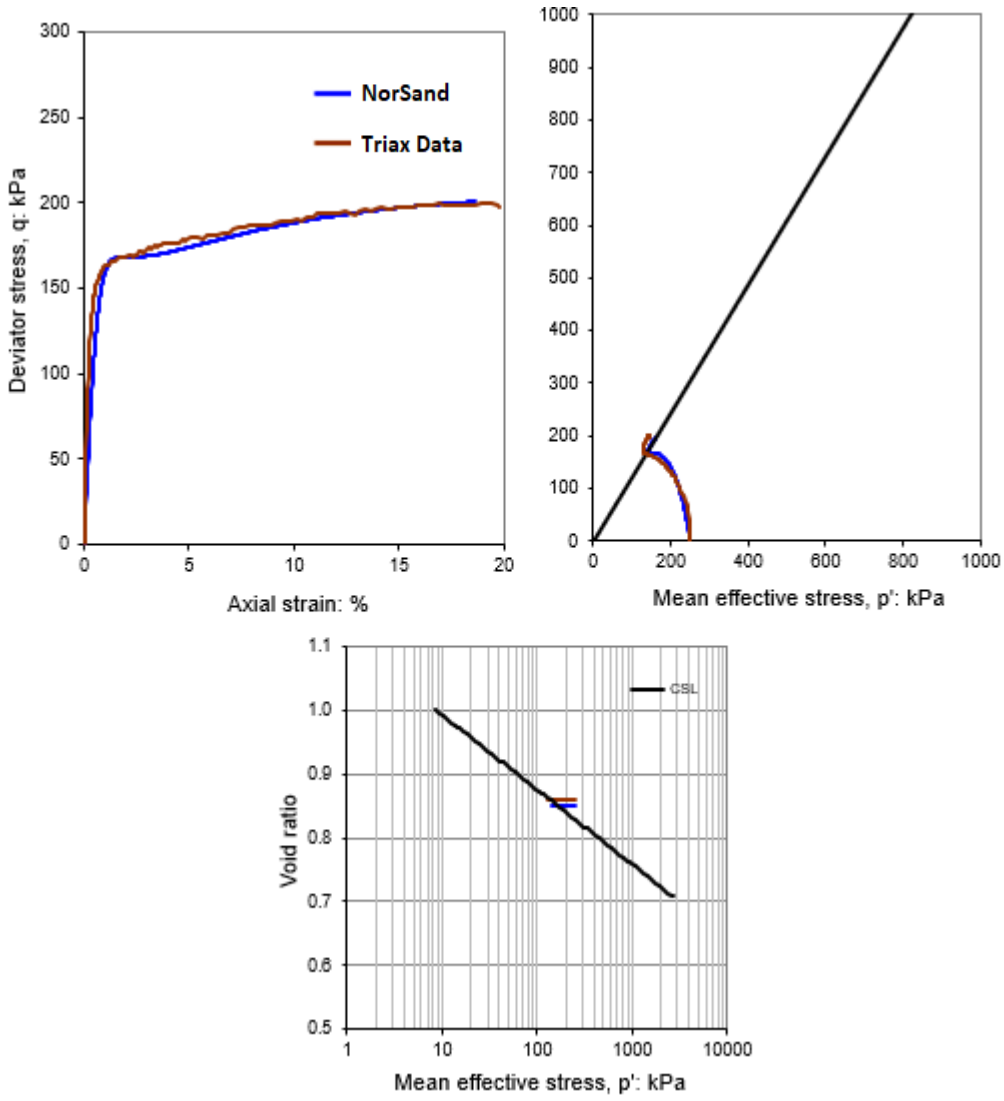

Figure B.12. Comparison of UMT-CU-1.030 actual test results versus NorSand simulation.

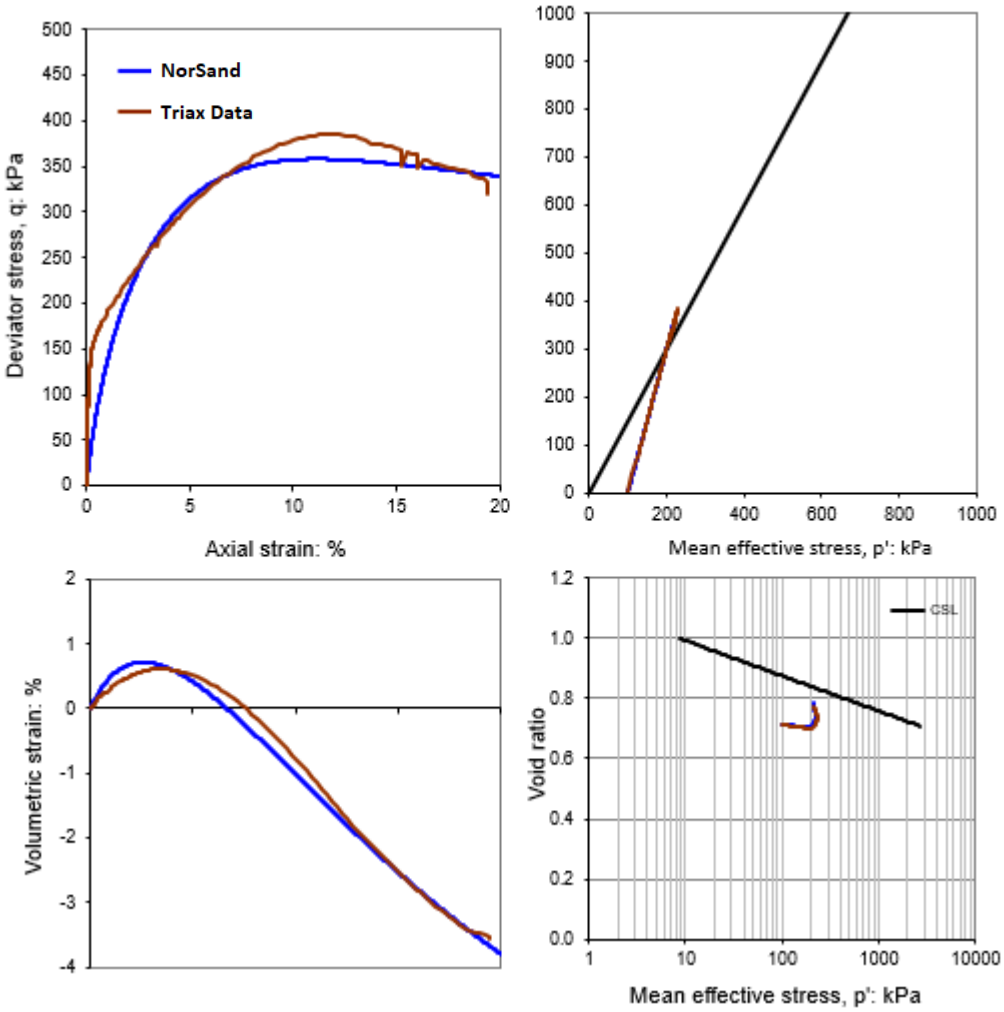

Figure B.13. Comparison of CMT-CD-0.71 actual test results versus NorSand simulation.

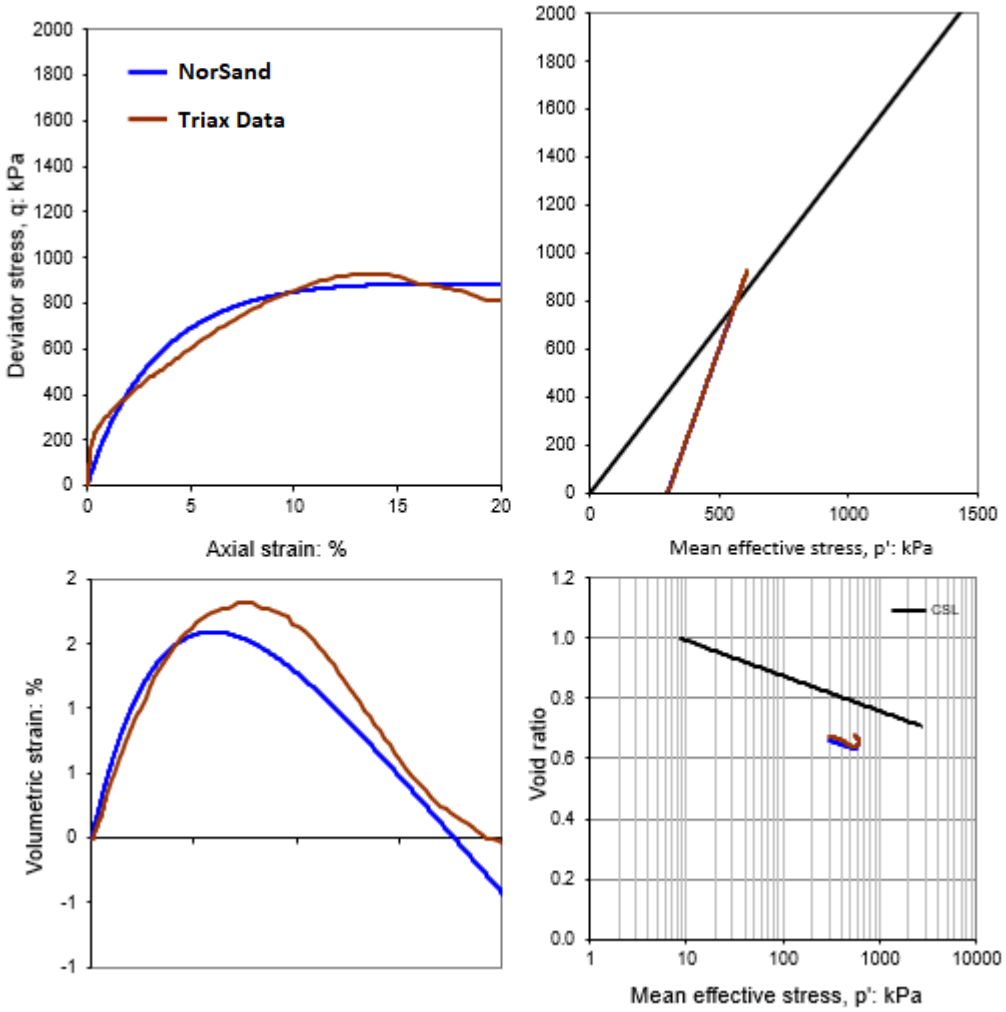

Figure B.14. Comparison of CMT-CD-0.67 actual test results versus NorSand simulation.

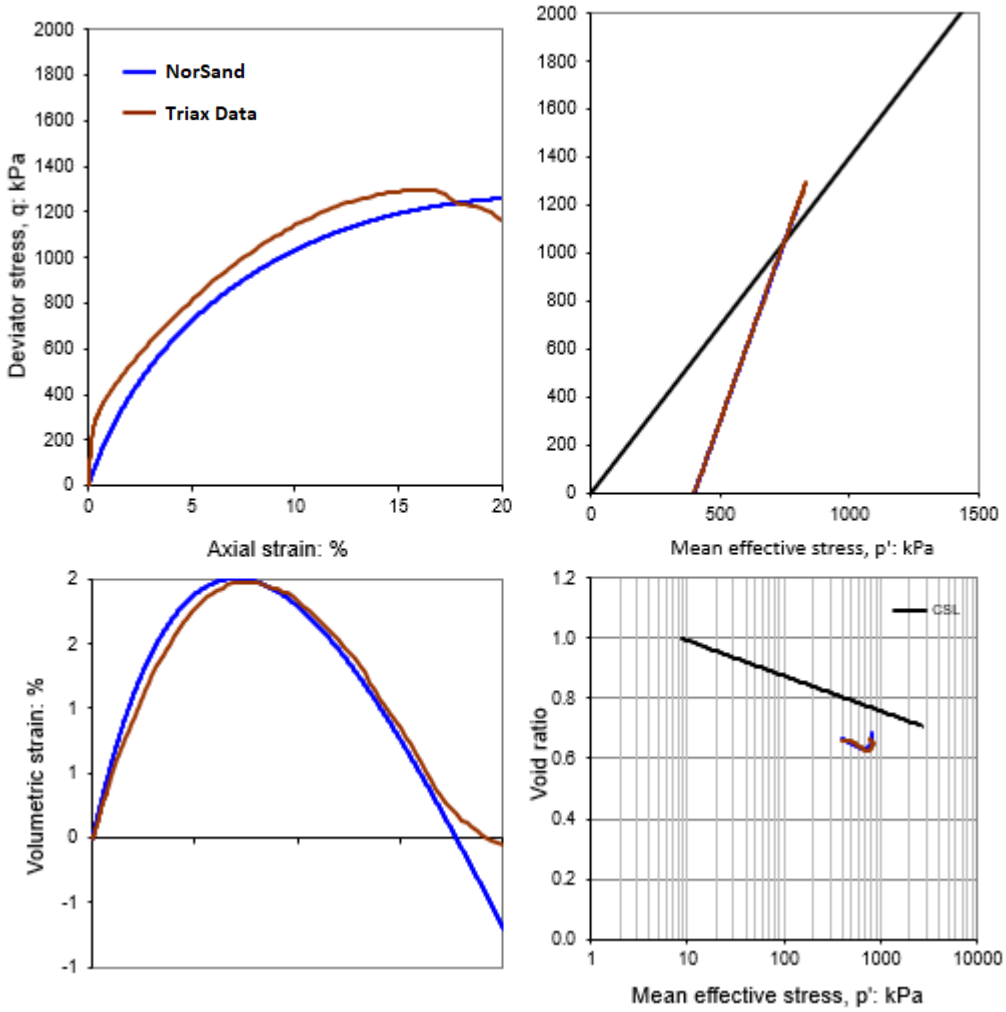

Figure B.15. Comparison of CMT-CD-0.66 actual test results versus NorSand simulation.

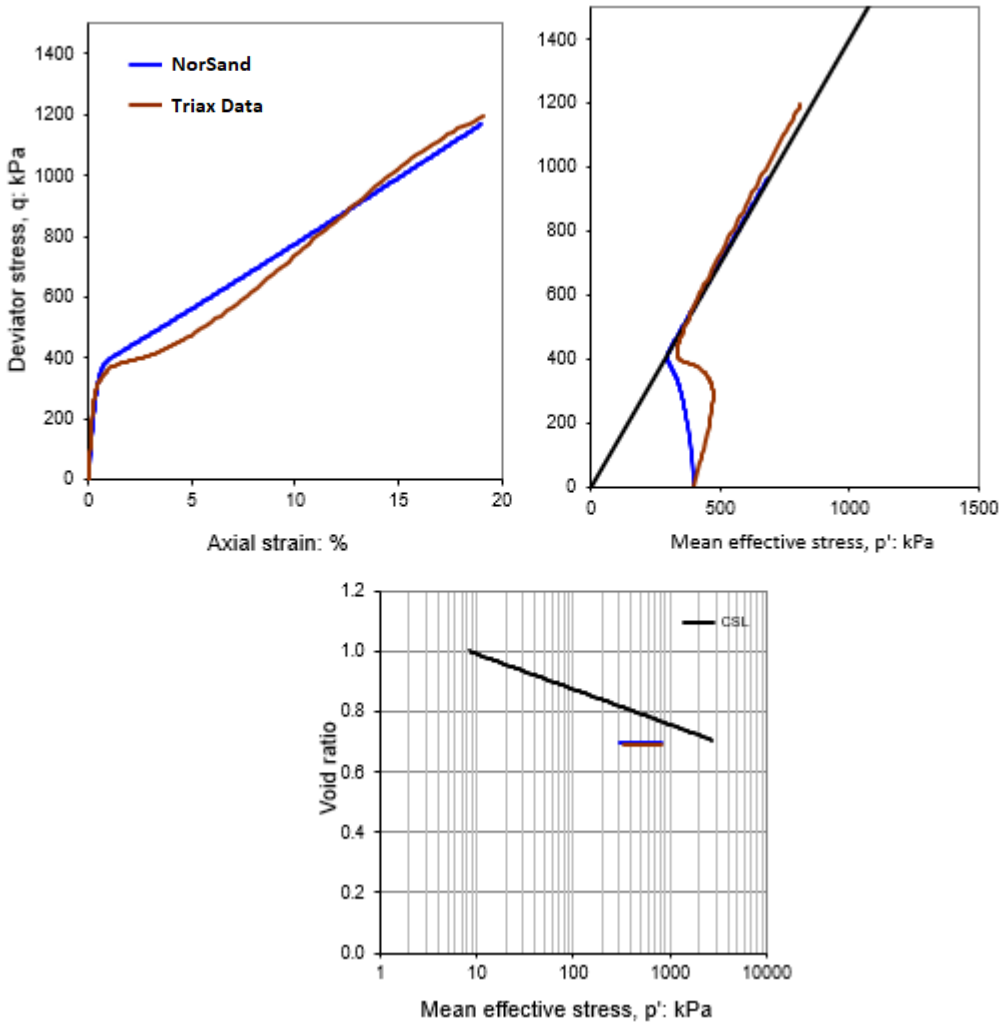

Figure B.16. Comparison of CMT-CU-0.69 actual test results versus NorSand simulation.

References

Al-Tarhouni, M. 2008. Liquefaction and post-liquefaction behaviour of gold mine tailings under simple shear loading. Master's Thesis, Department of Civil and Environmental Engineering, Carleton University, Ottawa, Ontario, Canada.

American Society of Civil Engineering, Committee on Soil Dynamics of the Geotechnical Engineering Division 1978. Definition of terms related to liquefaction. Journal of the Geotechnical Engineering Division, Vol. 104, No. GT9, pp. 1197-1200.

Aref, K. 1989. A study of the geotechnical characteristics and liquefaction potential of paste backfill. Ph.D. Thesis, McGill University, Montreal, PQ, Canada.

ASTM C136 / C136M-14, Standard Test Method for Sieve Analysis of Fine and Coarse Aggregates, ASTM International, West Conshohocken, PA, 2014, www.astm.org.

ASTM C150 / C150M-19a, Standard Specification for Portland Cement, ASTM International, West Conshohocken, PA, 2019, www.astm.org

ASTM C618-17, Standard Specification for Coal Fly Ash and Raw or Calcined Natural Pozzolan for Use in Concrete, ASTM International, West Conshohocken, PA.

ASTM D422-63(2007)e2, Standard Test Method for Particle-Size Analysis of Soils (Withdrawn 2016), ASTM International, West Conshohocken, PA, 2007, www.astm.org

ASTM D4318-05, Standard Test Methods for Liquid Limit, Plastic Limit, and Plasticity Index of Soils, ASTM International, West Conshohocken, PA, 2005, www.astm.org

ASTM D5084-16a, Standard Test Methods for Measurement of Hydraulic Conductivity of Saturated Porous Materials Using a Flexible Wall Permeameter, ASTM International, West Conshohocken, PA, 2016, www.astm.org

ASTM D5102-09, Standard Test Method for Unconfined Compressive Strength of Compacted Soil-Lime Mixtures (Withdrawn 2018), ASTM International, West Conshohocken, PA, 2009, www.astm.org

ASTM D854-06e1, Standard Test Methods for Specific Gravity of Soil Solids by Water Pycnometer, ASTM International, West Conshohocken, PA, 2006, www.astm.org

Beaty, M. & Byrne, P.M. (1998). An effective stress model for predicting liquefaction behaviour of sand. In P. Dakoulas, M. Yegian, & R. D. Holtz (Eds.), Geotechnical Earthquake Engineering and Soil Dynamics III, ASCE Geotechnical Special Publication No. 75, Vol. 1, Proceedings of a Specialty Conference (pp. 766-777). Seattle: ASCE.

Beaty, M.H. and Byrne, P.M., (2011). Ubcsand constitutive model version 904ar. Itasca UDM Web Site, page 69.

Been, K., & Jefferies, M. (2015;2016;). Soil liquefaction: A critical state approach, second edition (Second ed.). Boca Raton: CRC Press. doi:10.1201/b19114

Been, K., Brown, E. T., & Hepworth, N. (2002). Liquefaction potential of paste fill at neves corvo mine, portugal. Mining Technology, 111(1), 47-58. 10.1179/mnt.2002.111.1.47

Belem, T., and Benzaazoua, M. 2008. Design and application of underground mine paste backfill technology. Geotechnical and Geological Engineering, 26:147–174.

Benzaazoua, M., Belem, T., and Bussière, B. 2002. Chemical factors that influence the performance of mine sulphidic paste backfill. Cement and Concrete Research, 32(7): 1133- 1144.

Benzaazoua, M., Fall, M., Belem, T. 2004. A contribution to understanding the hardening process of cemented paste fill. Journal of Mineral Engineering, 17(2):141–152.

Benzaazoua, M., Ouellet, J., Servant, S., Newman, P., and Verburg, R. 1999. Cementitious backfill with high sulfur content: physical, chemical, and mineralogical characterization. Cement and Concrete Research 29(5): 719-725.

Boulanger, R. W., and Idriss, M. I. (2015). “Magnitude scaling factors in liquefaction triggering procedures.” Soil Dyn. Earthquake Eng., 79, 296-303.

Boulanger, R. W., Meyers, M. W., Mejia, L. H., and Idriss, I. M. (1998). “Behaviour of a fine-grained soil during the Loma Prieta earthquake.” Can. Geotech. J., 35(1), 146–158.

Byrne, P.M., Roy, D., Campanella, R.G. and Hughes, J. (1995). “Predicting liquefaction response of granular soils from pressuremeter tests. ASCE National Convention, San Diego, Oct. 23-27, ASCE Geotechnical Special Publication 56, pp. 122-135.

Castro, G., and Poulos, S.J. 1977. Factors affecting liquefaction and cyclic mobility. ASCE Journal of Geotechnical Engineering Division, 103:501-516.

Charlie, W.A., and Veyera, G. 1985. Explosive induced porewater pressure increases. Proceedings of the Eleventh International Conference on Soil Mechanics and Foundation Engineering, Vol. 2, pp. 997-1000.

Chu, J., Wanatowski, D., Loke, W. L., & Leong, W. K. (2015). Pre-failure instability of sand under dilatancy rate controlled conditions. Soils and Foundations, 55(2), 414-424. doi:10.1016/j.sandf.2015.02.015

Cincilla, W.A., Landriault, D.A., and Verburg, R. 1997. Application of paste technology to surface disposal of mineral wastes. Proceedings of the Fourth International Conference on Tailings and Mine Waste '97, Fort Collins, Colorado, USA.

Clough, G.W., Iwabuchi, J., Rad, N.S., and Kuppusamy, T. 1989. Influence of cementation on liquefaction of sands. Journal of Geotechnical Engineering, 115:1102-1117.

Collins R. J. and S. K. Ciesielski. (1994). Recycling and Use of Waste Materials and By-Products in Highway Construction. National Cooperative Highway Research Program Synthesis of Highway Practice 199, Transportation Research Board, Washington, DC.

Crowder, J.J. 2004. Deposition, consolidation, and strength of a non-plastic tailings paste for surface disposal. Ph.D. Thesis, University of Toronto, Toronto, Ontario, Canada.

Davies, M., (2001). Impounded mine tailings: what are the failures telling us? Can. Min. Metall. Bull., 94 (2001), pp. 53-59.

Davies, M., (2002). Tailings impoundment failures: are geotechnical engineers listening? Geotech. News 20, 31–36.

Dobry, R., and Alvarez, L. 1967. Seismic failures of Chilean tailings dams. Journal of the Soil Mechanics and Foundations Division, 93:237-260.

Erten, D., & Maher, M. H. (1995). Cyclic undrained behavior of silty sand. Soil Dynamics and Earthquake Engineering, 14(2), 115-123. 10.1016/0267-7261(94)00035-F

Etezad, M. Kam, S., and Addis, P. (2016). Liquefaction susceptibility assessment of tailings for upstream dam raising. Geovancouver.

Fall, M., Benzaazoua, M., and Ouellet, S. 2005. Experimental characterization of the influence of tailings fineness and density on the quality of cemented paste backfill. Minerals Engineering, 18:41–44.

Fall, Mamadou & Benzaazoua, Mostafa. (2003). Advances in predicting performance properties and cost of paste backfill. Tailings and Mine Waste. 73-85.

Federal Highway Administration, (2017). “Fly Ash Facts for Highway Engineers, Chapter 3 - Fly Ash in Portland Cement Concrete”. Retrieved on 9/02/2019 from https://www.fhwa.dot.gov/pavement/recycling/fach03.cfm

Fourie, A.B., and Papageorgiou, G. 2001. Defining an appropriate steady state line for Merriespruit gold tailings. Canadian Geotechnical Journal, 38:695-706.

Fragaszy, R.J., and Voss, M.E. 1981. Laboratory verification of blast-induced liquefaction mechanism. USAF-Office of Scientific Research, AFOSR: 81-0085, 52 p.

Garga, V.K., and McKay, L.D. 1984. Cyclic triaxial strength of mine tailings. ASCE Journal of Geotechnical Engineering, 110:1091-1105.

Golder Associates, personal communication, July 15, 2017.

Gorakhki, M. H. & Bareither, C. A. (2017). Unconfined compressive strength of synthetic and natural mine tailings amended with fly ash and cement. Journal of Geotechnical and Geoenvironmental Engineering, 143(7), 4017017. 10.1061/(ASCE)GT.1943-5606.0001678

Grabinsky, M.W., and Simms, P. 2006. Self-desiccation of cemented paste backfill and implications for mine design. In Proceedings of the 9th International Seminar on Paste and Thickened Tailings, Limerick, 3-7 April 2006, Ireland.

Grice, A.G. 1998. Underground mining with backfill. The 2nd Annual Summit-Mine Tailings Disposal Systems, 24–25 November 1998, Brisbane, Australia, 14 pp.

Helinski, M. (2008). “Mechanics of mine backfill.” Ph.D. thesis, School of Civil and Resource Engineering, Univ. of Western Australia, Perth, Australia.

Idriss, I. M. (1999). “An update to the Seed-Idriss simplified procedure for evaluation liquefaction potential.” Proc, TRB Workshop on New Approaches to Liquefaction Analysis, Earthquake Engineering to Extreme Events (MCEER), Buffalo, NY.

Ishihara, K. 1996. Soil Behaviour in Earthquake Geotechnics. Oxford Science Publication, England.

Ishihara, K., Troncoso, J., and Kawase, Y. 1980. Cyclic strength characteristics of tailings materials. Soils and Foundations, 20:127-142.

James, M., Aubertin, M., Wijewickreme, D., and Wilson, W. (2011). “A laboratory investigation of the dynamic properties of tailings.” Can. Geotech. J., 48(11), 1587–1600.

Jefferies, M.G. 1993. “NorSand: a simple critical state model for sand”. Géotechnique 43, 91-103.

Kossoff, D., Dubbin, W. E., Alfredsson, M., Edwards, S. J., Macklin, M. G., & Hudson-Edwards, K. A. (2014). Mine tailings dams: Characteristics, failure, environmental impacts, and remediation. Applied Geochemistry, 51, 229-245. doi:10.1016/j.apgeochem.2014.09.010

Kramer, S. 1996. Geotechnical Earthquake Engineering. Prentice Hall, New Jersey, USA.

Ladd, R. S., (1978). “Preparing Test Specimen using Undercompaction,” Geotechnical Testing Journal, Vol. 1, No. 1, pp. 16-23.

Landriault, D. 1995. Paste backfill mix design for Canadian underground hard rock mining. The 12th Annual Operators Conference, Timmins, Ontario, pp. 1-10.

Le Roux, K., Bawden, W.F., and Grabinsky, M.F. 2004. Liquefaction analysis of early-age cemented paste backfill. Minefill 2004, Beijing, China.

Lee, K.L., and Seed, H. B. 1967. Cyclic stress conditions causing liquefaction of sand. Journal of the Soil Mechanics and Foundations Division, ASCE, 933 (SMI).

Li, T., Singh, U., Coxon, J., Grice, T.G., and Sainsbury, D. 2002. Development and application of paste fill using dry tailings. First International Seminar on Deep and High Stress Mining, Perth, 10 pp.

Livingston, A. & Bumrongjaroen, W. (2005). Optimization Of Silica Fume, Fly Ash And Cement Mixes For High Performance Concrete. 10.13140/2.1.3770.4961.

Martin, T. & Mcroberts, Ed. (1999). Some considerations in the stability analysis of upstream tailings dams. Tailings and MineWaste '09, Proceedings 13th International Conference OnTailings and MineWaste.

Mohamed, A.M.O., Hossein, M., and Hassani, F.P. 2003. Role of fly ash and aluminum addition on ettringite formation in lime-remediated mine tailing. Cement, Concrete and Aggregates, 25(2): 49-58.

Mozaffaridana, M. (2011). Using thermal profiles of cemented paste backfill to predict strength, Master's thesis, University of Toronto.

Neville, A.M. 1995. Properties of Concrete. Fourth Edition, Pearson Education Limited, UK.

Okusa, S., Anma, S., and Maikuma, H. 1980. Liquefaction of mine tailings in the 1978 IZUOHSHIMAKINKAI earthquake, central Japan. Proceedings, 7th World Conference on Earthquake Engineering, Istanbul, Turkey, Vol. 3.

Omar, T., & Sadrekarimi, A. (2015). Effect of triaxial specimen size on engineering design and analysis. International Journal of Geo-Engineering, 6(1), 1-17. doi:10.1186/s40703-015-0006-3

Ouellet, J., Benzaazoua, M., and Servant, S. 1998. Mechanical, mineralogical and chemical characterization of a paste backfill. Tailings and Mine Waste '98, Proceedings, 5th International Conference, Colorado.

Papadakis, V. G. (2000). Effect of fly ash on portland cement systems: Part II. high-calcium fly ash. Cement and Concrete Research, 30(10), 1647-1654. doi:10.1016/S0008-8846(00)00388-4

Pierce, M. E. (1997). Laboratory and numerical analysis of the strength and deformation behaviour of paste backfill. Master's thesis, Queen's university, Kingston, Ontario, Canada.

Poulos, S.J. 1981. The steady state of deformation. Journal of the Geotechnical Engineering Division, ASCE 107:553-562.

Poulos, S.J., Robinsky, E.I., and Keller, T.O. 1985. Liquefaction resistance of thickened tailings. Journal of Geotechnical Engineering, 111:1380-1394.

Prakash, S. (1981), “Soil Dynamics”, McGraw-Hill Book Co., New York, Reprinted by S.P. Foundation, Rolla, 1991.

Ramlochan, T., Grabinsky, M.W., and Hooton, R.D. 2004. Microstructural and chemical investigations of cemented paste backfills. Tailings and Mine Waste '04, pp. 293-304.

Revell, M. B., and Sainsbury, D. P. (2007). “Paste bulkhead failures.” Minefill, Melbourne, Australia.

Revell, M. 2000. Cannington backfill taking the pig out of paste. Paste Technology Seminar, April 2000, Perth, Australia, pp 1–12.

Rischbieter, F. 1977. Soil liquefaction - A survey of research. Proceedings, 5th International Symposium on Military Application of Blast Simulation, Royal Swedish Fortifications Administration, Stockholm, Sweden, pp. 7:1:1-7:1:24.

Roscoe, K.H., and Burland, J.B. 1968. On the generalized stress– strain behaviour of ‘wet’ clay. In Engineering plasticity. Edited by J. Heyman and F.A. Leckie. Cambridge University Press, London, UK. pp. 535–609.

Saebimoghaddam, A. (2010). “Liquefaction of early-age cemented paste backfill.” Ph.D. thesis, Dept. of Civil Engineering, Univ. of Toronto, Toronto.

Schofield, A., and Wroth, C.P., (1968). Critical State Soil Mechanics. McGraw-Hill, London, UK.

Scrivener, K.L. 2004. Backscattered electron imaging of cementitious microstructures: Understanding and quantification. Cement and Concrete Composition, 26:935-945.

Seed, H. B., and Idriss, I. M. (1982). “Ground motions and soil liquefaction during earthquakes.” EERI Monograph, Earthquake Engineering Research Institute, Berkeley, CA.

Simon, D. (2005). Microscale Analysis of Cemented Paste Backfill. Ph.D. Thesis, University of Toronto.

Sladen, J.A. and Handford, G. (1987) A potential systematic error in laboratory testing of very loose sands. Canadian Geotechnical Journal, 24(3), 462–466.

Soroka, I. 1980. Portland Cement Paste and Concrete. John Wiley& Sons, pp 338.

Stone, D.M.R. 1993. The optimization of mix designs for cemented rockfill. Proceedings of Fifth International Symposium on Mining with Backfill, MINEFILL’93, Johannesburg, SAIMM, pp 249–253.

Suazo, G., Doherty, J., & Fourie, A. (2017;2016). Cyclic shear response of cemented paste backfill. Journal of Geotechnical and Geoenvironmental Engineering, 143(1), 4016082. 10.1061/(ASCE)GT.1943-5606.0001581

Tenbergen, R.A. 2000. Paste dewatering techniques and paste plant circuit design. Tailings and Mine Waste’00, Balkema. ISBN 90 5809 126 0.

Thomas, M., Shehata, M., & Shashiprakash, S. (1999). The use of fly ash in concrete: classification by composition10.1520/CCA10423J

Transportation Development Foundation, (2011). “The Economic Impacts of Prohibiting Coal Fly Ash Use in Transportation Infrastructure Construction”. American Road & Transportation Builders Association. Retrieved on 9/01/2019 from https://www.artba.org/wp-content/ uploads/2017/06/study2011flyash.pdf.

U.S. Environmental Protection Agency (2003). Resource Conservation and Recovery Act Orientation Manual, Washington, DC.

Vaid, Y.P. and Thomas, J. (1995) Liquefaction and post liquefaction behaviour of sand. Journal of Geotechnical and Geoenvironmental Engineering, 121(2), 163–173.

Vaid, Y.P., and Chern J.C. 1985. Cyclic and monotonic undrained response of saturated sands. In Advances in the Art of Testing Soils under Cyclic Conditions: Proceeding of a session held in conjunction with the ASCE Convention., pp. 120-147.

Wijewickreme, D., Sanin, M.V., and Greenaway, G.R. 2005. Cyclic shear response of fine-grained mine tailings. Canadian Geotechnical Journal, 42:1408-1421.

Biographical Information

Amin B. Ghorbanpour completed his undergraduate degree (B. Sc. Civil Engineering) at the Baha"i Institute for Higher Education (BIHE), Tehran, in March 2012. In December 2013, he completed his Master of Science program in Civil-Geotechnical Engineering (MSCE) at The University of Texas at Arlington (UTA). He joined Golder associates Inc. (Golder) as a geotechnical engineer in 2014. During his full-time consulting career at Golder he completed his doctoral program studying the static and cyclic liquefaction of mine tailings and Cemented Paste Backfill.